QUANTIFICATION AND CHARACTERIZATION OF MEASURED NITROUS OXIDE EMISSION FROM PERENNIAL GRASSES

A Dissertation

Presented to the Faculty of the Graduate School

of Cornell University

in Partial Fulfillment of the Requirements for the Degree of

Doctor of Philosophy

by

Cedric Wood Mason

August 2016

QUANTIFICATION AND CHARACTERIZATION OF MEASURED NITROUS OXIDE EMISSION FROM PERENNIAL GRASSES

Cedric Wood Mason, Ph.D.

Cornell University 2016

Soils, especially those that are agriculturally managed, are a primary source of atmospheric nitrous oxide, but quantification of emission from soils over large spatial and temporal scales is quite uncertain to due to a high degree of heterogeneity in the processes within soils that regulate production of nitrous oxide and its transmission to the atmosphere. There is very little knowledge of the magnitude and trends in nitrous oxide emissions from perennial grass bioenergy crops in particular. Arrays of enclosed chambers can be used to measure emission rates at discrete points across a soil surface, but these must be spatially and temporally interpolated in order to determine emissions over broader areas and timespans, and this can induce errors. The eddy covariance method can be used to continuously monitor nitrous oxide emissions at the field scale, but this approach poses instrumental and computational challenges. We conducted studies during the growing season of years 2013 and 2014 using closed chambers to monitor nitrous oxide emissions from four different perennial grass ecosystems, and used those observations to estimate long-term emissions from each system. We used a bootstrapping technique to estimate the uncertainty in spatially upscaled estimates coupled with a monte carlo approach to estimate uncertainty over integrated time periods. We examined the results of the chamber studies to identify trends in the occurrence of nitrous oxide emission hotspots. We also compared eddy covariance measurement of nitrous oxide to the spatially and temporally upscaled emission estimates that were established using the closed chambers. We conclude that approximately 2.5% of applied nitrogen is lost as nitrous oxide in these fertilized perennial grass systems, and that

hotspots constitute about 1/3rd of these emissions. The field scale nitrous oxide emission estimates from eddy covariance did not contradict the upscaled estimates from closed chambers, but closed chambers seem to offer more accurate quantification at low emission rates.

BIOGRAPHICAL SKETCH

Cedric Wood Mason was born in 1981 in Denver Colorado. The second of five children, he lived most of his childhood and adolescence in Massachusetts and Vermont. In school he excelled at physical science and mathematics but also developed and cultivated a strong interest in the natural world. At Franklin and Marshall College in Lancaster, Pennsylvania he studied Physics and Music, and graduated with a B.A. in 2003. From 2003 to 2007 Cedric lived in New York City where he worked as a research assistant at the Lamont Doherty Earth Observatory, helping to conduct paleomagnetic research. In 2007, He returned to Vermont to pursue his growing interest in sustainable agriculture and worked for several years at Cedar Circle Farm. Cedric moved to Ithaca, New York in 2011 to join the Soil and Water Group at Cornell University, and completed an M.S. in agricultural and biological engineering in 2014.

This dissertation is dedicated to all of the hard working and caring people in my life, for whom I am very grateful. I especially would like to thank Bruce Mason, Melissa Warner, and my five siblings: Sthea, Rhapsody, Laurel, and Jed. I must also recognize the importance of the many teachers and mentors that have shaped my experience, including Leroy Thorpe, Mrs. Wolworth, Mr. Menin and Mr. Gilulli, Mr. Malukas, Jim Thomas, Mr. Demont and Mr. Baio, Dr. Adkins, Dr. Kent, Will Allen and John Melquist, and of course Cathelijne Stoof, Tammo Steenhuis, Brian Richards, and Christine Goodale. I would also like to recognize Hamzeh Alsalhi and Marina Molodovskaya for their help with my research. Many thanks to my friends who have been with me along the way both at school and otherwise, including Ian Rodgers, Brian Stevens, John Elliot, Ethan Cole, Devin Kelly, the NYC crew, the Cedar Circle Farmers, Talk Crazy, and of course very special thanks to the wonderful people of Ithaca, New York. Thanks to Maurice Haltom and my yoga teachers, and my teammates the Greenstar Naturals! Finally, this work is dedicated to the spirit of life, freedom, and truth, with hope for peace and harmony.

ACKNOWLEDGMENTS

This research was supported by Agriculture and Food Research Initiative Competitive Grant no. 2011-67009-20083 from the USDA National Institute of Food and Agriculture, and by the Cross-scale Biogeochemistry & Climate Integrative Graduate Education and Research Traineeship (IGERT) NSF program at Cornell University, with additional funds provided through Cornell University's College of Agriculture and Life Sciences (CALS). I would also like to acknowledge the New York State Department of Environmental Conservation (NYSDEC) for their support early in my graduate career.

TABLE OF CONTENTS

LIST OF FIGURES

LIST OF TABLES

PREFACE

The material in this dissertation was composed with the primary intention of providing material for the dissertation of the author, and to contribute to discourse on the topic of greenhouse gas emission from soils by describing original research and findings. It constitutes a distilled version of the focus of the author's academic research at the Soil and Water Lab at Cornell University, which was undertaken over the span of several years. Each chapter covers a more-or-less single, well defined topic of interest among those working to better understand, study, and control nitrous oxide emissions from soils. Chapter 1 deals with quantifying the magnitude and uncertainty of nitrous oxide emissions from an agricultural field, Chapter 2 investigates the phenomenon of nitrous oxide hotspots in an agricultural landscape and their contribution to overall emissions, and Chapter 3 compares and evaluates two common methods for determining field scale nitrous oxide losses. While it is the intention of the author to subsequently publish each of the three chapters independently in peer-review journals, this dissertation is not intended to fill that role per se, but to fully explain the objectives, methods, and findings of each major facet of the research.

CHAPTER 1

Growing season nitrous oxide emissions from perennial grass bioenergy crops in the Northeast U.S. estimated using stochastic methods applied to soil chamber data[*]

[*]Authors: Cedric W. Mason, Cathelijne R. Stoof, Brian K. Richards, Christine L. Goodale, Tammo S. Steenhuis

Introduction

Perennial grasses such as switchgrass (*Panicum virgatum*) and reed canarygrass (*Phalaris arundinaceae*) are viable crops in the Northeast U.S. where they are well-suited to seasonally wet, marginal, and otherwise unused farmland (Stoof, et al., 2014). In this region, production of these grasses can provide bioenergy feedstock to support regional energy needs without competing for prime farmland used for food production, all while providing valuable ecosystem services such as soil carbon sequestration (Bessou, et al., 2011) and an additional source of income for the regional agricultural producers. However, the conversion of previously fallow land to perennial grass crops could have detrimental effects on soil, water, and air chemistry. Emissions of nitrous oxide (N_2O, a potent greenhouse gas) are particularly concerning (Adler, et al., 2007, Hellebrand, et al., 2008); much of the land base in the Northeast U.S. that could be used for these bioenergy crops is wetness-prone, and soil moisture has been shown to be a critical factor in driving N_2O emissions (Li, 2007, Rabot, et al., 2014, Smith, et al., 1998). It is thought that N_2O emissions from agricultural soil are enhanced by nitrogen fertilizer (Davidson, 2009), can be triggered by rainfall (Van Kessel, et al., 1993, Wagner-Riddle, et al., 2007), and occur under conditions of approximately 40-90% water filled pore space (Singurindy, et al., 2009, Smith, et al., 1998). However, research pertinent particularly to N_2O emissions from perennial grasses grown on wet soil for bioenergy is sparse, and the impact of various cultivation practices (such as fertilizer timing) for these cropping systems on N_2O emissions is not well studied.

N_2O, a product of microbially mediated nitrification and denitrification in soils, is a challenging trace gas to monitor because of high spatial and temporal variation (Ambus and Christensen, 1994, Barton, et al., 2015, Groffman, et al., 2009, Parkin and Venterea, 2010). In

soils, a large proportion of annual N_2O emission occurs during brief episodes (Molodovskaya, et al., 2012, Parkin, 2008, Wagner-Riddle, et al., 2007) and from isolated patches of the larger landscape ("hotspots") (McClain, et al., 2003). The spatial variability of emissions has been shown to produce observations that form a log-normal, or positively skewed frequency distribution (Ambus and Christensen, 1994, Corre, et al., 1996, Yates, et al., 2006) which is explained as the result of patchy distribution of anaerobic microsites in soil (Parkin, 1987). Variation within these distributions can be described by a coefficient of variation (CV) and skewness, and skewed datasets are sometimes log-transformed for statistical work (Yanai, et al., 2003), although transformation does not necessarily yield normality (Van Kessel, et al., 1993). However, these approaches do not clearly convey uncertainty or confidence intervals about the central tendency of such distributions due to the variability in measured N_2O flux rates. An improved grasp of the uncertainty of an upscaled spatial mean from aggregated static chamber observations in these systems can help constrain regional emission inventories and climate prediction, and facilitate comparison of observations with model predictions which are commonly based on course-scale representations of the soil environment (Groffman, et al., 2009).

The purpose of this research is to 1) observe and quantify growing season N_2O emissions from perennial grass bioenergy crops on wetness-prone soils, 2) examine temporal emission trends and differences in emissions due to crop type and cultivation practice, and 3) investigate the effect of the positively skewed spatial heterogeneity of flux observations on uncertainty of upscaled estimates.

Methods

Study site

This study was conducted at a site near Ithaca, New York, USA (42N 28.20', 76W 25.94'). The site was chosen because it is situated on marginal, former farmland that has historically been too wet to permit reliable access with farm equipment, and because variations in the surface topography and soil drainage class create a naturally occurring array of soil moisture conditions. Prior to the onset of this research, the site was in a long-term (over 50 years) fallow state, mowed several times per decade to prevent successional growth. Existing vegetation was primarily legacy reed canarygrass (*Phalaris arundinaceae*) with assorted other grasses and forbs most notably goldenrod (*Solidago* sp). Sixteen adjacent strips, each 14.6m wide, approximately 200m long, and separated by access lanes 1.8m wide, were demarcated and assigned in randomized complete block format to one of the four treatments of the study (with the two strips on the extreme ends of the site assigned as control treatments to act as a buffer to activities adjacent to the site). Strips were oriented along the topography-induced variations in soil drainage so that the strip plots captured this variability in soil drainage class. In this way, each treatment was quadruplicated and distributed randomly along the North-South axis of the field (Fig. S1.1). Precipitation was monitored by a tipping bucket rain gauge (3665R, Spectrum Technologies) installed at the site.

Treatments

We cultivated and studied three different bioenergy perennial grass production regimes, and retained the existing land cover described above as a fallow control. The non-control strips were prepared in the mid-summer of 2011 for seeding with reed canarygrass (*Phalaris arundinaceae* L., v. Bellevue) or switchgrass (*Panicum virgatum* L. v. Shawnee, a selection from

Cave-in-Rock, an upland ecotype). These strips were sprayed with glyphosate herbicide, then mowed, plowed, disked, and harrowed prior to seeding in accordance with common agricultural practices for these crops. Four strips were planted with reed canarygrass that was subsequently fertilized annually in mid-spring with 75 kg-N ha^{-1} applied as ammonium sulfate ($(NH_4)_2SO_4$). The remaining eight strips were seeded with switchgrass, four of which received 75 kg-N ha^{-1} ammonium sulfate ($(NH_4)_2SO_4$) annually in late spring (except for 2012), the remaining four switchgrass strips received no fertilizer. A glyphosate herbicide was applied to all eight strips of switchgrass annually in spring beginning in 2013 while switchgrass was still dormant to reduce competition from cool-season weeds, especially legacy reed canarygrass.

Flux monitoring

Emissions of N_2O were observed periodically during the 2013 and 2014 growing seasons using static chambers installed in three of the replicate strips of each treatment, as described by Parkin and Venterea (2010). In each of the 12 strips that were observed, 10 chambers constructed from plastic pails were installed along the centerline of each strip; two chambers at each of five subplots that were situated to capture the full range of soil moisture within each strip (Fig. S1.1). Chamber bases were installed in 2012 and left in place throughout the duration of the study with minor maintenance as required. Periodic flux monitoring, performed by a team of 6 or more researchers, consistently commenced during mid-day (10:30 – 12:30 hrs) and lasted for 30 minutes for each chamber, with 4 samples typically withdrawn with a syringe at 10 min intervals during chamber closure. Standards used for calibrating field samples were prepared on-site from certified gas mixtures immediately after sample collection was completed. Samples were collected on dates and from treatments indicated in Table 1.1, beginning as early as April and ending as late as November in a given year.

Table 1.1: Observation dates of static chamber N_2O fluxes from the Control, Switchgrass, Reed Canarygrass + N, and Switchgrass + N treatments. Numerals indicate the number of days elapsed since most recent fertilizer application date, if applicable. If fertilizer had not been previously applied, a check mark indicates that data was collected.

Date	Control	Switchgrass	Reed Canarygrass +N	Switchgrass +N
2013-04-01	✓	✓	314	✓
2013-05-14	✓	✓	14	✓
2013-06-12	✓	✓	43	7
2013-07-11	✓	✓	72	36
2013-08-14	✓	✓	106	70
2013-09-17	✓	✓	140	104
2013-10-22	✓	✓	175	139
2013-11-20	✓	✓	204	168
2014-05-06	✓		371	
2014-05-20	✓		13	
2014-05-29	✓	✓	22	358
2014-06-06	✓	✓	30	4
2014-06-12		✓		10
2014-06-19	✓	✓	43	17
2014-07-16	✓	✓	70	44
2014-08-14	✓	✓	99	73
2014-09-24	✓	✓	140	114
2014-11-12	✓	✓	189	163

Concentrations of N_2O were determined for each field sample using a gas chromatograph (Agilent Technologies 6890N) equipped with a Supel-Q plot 30 m capillary column, a μECD detector, and a cryo-cooler, and controlled with Chemstation software (Agilent Technologies, 2004). The gas chromatograph's analysis program was optimized for N_2O detection by using splitless injection, an inlet purge time of 0.73 sec., ultrapure helium carrier gas at a flow rate of 2.6 mL/min., a makeup gas of $ArCH_4$ at a flow rate of 8.2 mL/min., and an oven temperature of -22 deg. C. Automatic peak integration features of the Chemstation software were used to calculate the N_2O peak area from the output signal.

Once N_2O concentrations were determined for the field samples, fluxes were calculated for each chamber using Eq. 1.

$$F_{N2O} = \frac{dC}{dt}\frac{V}{A}\frac{M_{N2O}}{V_m} \qquad \text{Equation 1}$$

In Eq. 1, $\frac{dC}{dt}$ is the slope of the linear regression of chamber headspace N_2O concentration with respect to chamber closure time, V is chamber volume, A is the area of the chamber footprint, M_{N2O} is the molecular mass of N_2O, and V_m is molar volume. The linear fits from which $\frac{dC}{dt}$ was derived were checked visually for each instance, and if there was not a clear trend among the constituent concentrations, data was discarded. Only flux calculations based on three or more time series samples with a clear temporal trend were retained.

Cumulative emissions

Cumulative growing season emissions were calculated for each treatment in years 2013 and 2014 separately following the linear interpolation approach outlined by Dunmola, et al. (2010). All of the available chamber N_2O flux observations were used in the cumulative emissions calculations and thus the frequency of observation and the time span of observation

varied slightly between the two years. For each treatment, the observation period for each year lasted from the first observation of that year to the last observation of that year. Cumulative emissions for each year were calculated from the "area under the curve" bounded by chamber means and discrete observation dates (linear interpolation). For each cumulative calculation, the time series was split into segments based on the discrete sampling dates, and the cumulative emission for each segment was determined from the average of the treatment means at either end and multiplied by the duration of the time segment. The segments were then summed to estimate the total emissions during the full period. Note that chambers within each cropping treatment were aggregated across all soil moisture regimes in this overall assessment. The impact of soil moisture and soil temperature on N_2O emissions will be assessed in a separate analysis (Chapter 2).

Non-normality of the skewed flux distributions invalidates the use of simple methods to determine the confidence interval for the treatment means and cumulative emissions via calculation of the standard error. To determine the uncertainty of the final cumulative flux measurements, a stochastic process was used to simulate the range of values that result from uncertainty in the treatment means due to skewed (non-normal) spatial heterogeneity of emissions and discrete spatial sampling. For each treatment on a given date, an ensemble of 10,000 possible means was created using a bootstrapping technique to simulate the resulting mean from different permutations of physical chamber placement. In the ensemble, each permutation's mean was created by drawing *N* random samples with replacement from the pool of actual chamber flux observations for the treatment on a given date, where *N* is the number of flux values in the pool (*N* was typically 30, but sometimes slightly less due to lost or discarded data). Assuming that the underlying distribution of fluxes across the soil surface is the same as

the distribution of the actual flux observations, the distributions within the ensembles represent the uncertainty of the true treatment means induced by discrete spatial sampling over a heterogeneously emitting land surface with a skewed (non-normal) distribution of fluxes. Once an ensemble of means was created for each treatment on each observation date, the cumulative emission calculations were performed as described above, but with a single mean drawn randomly from the ensemble to serve as the treatment mean. This was repeated 10,000 times, in turn producing an ensemble of cumulative emissions values for a full period. From this final ensemble, upper and lower bounds of a 95% confidence interval were established by finding the values of the 2.5% and 97.5% quantiles. The mean and median of the final ensemble were also established.

We used the method of moments (arithmetic mean) to determine all means/averages in this study. The method of moments was reported to be unbiased and does not underestimate the population mean for skewed sample distributions (Parkin, et al., 1988).

Emissions as percent of nitrogen loading

The values of the mean and confidence intervals of the cumulative emissions were used to calculate the increase in emissions from fertilized treatments over the non-fertilized treatments as a percent of the nitrogen applied as fertilizer (emission factor). The increase (as percent of nitrogen applied) was established by subtracting the mean cumulative emission of the non-fertilized treatment from that of the fertilized treatment, then dividing by the nitrogen loading rate. For the lower bound of the increase (as percent nitrogen applied), the value of the upper confidence interval for the unfertilized treatment was subtracted from the value of the lower confidence interval for the fertilized treatment and divided by the nitrogen loading rate. For the upper bound of the increase, the value of the lower confidence interval for the unfertilized

treatment was subtracted from the value of the upper confidence interval for the fertilized treatment and divided by the nitrogen loading rate.

Statistical analysis

Exploratory analysis of the chamber flux data revealed that the flux observations include numerous outliers and exhibit a positive skew to the overall distribution. A positive skew to both the spatial and temporal distribution of discrete N_2O fluxes has been reported in other research (Corre, et al., 1996, Wagner-Riddle, et al., 2007). In contrast to standard ANOVA tests, the Kruskal-Wallace rank sum test is a statistical significance test that can be applied to non-normally distributed data. We explored potential differences between treatments within each year, and between years for each treatment using the Kruskal-Wallace rank sum test. Because the sampling schedule was changed from roughly monthly in 2013, to a schedule of more frequent observations during expected peak emissions in May and June of 2014 (Table 1.1), we used subsets of the data to make comparable groups for statistical analysis. For across-years comparisons, groups were assembled to provide an equal number of observations made at similar time intervals after fertilizer application. If treatments were not fertilized, the groups were constructed so that they both represent similar time periods within the growing season (see Appendix A, Table S1.1). For within-year comparisons of different treatments, groups were chosen so that if both treatments were fertilized, there was an equal number of observations made at similar time intervals after fertilizer application. If only one, or none of the compared treatments were fertilized, emphasis was placed on an equal number of simultaneous observations over a similar period (Appendix A, Tables S1.2 through S1.7).

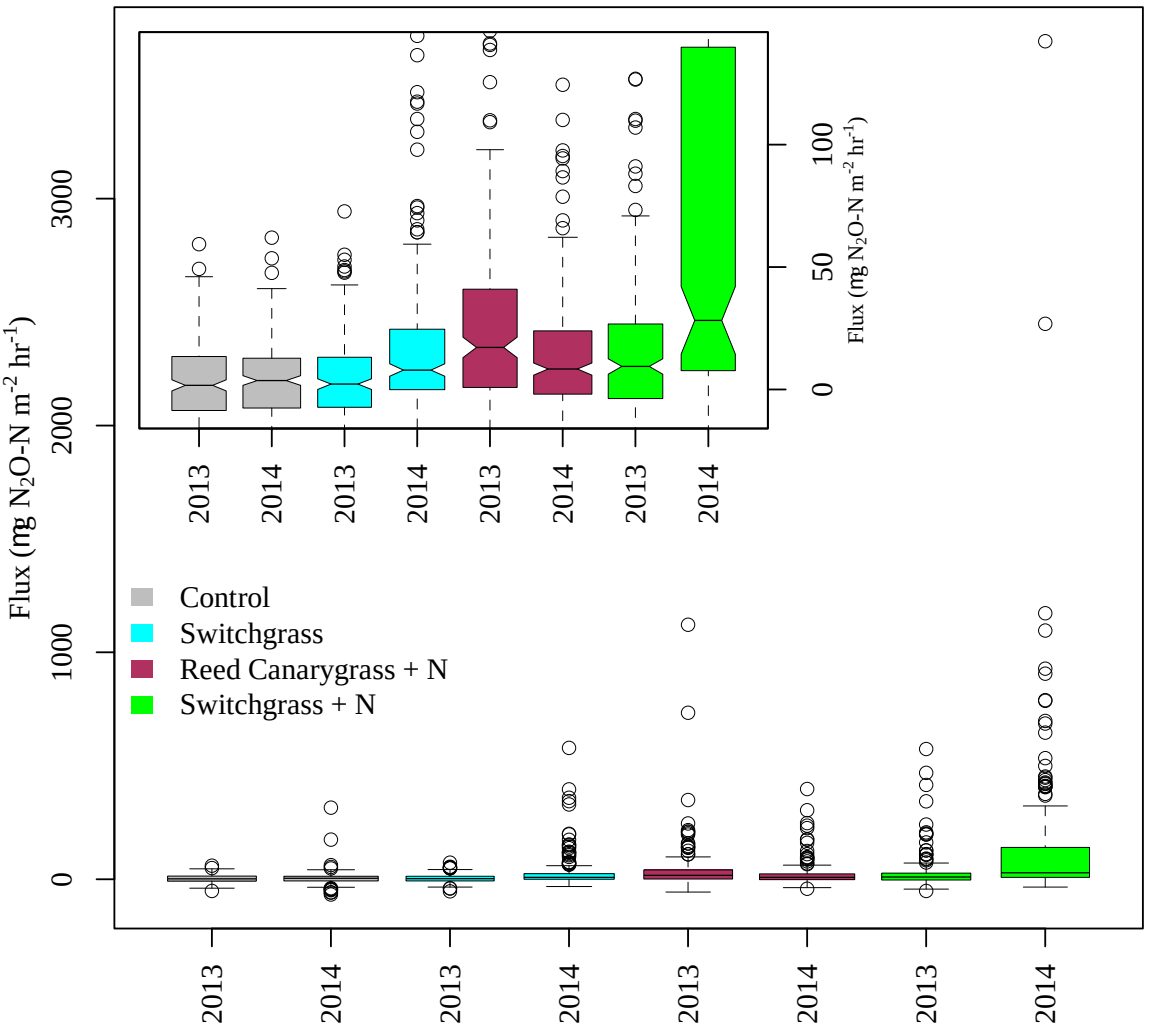

Figure 1.1: Boxplots of chamber N_2O flux observations for each treatment in years 2013 and 2014. The inset shows a magnified view of the central range of the bars and flux values.

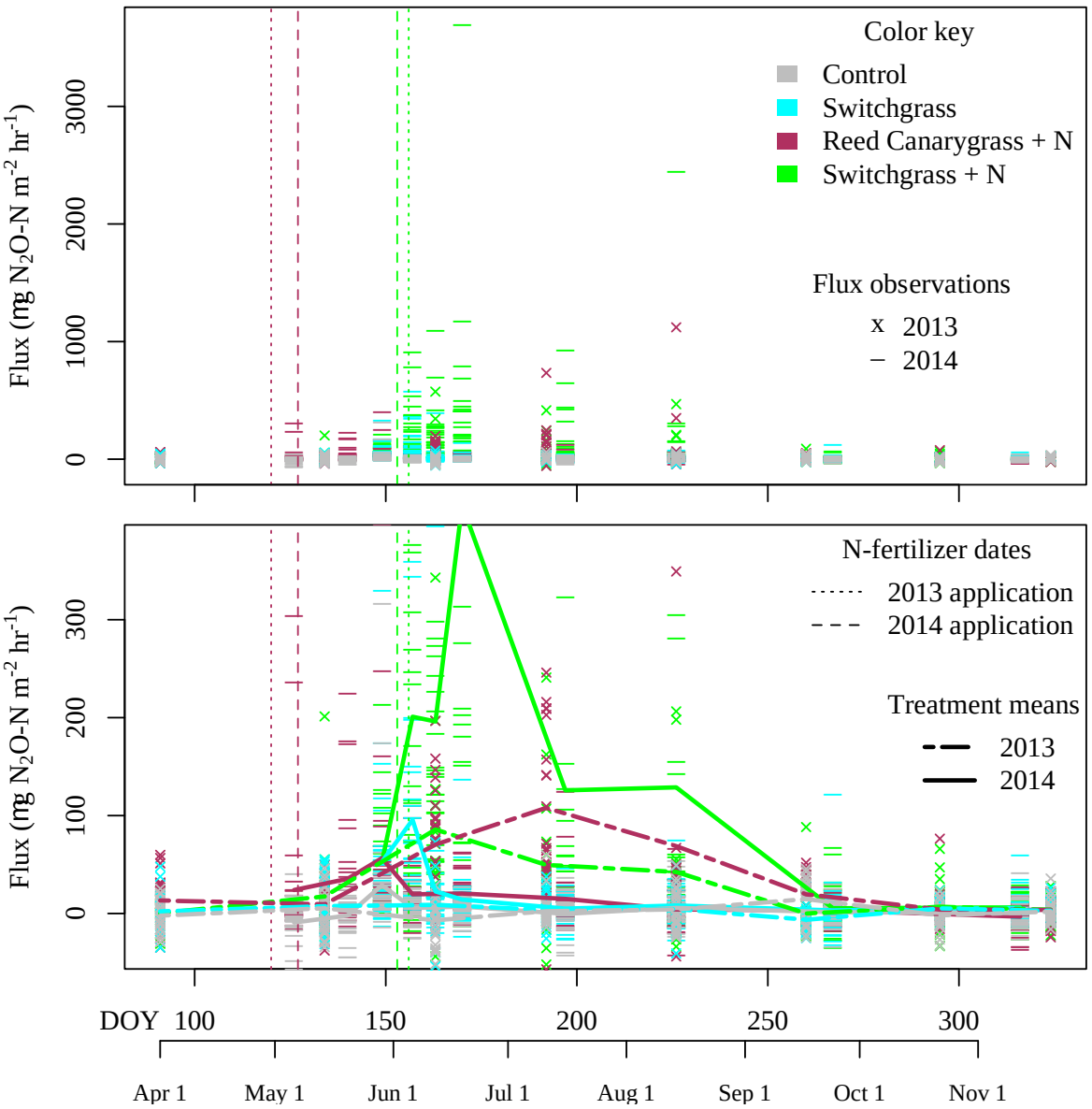

Figure 1.2: Chamber observations (top) of N_2O and temporal progression of the resulting treatment means (bottom) for years 2013 and 2014. Vertical dotted and dashed lines indicate dates of N-fertilizer application.

Data processing

Chamber headspace sample calibration, flux calculations, quality control, cumulative emissions calculations, stochastic processes, graphical plots, and statistical tests were performed with R software (R Core Team, 2011).

Results

Fluxes

Chamber flux observations of N_2O (as N_2O-N) are presented in Fig. 1.1 and Fig. 1.2. Fluxes were quite variable in both space and time, and between treatments. Within the control chambers, fluxes were generally low in magnitude and had little variation in comparison to fluxes from switchgrass, reed canarygrass + N, and switchgrass + N. Distributions were near normal for the control and more positively skewed for the other treatments. Instances of N_2O uptake (negative emission values) were small in magnitude and frequency compared to instances of positive emissions. Variation among the means of the treatments was much smaller than variation in individual flux observations (Fig. 1.2). For both 2013 and 2014, observations of elevated flux were more common in summer months (June, July, August) following fertilization, and almost completely absent from September to November (Fig. 1.2).

Treatment means and confidence intervals

The mean chamber flux for each treatment is plotted over the course of the sampling schedule in Fig. 1.2, and the medians of the ensemble of means in Fig. 1.3 and Fig. 1.4. In 2013, the mean flux from the control and switchgrass treatments were both relatively low and showed little temporal trend over the course of the growing season, whereas the means in the reed canarygrass + N and switchgrass + N treatments increased and then returned to baseline levels

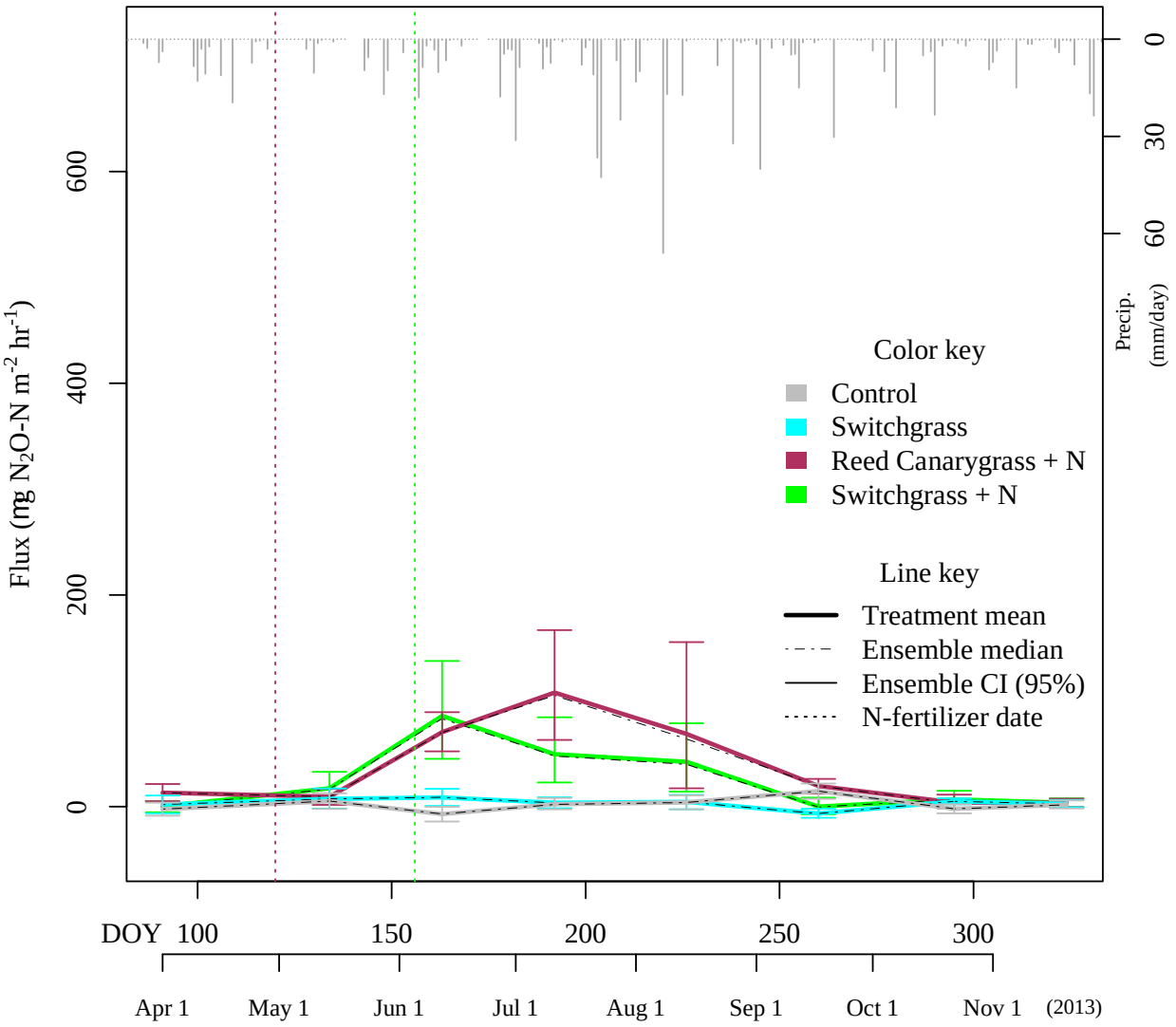

Figure 1.3: Treatment means over the course of year 2013. The 95% confidence intervals (CI) and ensemble medians from the bootstrapping procedure are also shown. Vertical dotted lines indicate dates of N-fertilizer application.

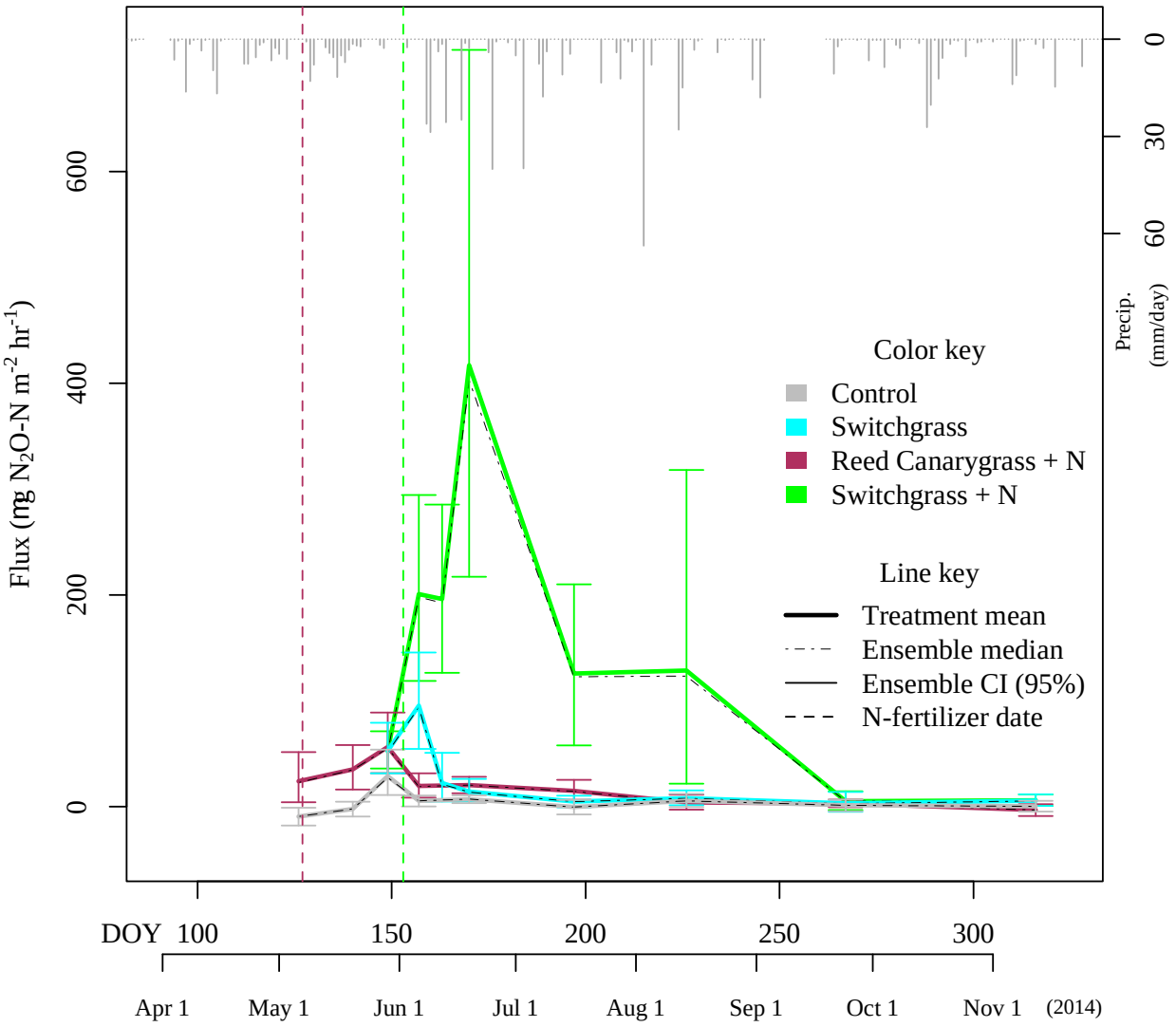

Figure 1.4: Treatment means over the course of year 2014. The 95% confidence intervals (CI) and ensemble medians from the bootstrapping procedure are also shown. Vertical dashed lines indicate dates of N-fertilizer application.

over the course of the growing season. In 2014, the means of the control, switchgrass, and reed canarygrass +N were elevated briefly around DOY 150 and quickly returned to baseline levels, while in the switchgrass + N treatment, the mean flux rose quite abruptly and remained elevated for a longer period before returning to baseline levels.

Confidence intervals at a 95% level are presented along with the treatment means in Fig. 1.3 and Fig. 1.4. These confidence intervals that were derived from the distribution of the ensemble of plausible means generated by the bootstrapping procedure represent the uncertainty in the treatment means due to discrete spatial sampling. The asymmetry of the confidence intervals for the means (and the difference between the mean and the ensemble median) generally increase with the degree of skew of the actual chamber flux observations, and generally the extent of the confidence intervals increases with the magnitude of the mean; periods of low mean flux have small confidence intervals compared to periods of elevated mean flux.

Cumulative emissions

The results of the cumulative emissions calculations are shown in Fig. 1.5 and Table 1.2. The control treatment consistently had low emissions and low uncertainty, while the other three treatments exhibited higher emissions. The highest cumulative emissions in both years were from the fertilized treatments. The confidence intervals (that were derived from the ensemble of plausible cumulative emission values) tend to increase with higher cumulative emissions estimates. Table 1.3 shows the increase in cumulative emissions from the two fertilized treatments over each of the non-fertilized treatments, as a percentage of the nitrogen addition due to annual fertilizer application.

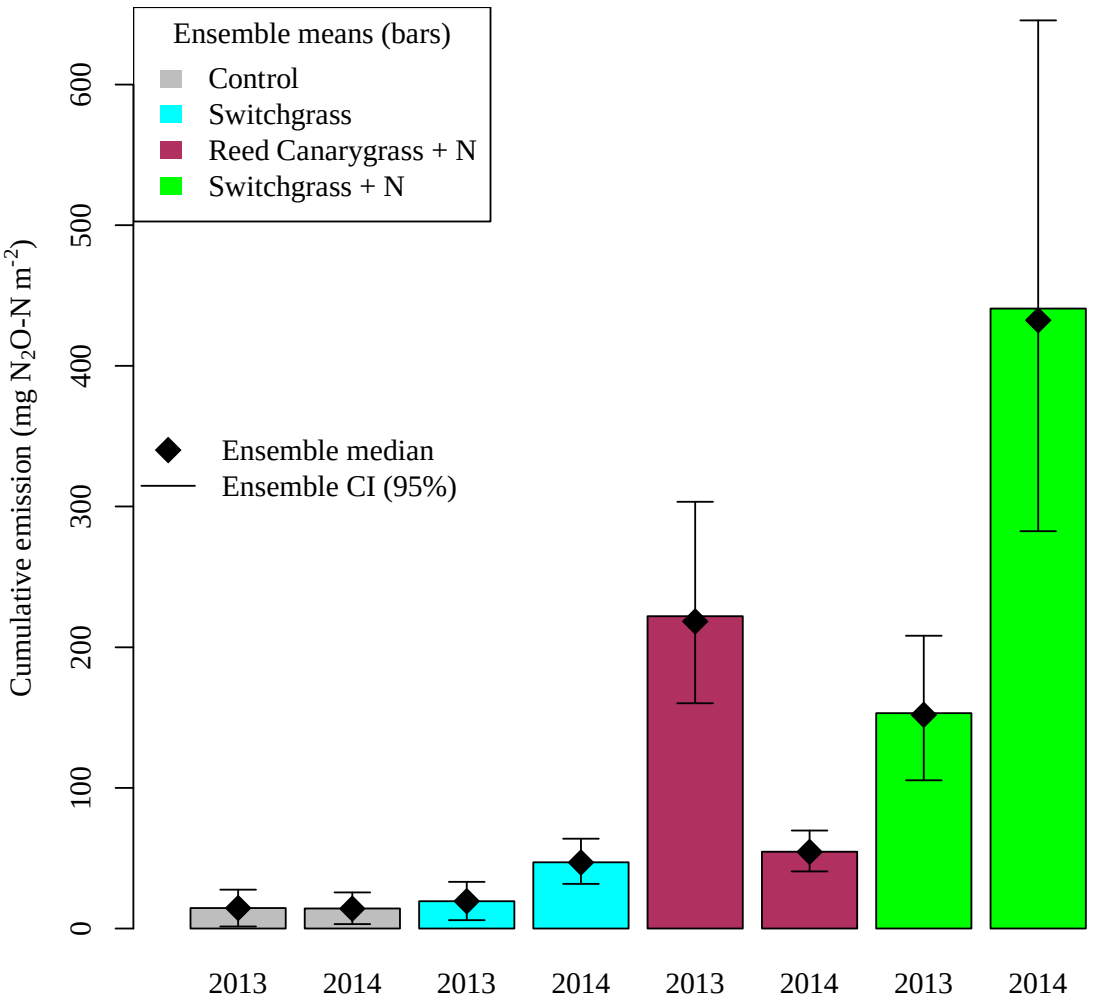

Figure 1.5: Barplots showing mean estimates of cumulative growing season N_2O emissions for each treatment and year. Confidence intervals (CI, 95%) and medians of stochastic ensembles are also shown.

Table 1.2: Mean estimates and confidence intervals (CI) for cumulative growing season emissions (mg N_2O-N m^{-2}) for fallow control (CONTROL), switchgrass (SWG), reed canarygrass + N (RCGN), and switchgrass + N (SWGN) in years 2013 and 2014.

Year	Treatment	Start date	End date	Mean	Median	CI lower	CI upper
2013	CONTROL	4/1/13	11/20/13	14.4	14.5	1.5	27.0
2014	CONTROL	5/6/14	11/12/14	14.4	14.3	3.2	25.7
2013	SWG	4/1/13	11/20/13	19.4	19.4	5.5	33.2
2014	SWG	5/29/14	11/12/14	47.3	46.9	32.1	64.2
2013	RCGN	4/1/13	11/20/13	221.9	218.6	159.2	304.3
2014	RCGN	5/6/14	11/12/14	54.7	54.6	40.5	69.8
2013	SWGN	4/1/13	11/20/13	153.5	152.3	106.0	208.9
2014	SWGN	5/29/14	11/12/14	439.2	430.8	279.5	648.0

Table 1.3: Mean estimates and confidence intervals (CI) for cumulative growing season emissions increase over fallow control (CONTROL) and switchgrass (SWG), as percent of applied nitrogen, for reed canarygrass + N (RCGN) and switchgrass + N (SWGN) in years 2013 and 2014.

				Cumulative flux increase over CONTROL as % of N applied			Cumulative flux increase over SWG as % of N applied		
Year	Treatment	Start date	End date	Mean	Lower CI	Upper CI	Mean	Lower CI	Upper CI
2013	RCGN	4/1/13	11/20/13	2.8	1.8	4.0	2.7	1.7	4.0
2014	RCGN	5/6/14	11/12/14	0.5	0.2	0.9	0.1	-0.3	0.5
2013	SWGN	4/1/13	11/20/13	1.9	1.0	2.8	1.8	1.0	2.7
2014	SWGN	5/29/14	11/12/14	5.7	3.4	8.6	5.2	2.9	8.3

Table 1.4: *P*-values resulting from Kruskal-Wallace rank sum tests on equalized groups of fallow control (CONTROL), switchgrass (SWG), reed canarygrass + N (RCGN), and switchgrass + N (SWGN).

		2013				2014			
		CONT	RCGN	SWG	SWGN	CONT	RCGN	SWG	SWGN
2013	CONT								
	RCGN	4.4e-15							
	SWG	0.55	1.2e-13						
	SWGN	2.0e-06	0.0002	2.0e-05					
2014	CONT	0.74							
	RCGN		1.1e-08			1.1e-05			
	SWG			0.002		0.0006	0.49		
	SWGN				0.0006	7.0e-16	3.7e-09	5.7e-12	

Kruskal-Wallace rank sum test

The *p*-values for the Kruskal-Wallace rank sum tests are presented in Table 1.4. The results of the annual comparisons show that the chamber fluxes in 2013 were significantly different from those of 2014 for all the treatments, except the control which did not differ across years. This indicates that in the switchgrass, reed canarygrass + N, and switchgrass + N, the distribution of fluxes changed significantly from year-to-year. For the year 2013, the Kruskal-Wallace test results show that all treatments had significantly different flux distributions from one another, except that the switchgrass did not differ significantly from the control. For 2014, all treatments had significantly different flux distributions from one another, except that the switchgrass was not significantly different from the reed canarygrass + N. The results of the Kruskal-Wallace rank sum tests (Table 1.4) are consistent with the means and confidence intervals from the cumulative emissions calculations (Fig. 1.5).

Discussion

Effect of nitrogen fertilizer

The treatments that received nitrogen fertilizer consistently had significantly greater cumulative N_2O emissions than the treatments that did not. This trend is evident in Fig. 1.5 and Table 1.4. An exception to the fertilizer's stimulatory effect on emissions is evident in the comparison of unfertilized switchgrass and reed canarygrass + N in year 2014. In this one case, a significant effect of fertilizer application on emissions was not observed and this indicates that there could be other factors at play that mitigate the fertilizer effect, and that conversion from fallow to unfertilized perennial grass can increase N_2O emissions.

It has been widely reported that nitrogen fertilizer application increases N_2O emission from soils (Adler, et al., 2007, Rees, et al., 2013, Sainju, et al., 2012), and this research confirms this connection. The values for percent applied N that is emitted as N_2O (emission factor) for each treatment (Table 1.3) can be compared to the IPCC emission factor of 1.25% (+/- 1%) (Houghton, 1997), and to 2.5%; the value proposed by Davidson (2009). In the context of this metric, the value of percent increase for reed canarygrass + N and switchgrass + N is best taken as the increase over emissions from the non-fertilized switchgrass (rather than the control) because the non-fertilized switchgrass was plowed and seeded similarly to the fertilized plots, and this comparison allows the isolation of the effect of nitrogen fertilizer application from the other management practices involved in land conversion such as tillage, which did not take place in the control. While there was some variation of the percentage of nitrogen emitted as N_2O between reed canarygrass + N and switchgrass + N, and across years, and only 2 of 4 confidence intervals accommodate either Davidson's or the IPCC's value, the overall average percent N emitted as N_2O is 2.45% (95% confidence interval is 1.33% - 3.88%) which agrees very well with the value of Davidson. However, if winter and/or spring emissions are significant in these fertilized perennial grass crops, the annual figure could be higher than the above emission factor. Winter and early spring N_2O fluxes were not measured in this study, but thaw induced emission events have been observed to comprise a significant proportion of annual emissions in temperate soils (Risk, et al., 2013). Another study of long-term N_2O emissions from agricultural soils yielded an annual emission factor of 3.16% with a 95% confidence interval of -0.89% to 7.21% (Beheydt, et al., 2007), and winter and spring fluxes (not monitored in this study) could explain this discrepancy. It should be noted that there was a wide variety of moisture conditions at the site; some areas were poorly drained and were consistently wet, whereas other areas of the field

were moderately well drained. It is likely that certain areas that fell often within the broad window of 40-90% WFPS (Singurindy, et al., 2009, Smith, et al., 1998) were responsible for a disproportional amount of the total emissions. A limitation of the present analysis is that all chamber replicates (which were located to capture the range of soil drainage conditions within each strip) are assigned equal weight; a "treatment mean" thus presumes an equal spatial occurrence of each drainage condition within the field. The controlling role of soil wetness and implications of its spatial structure on a spatially–aggregated emission potential are being analyzed separately in greater detail. However, given reasonable agreement between the cumulative emissions estimates produced by this study and the emission factors presented above, we suggest that the soils and hydrologic conditions at our study site do not seem to give rise to emission factors that are much different than those observed at other agricultural soils and sites.

Reed canarygrass + N and switchgrass + N had significantly different emissions compared to each other in year 2013, and again in year 2014. One key difference in cultivation practice between these two grasses was the fertilizer application date. Reed canarygrass, being a cool-season grass that resumes growth early, was fertilized earlier in the spring when soil temperatures were lower, and this could have reduced the rate of nitrification and denitrification, and thus N_2O production. Switchgrass fertilization is generally delayed because as a warm-season C4 grass, switchgrass does not emerge from dormancy until up to a month later. However, the temperature effect alone does not appear to dominate the variability because there was not a consistent trend in the response over both years; in year 2013 reed canarygrass + N had higher emissions, while in year 2014 switchgrass + N had higher emissions. However, overall the Reed canarygrass + N treatment had lower emissions, and this could be because of the earlier (and cooler) N-fertilizer application date.

Given that in the fertilized treatments there was typically a pattern of early-summer rise and subsequent abatement as emissions returned to baseline in September, we can assume that the direct fertilizer effect was essentially concluded by the final observations in November 2013 and November 2014. Subsequent emissions during winter or spring (periods not observed in this study) are likely a result of a different mechanism (Mason, et al., 2016, Risk, et al., 2013). Soil temperature alone cannot explain winter or spring emissions as the product of the same process that was responsible for summertime emissions (observed in this study) because observations of baseline emissions in September occurred when soil temperature was still somewhat elevated (data not shown).

Annual variability of N_2O fluxes

While the cumulative emissions calculations seem to show differences year-to-year, those values cannot be used for statistical comparison across years because different sampling schedules were applied in each year. The Kruskal-Wallace rank sum tests were based on data that was equalized to enable comparison across years 2013 and 2014. Table 1.4 shows that switchgrass, reed canarygrass + N, and switchgrass + N each produced significantly different chamber fluxes in the two years of this study, while the control did not change significantly between years. Previous research has shown that annual variation in N_2O emissions at a site can be considerable (Rees, et al., 2013).

In the reed canarygrass + N and switchgrass + N (where nitrogen was applied equally in both years) there is a clear difference in emissions across years; in both cases the Kruskal-Wallace rank sum tests indicate that the changes are significant (Table 1.4). In Fig. 1.2, Fig. 1.3, and Fig. 1.4, the difference between years in both cases appears consistent throughout the high emissions period, suggesting that this manifestation of annual variability was not driven by just a

few chance chamber fluxes (hotspots), or even one or two campaigns that by happenstance occurred during peak emission (hot-moments), but that some other factor changing from year-to-year influenced emissions. Furthermore, it is notable that emissions from reed canarygrass + N and switchgrass + N did not evolve in the same way; reed canarygrass + N emissions decreased from year 2013 to 2014, while in the switchgrass + N emissions increased.

It is possible that this phenomenon is the result of various precipitation patterns associated with the timing of N-fertilizer applications. Instances where N-fertilizer was applied during relatively dry periods (Fig. 1.3 reed canarygrass + N fertilization, and Fig. 1.4 switchgrass + N fertilization) were followed by high emissions for the rest of the season, whereas when N-fertilizer was applied during wet periods (Fig. 1.3 switchgrass + N fertilization, and Fig. 1.4 reed canarygrass + N fertilization), subsequent emissions were generally lower. This is consistent with the observations of Rabot, et al. (2014) and results of Brumme, et al. (1999) who reported that precipitation following dry periods can result in increased N_2O emissions. Yates, et al. (2006) suggests that extended dry periods can enhance the N_2O production triggered by subsequent precipitation events. In addition, it has been shown that "Nitrous oxide emissions are crucially dependent on the interaction between timing of N fertilizer application and weather" (Harrison and Webb, 2001), and that ammonia losses from surface-applied ammonium sulfate are greater for wet soil than dry (Fenn and Escarzaga, 1977). Rainfall is certainly a key mechanism that dissolves and transports surface-applied ammonium sulfate into the soil matrix where it becomes accessible to nitrifiers and denitrifiers, as well as influencing soil moisture and ammonia losses. The observed annual variability in emissions from Reed canarygrass + N and Switchgrass + N in this research can be explained by increased ammonium losses when ammonium sulfate fertilizer was broadcast in wet conditions, and better ammonium (and

eventually nitrate) retention when the fertilizer was broadcast during sustained dry periods and eventually transported into the soil by heavy precipitation.

Effect of skewed distributions of fluxes on uncertainty of treatment means and cumulative estimates

This study employed a spatially discrete sampling design to monitor N_2O fluxes at points across a field surface, and, to varying degrees, the resulting flux observations display a positively skewed distribution. This tendency is more pronounced in the fertilized treatments (Fig. 1.1).

In this research we used a stochastic bootstrapping process to estimate the confidence intervals for the treatment means empirically. The resulting intervals are themselves asymmetric (Fig. 1.3, Fig. 1.4); this indicates that the effect of hotspots on the treatment mean (and subsequently the cumulative emission) is a positively-skewed confidence interval about the median. This occurs because there are more permutations of chamber placement that will under-represent the hotspots than permutations that will over-represent them. Thus, in this research, a single treatment mean based on one such discrete sampling is more likely to be lower than the true average than above it. However, over many trials, a minority of the sample estimates of the field mean will be higher than the true average because they over-represent the hotspots, and these few instances will "correct" the average over many trials due to their disproportionate magnitude. An implication of this phenomenon is that estimates of emissions from fluxes that display a positively skewed distribution will have a more certain lower-bound than their upper-bound.

Conclusion

This research shows that conversion of a wetness-prone long-term fallow field to perennial grasses for bioenergy feedstock results in increased emissions of N_2O, and that

nitrogen fertilizer application largely drives the increase in emissions. Overall, we estimated that 2.45% of the applied nitrogen was emitted as N_2O during the growing season from April to November, and this value agrees better with the estimate by Davidson than does the IPCC estimate. At present, Davidson's (2009) value of 2.5% appears appropriate for estimates of annual N_2O emissions from perennial grass bioenergy crops under a similar nitrogen loading rate on wetness-prone marginal lands in the Northeast U.S.

Nitrous oxide emissions varied significantly from year-to-year and this highlights the importance of long-term studies to assess gross emission rates. The timing of spring fertilizer application with respect to concurrent rainfall patterns could have a profound effect on subsequent growing season emissions of N_2O (Harrison and Webb, 2001) and further study of the mechanisms by which the ammonium nitrate fertilizer is physically and chemically broken down and assimilated into various nitrogen pathways could provide useful insight into the processes that produce N_2O emission from these soils.

The flux observations from this study follow a positively skewed distribution, and this is most pronounced in the fertilized treatments during mid-summer. The skewed distributions in turn result in asymmetric uncertainty of instantaneous means, and of cumulative estimates over time. We found that as a measure of central tendency, the mean accounts for the magnitude and frequency of hotspots, but ultimately with respect to N_2O emissions, it is better to consider distributions of possibilities than a mean value alone.

Works Cited

Adler, P.R., S.J. Del Grosso and W.J. Parton. 2007. Life-cycle assessment of net greenhouse-gas flux for bioenergy cropping systems. Ecol Appl 17: 675-691. doi:Doi 10.1890/05-2018.

Agilent Technologies. 2004. Chemstation software. Agilent Technologies.

Ambus, P. and S. Christensen. 1994. Measurement of N2O emission from a fertilized grassland: an analysis of spatial variability. Journal of Geophysical Research: Atmospheres 99: 16549-16555.

Barton, L., B. Wolf, D. Rowlings, C. Scheer, R. Kiese, P. Grace, et al. 2015. Sampling frequency affects estimates of annual nitrous oxide fluxes. Scientific reports 5.

Beheydt, D., P. Boeckx, S. Sleutel, C. Li and O. Van Cleemput. 2007. Validation of DNDC for 22 long-term N 2 O field emission measurements. Atmos Environ 41: 6196-6211.

Bessou, C., F. Ferchaud, B. Gabrielle and B. Mary. 2011. Biofuels, greenhouse gases and climate change. A review. Agronomy for Sustainable Development 31: 1-79. doi:10.1051/agro/2009039.

Brumme, R., W. Borken and S. Finke. 1999. Hierarchical control on nitrous oxide emission in forest ecosystems. Global Biogeochemical Cycles 13: 1137-1148.

Corre, M.D., C. van Kessel and D.J. Pennock. 1996. Landscape and seasonal patterns of nitrous oxide emissions in a semiarid region. Soil Sci Soc Am J 60: 1806-1815.

Davidson, E.A. 2009. The contribution of manure and fertilizer nitrogen to atmospheric nitrous oxide since 1860. Nature Geoscience 2: 659-662.

Dunmola, A.S., M. Tenuta, A.P. Moulin, P. Yapa and D.A. Lobb. 2010. Pattern of greenhouse gas emission from a Prairie Pothole agricultural landscape in Manitoba, Canada. Canadian Journal of Soil Science 90: 243-256.

Fenn, L.B. and R. Escarzaga. 1977. Ammonia Volatilization from Surface Applications of Ammonium Compounds to Calcareous Soils: VI. Effects of Initial Soil Water Content and Quantity of Applied Water1. Soil Sci Soc Am J 41: 358-363. doi:10.2136/sssaj1977.03615995004100020038x.

Groffman, P.M., K. Butterbach-Bahl, R.W. Fulweiler, A.J. Gold, J.L. Morse, E.K. Stander, et al. 2009. Challenges to incorporating spatially and temporally explicit phenomena (hotspots and hot moments) in denitrification models. Biogeochemistry 93: 49-77.

Groffman, P.M., E.A. Davidson and S. Seitzinger. 2009. New approaches to modeling denitrification. Biogeochemistry 93: 1-5.

Harrison, R. and J. Webb. 2001. A review of the effect of N fertilizer type on gaseous emissions. Advances in agronomy 73: 65-108.

Hellebrand, H.J., V. Scholz and J. Kern. 2008. Fertiliser induced nitrous oxide emissions during energy crop cultivation on loamy sand soils. Atmos Environ 42: 8403-8411.

Houghton, J.T. 1997. Revised 1996 IPCC guidelines for national greenhouse gas inventoriesIntergovernmental Panel on Climate Change.

Li, C. 2007. Quantifying greenhouse gas emissions from soils: Scientific basis and modeling approach. Soil Science and Plant Nutrition 53: 344-352. doi:10.1111/j.1747-0765.2007.00133.x.

Mason, C.W., C.R. Stoof, B.K. Richards, D.G. Rossiter and T.S. Steenhuis. 2016. Spring-Thaw Nitrous Oxide Emissions from Reed Canarygrass on Wetness-Prone Marginal Soil in New York State. Soil Sci Soc Am J.

McClain, M.E., E.W. Boyer, C.L. Dent, S.E. Gergel, N.B. Grimm, P.M. Groffman, et al. 2003. Biogeochemical hot spots and hot moments at the interface of terrestrial and aquatic ecosystems. Ecosystems 6: 301-312.

Molodovskaya, M., O. Singurindy, B.K. Richards, J. Warland, M.S. Johnson and T.S. Steenhuis. 2012. Temporal Variability of Nitrous Oxide from Fertilized Croplands: Hot Moment Analysis. Soil Sci Soc Am J 76: 1728-1740. doi:DOI 10.2136/sssaj2012.0039.

Parkin, T., J. Meisinger, J. Starr, S. Chester and J. Robinson. 1988. Evaluation of statistical estimation methods for lognormally distributed variables. Soil Sci Soc Am J 52: 323-329.

Parkin, T.B. 1987. Soil microsites as a source of denitrification variability. Soil Sci Soc Am J 51: 1194-1199.

Parkin, T.B. 2008. Effect of sampling frequency on estimates of cumulative nitrous oxide emissions. Journal of environmental quality 37: 1390-1395.

Parkin, T.B. and R.T. Venterea. 2010. Sampling Protocols. Chapter 3. Chamber-Based Trace Gas Flux Measurements. Sampling Protocols. R.F. Follett, editor.: p. 3-1 to 3-39.

R Core Team. 2011. R: A language and environment for statistical computing. R Foundation for Statistical Computing, Vienna, Austria.

Rabot, E., C. Hénault and I. Cousin. 2014. Temporal Variability of Nitrous Oxide Emissionsby Soils as Affected by Hydric History. Soil Sci Soc Am J 78: 434-444.

Rees, R., J. Augustin, G. Alberti, B. Ball, P. Boeckx, A. Cantarel, et al. 2013. Nitrous oxide emissions from European agriculture: an analysis of variability and drivers of emissions from field experiments. Biogeosciences 10: 2671-2682.

Risk, N., D. Snider and C. Wagner-Riddle. 2013. Mechanisms leading to enhanced soil nitrous oxide fluxes induced by freeze–thaw cycles. Canadian Journal of Soil Science 93: 401-414. doi:10.4141/cjss2012-071.

Sainju, U.M., W.B. Stevens, T. Caesar-Tonthat and M.A. Liebig. 2012. Soil greenhouse gas emissions affected by irrigation, tillage, crop rotation, and nitrogen fertilization. Journal of environmental quality 41: 1774-1786. doi:10.2134/jeq2012.0176.

Singurindy, O., M. Molodovskaya, B.K. Richards and T.S. Steenhuis. 2009. Nitrous oxide emission at low temperatures from manure-amended soils under corn (Zea mays L.). Agriculture, Ecosystems & Environment 132: 74-81. doi:10.1016/j.agee.2009.03.001.

Smith, K.A., P.E. Thomson, H. Clayton, I.P. McTaggart and F. Conen. 1998. Effects of temperature, water content and nitrogen fertilisation on emissions of nitrous oxide by soils. Atmos Environ 32: 3301-3309. doi:Doi 10.1016/S1352-2310(97)00492-5.

Stoof, C.R., B.K. Richards, P.B. Woodbury, E.S. Fabio, A.R. Brumbach, J. Cherney, et al. 2014. Untapped Potential: Opportunities and Challenges for Sustainable Bioenergy Production from Marginal Lands in the Northeast USA. BioEnergy Research. doi:10.1007/s12155-014-9515-8.

Van Kessel, C., D. Pennock and R. Farrell. 1993. Seasonal variations in denitrification and nitrous oxide evolution at the landscape scale. Soil Sci Soc Am J 57: 988-995.

Wagner-Riddle, C., A. Furon, N.L. Mclaughlin, I. Lee, J. Barbeau, S. Jayasundara, et al. 2007. Intensive measurement of nitrous oxide emissions from a corn-soybean-wheat rotation under two contrasting management systems over 5 years. Global Change Biol 13: 1722-1736. doi:DOI 10.1111/j.1365-2486.2007.01388.x.

Yanai, J., T. Sawamoto, T. Oe, K. Kusa, K. Yamakawa, K. Sakamoto, et al. 2003. Spatial variability of nitrous oxide emissions and their soil-related determining factors in an agricultural field. Journal of environmental quality 32: 1965-1977.

Yates, T., B. Si, R. Farrell and D. Pennock. 2006. Probability distribution and spatial dependence of nitrous oxide emission. Soil Sci Soc Am J 70: 753-762.

CHAPTER 2

Hotspots of nitrous oxide emission in fertilized and unfertilized perennial grasses on wetness-prone marginal land in New York State[†]

[†]Authors: Cedric W. Mason, Cathelijne R. Stoof, Brian K. Richards, Srabani Das, Christine L. Goodale, Tammo S. Steenhuis

Introduction

Nitrous oxide (N_2O) is an important greenhouse gas that contributes to climate change and is produced from agricultural soils via the microbiologically mediated processes of nitrification and denitrification (Ambus, 1998, Bateman and Baggs, 2005, Bessou, et al., 2011, Dunmola, et al., 2010, Li, 2007). Nitrification is thought to occur primarily under aerobic conditions by nitrifying bacteria, and denitrification is considered to occur in anaerobic soil microsites (Parkin, 1987) as a result of activity by bacteria, as well as by fungi (Bateman and Baggs, 2005, Kester, et al., 1997, Rütting, et al., 2013). Emissions of N_2O have been generally reported to exhibit wide spatial variability (Barton, et al., 2015, Schelde, et al., 2012), resulting in highly skewed frequency distributions that are described as "approximately log-normal" (Ball, et al., 1997, Hellebrand, et al., 2008, Parkin, 1987, Van Kessel, et al., 1993) and "reverse J-shaped" (Yates, et al., 2006). These skewed distributions give rise to a minority of extreme outliers, dubbed "hotspots", and these hotspots indicate regions of enhanced biogeochemical activity compared to the surrounding area (McClain, et al., 2003). Rapid denitrification is presented as a likely cause of N_2O hotspots (Ambus, 1998) due to association of N_2O hotspots with high soil moisture and availability of labile carbon (Dunmola, et al., 2010). In addition, denitrification often exhibits skewed frequency distributions in soils (Christensen, et al., 1990, Parkin, 1987, Van Kessel, et al., 1993), similar to spatial patterns of N_2O emission.

Environmental factors that can vary by site, climate, and management practice (Rees, et al., 2013) are thought to mediate denitrification rates by influencing the presence of organic matter (Christensen, et al., 1990, Parkin, 1987), oxygen availability (Christensen, et al., 1990), and NO_3 availability (Van Kessel, et al., 1993). High soil moisture inhibits the diffusion of O_2 into soil pores (Bateman and Baggs, 2005, Christensen, et al., 1990), thus controlling rates of

nitrification and denitrification (Kester, et al., 1997), and soil moisture plays a role in the diffusion of dissolved substrates (such as NO_3) through the soil matrix (Bateman and Baggs, 2005). In addition, the potential for N_2O to escape from soil pores before further reduction to N_2 is affected by soil moisture status (Li, 2007, Yates, et al., 2006). The degree to which O_2 permeates soil pores, and to which N_2O escapes soil pores by diffusion, is also influenced by soil structure characteristics such as pore connectivity and bulk density (Ball, et al., 1997). Temperature is also an important driver of both nitrification and denitrification in soils (Smith, et al., 1998) because of its effect on microbial kinetics that mediate those processes, and because temperature strongly influences soil respiration rates which in turn can affect O_2 availability. N_2O hotspots are thought to occur where none of the underlying multiplicative factors is limiting (Yates, et al., 2006), resulting in high biogeochemical reaction and emission rates.

Due in part to the relative rarity of natural hotspots, knowledge of the contribution of hotspots to overall emissions, the conditions where hotspots occur, and spatial and temporal trends in hotspot occurrence is quite limited for N_2O. One investigation found that "intermediate scale" N_2O hotspots were the source of approximately $1/3^{rd}$ of the summer N_2O emissions from a riparian buffer zone in the Netherlands despite constituting only 4% of the land surface area (Van den Heuvel, et al., 2009), and another (Parkin, 1987) showed that 85% of N_2O production in a soil core originated from a tiny fraction (< 1%) of the core volume. While it is thought that production of N_2O can result from denitrification in saturated conditions, Dunmola, et al. (2010) showed that emissions of N_2O were mostly from soils between 50% and 80% WFPS, and did not occur at higher moisture levels probably because poor air permeability under such conditions promotes complete denitrification of N_2O to N_2. There is little information available informing how the spatial dependence of N_2O emissions (and hotspots) changes (or is stable) over time

(Yates, et al., 2006). While some research has shown moderate-to-weak spatial dependence of N_2O emissions (Yanai, et al., 2003, Yates, et al., 2006), Van Kessel, et al. (1993) showed that an observed spatial pattern of denitrification was stable over time, and this could be due to the influence of topography on preferential hydrologic flow paths that transport reactants (McClain, et al., 2003). Similarly, Corre, et al. (1996) found that hotspots of N_2O emission occur in higher numbers at footslope locations compared to an elevated shoulder complex and that the landscape-scale pattern was consistent with time. Temporally, N_2O emission generally follows a seasonal pattern, increasing at spring-thaw and after fertilization in early summer, followed by a decrease in late summer and baseline emissions in autumn (Brumme, et al., 1999, Corre, et al., 1996, Dunmola, et al., 2010), and it is thought that this seasonal pattern is determined in temperate climates by temperature and rainfall (Hellebrand, et al., 2008). N_2O hotspots in particular have been observed predominantly during high temperature periods (Hellebrand, et al., 2008).

Mechanistic models can help estimate global emissions of N_2O and evaluate mitigation strategies (Li, 2007). Hotspots, however, are difficult to simulate because models typically use an average value for parameters such as soil moisture and labile carbon across large grid sizes, where in reality, variation exists at a fine scale due to the influence of factors including plant rooting patterns, subsurface soil aggregates, and microtopography (Groffman, et al., 2009). Because denitrification (and thus N_2O production) rates tend to correlate non-linearly with many soil parameters, the use of low-resolution grids that represent soil and other factors homogeneously is problematic (Li, 2007). To improve mechanistic denitrification models (that also predict N_2O emission), additional research into the nature and occurrence of natural hotspots at different scales, and improved prediction of hotspot spatial distribution is necessary (McClain,

et al., 2003). Additional field measurements of hotspots can provide the knowledge needed to construct better models (Groffman, et al., 2009).

In this study, we investigated N_2O hotspots at the field scale in the context of perennial grass bioenergy crops on marginal, recently converted farmland in the Northeast U.S. In this study, our primary research questions are: 1) What is the contribution of these hotspots to overall emissions of N_2O? 2) What are the conditions of soil moisture and soil temperature under which N_2O emission hotspots occur? 3) What are the temporal and spatial patterns of N_2O hotspot occurrence?

Methods

Research site

A seasonally wet, previously fallow farm field near Ithaca, NY (N 42° 28.20', W 76° 25.94') was used for production of perennial grass crops. The field is generally flat with slightly undulating topography that presents a wide range of soil moisture conditions. Drainage class of the silt loam soil at the site ranges from moderately well drained to poorly drained, with a shallow fragipan that results in seasonal saturation or near saturation. The field characteristics are further described in Chapter 1.

Treatments

During the summer of 2011 in preparation for this study, the field was divided into 16 adjacent strips, each strip 14.6 m wide and covering approximately 0.4 ha. Sets of four strips were selected at random and assigned to one of four treatments: a fallow unconverted control of assorted grasses and forbs that preexisted at the site, unfertilized Switchgrass (*Panicum virgatum* L., v. Shawnee), Reed canarygrass (*Phalaris arundinaceae* L., v. Bellevue) fertilized with 75 kg-N ha^{-1}, and Switchgrass fertilized with 75 kg-N ha^{-1}. Thus each treatment was represented by

four strips randomly distributed across the field. Strips for the Switchgrass, Reed canarygrass + N and Switchgrass + N treatments were prepared for seeding by initially mowing, plowing, and applying herbicide, while the control was left unaltered. Fertilizer was applied as ammonium sulfate ($(NH_4)_2\ SO_4$) to the Reed canarygrass + N treatment on May 22 2012, April 30 2013, and May 07 2014, and to the Switchgrass + N treatment on June 05 2013, June 02 2014, and May 21 2015 (no fertilizer was applied to the Switchgrass + N in 2012, as is typical for the early establishment phase). In both the Switchgrass and Switchgrass + N treatments, a glyphosate herbicide was applied in the spring, preceding fertilizer application, to reduce weed competition with the warm-season Switchgrass crop. Grass biomass was harvested from all treatments except the control annually in mid-autumn beginning in year 2013 using conventional mowing and baling equipment for forage crops.

N_2O flux observations

N_2O emissions were monitored periodically during years 2013, 2014, and 2015 using the static chamber method. Chambers were constructed and operated according to the recommendations of Parkin and Venterea (2010). Each chamber footprint area was 0.07 m^2, with deployments lasting 30 minutes during which time 4 headspace samples were withdrawn and injected into evacuated glass vials (10 ml nominal capacity). Concentration of headspace N_2O was determined by gas chromatography and a flux rate was subsequently determined. A full description of the equipment, operational techniques, and flux calculation is given in Chapter 1. On dates of observation, N_2O emissions were monitored at midday (hrs. 10:30 to 12:30) in three of the four strips (consistently) of each treatment, with 5 pairs ("subplots") of chambers permanently placed along each strip situated to capture the full range of soil moisture conditions

Table 2.1: Observation dates of static chamber N_2O fluxes from the Control, Switchgrass, Reed Canarygrass + N, and Switchgrass + N treatments. Numerals indicate the number of days elapsed since the last fertilizer application date, if applicable. If fertilizer had not been previously applied, a check mark indicates that data was collected.

Data collected and Days since N fertilization				
Date	Control	Switchgrass	Reed Canarygrass +N	Switchgrass +N
2013-04-01	✓	✓	314	✓
2013-05-14	✓	✓	14	✓
2013-06-12	✓	✓	43	7
2013-07-11	✓	✓	72	36
2013-08-14	✓	✓	106	70
2013-09-17	✓	✓	140	104
2013-10-22	✓	✓	175	139
2013-11-20	✓	✓	204	168
2014-05-06	✓		371	
2014-05-20	✓		13	
2014-05-29	✓	✓	22	358
2014-06-06	✓	✓	30	4
2014-06-12		✓		10
2014-06-19	✓	✓	43	17
2014-07-16	✓	✓	70	44
2014-08-14	✓	✓	99	73
2014-09-24	✓	✓	140	114
2014-11-12	✓	✓	189	163
2015-07-07	(Strip P only)			47
2015-07-22	(Strip P only)			62

available. Thus N_2O emissions of each treatment were monitored with 30 chambers operated simultaneously on dates indicated in Table 2.1.

Hotspot identification

Emission hotspots are patches of the soil surface that exhibit substantially different emissions compared to the surrounding areas. To identify hotspots in this study we applied the statistical definition used by Corre, et al. (1996), Van den Heuvel, et al. (2009), and Van Kessel, et al. (1993), whereby individual observations within a dataset that exceed a threshold value are considered to be hotspots. The hotspot threshold (T_{hs}), described in Eq. 1, is established as the median (M) plus three times the interquartile range ($Q_3 - Q_1$) for the dataset.

$$T_{hs} = M + 3(Q_3 - Q_1) \qquad \text{Eq. 1}$$

In this research, a threshold and hotspots were identified independently for each treatment on each date of observation. The flux observations from a given treatment on a given date that were not classified as hotspots are referred to as the "background" emissions.

Soil temperature, soil moisture, groundwater monitoring, and precipitation

Soil temperature and soil moisture were measured manually at the chamber locations immediately after chamber headspace sampling was completed, typically between hrs. 13:00 and 16:00. Soil temperature was observed by inserting 3 thermocouple thermometers into the upper 2.5 cm of soil between the pair of chambers at each subplot, and the average of the 3 readings was assigned to both chambers. Soil moisture was assigned similarly, determined from the average of 3 measurements between each pair of chambers using a time domain reflectometry (TDR) soil moisture sensor equipped with 12 cm probes (Hydrosense™, Campbell Scientific Australia Pty. LTD.). The TDR instrument determines percent volumetric water content (% VWC) using a factory calibration. We converted soil moisture values from % VWC to percent

water filled pore space (% WFPS) by scaling the instrument's values based on a linear trend that was established from the average % VWC values observed for saturated (100% WFPS) and dry (0% WFPS) conditions. Because there was some variation in the values of % VWC for saturated conditions, and the average of said values was used for calibration, some of the resulting calibrated soil moisture values appear to exceed 100% WFPS, however this is simply a result of variation in instrument readings for saturated soils and the calibration method. Thus the calibrated soil moisture values presented here are approximations of the actual % WFPS. To establish long-term wetness ranking among subplots, the instantaneous values of % WFPS at each subplot were converted to ratios of the simultaneous field average. These ratios were then averaged over the duration of the study, and binned into quintiles, with Quintile 1 reflecting wettest conditions.

At each of the subplots where the chamber bases were situated, perched water table depths were monitored using shallow wells that consisted of a slotted and screened PVC pipe (2 cm diameter, 1.2m long), installed vertically, flush with the soil surface and covered with a loose-fitting (3 cm diameter) PVC cap. Perched water table depths were monitored at least monthly (typically concurrent with N_2O emissions chamber measurements) using a custom depth measurement device that provided audible sensing of the water surface. Flooded subplots were assigned a depth of zero.

Precipitation was recorded by a tipping-bucket rain gauge (model 366R, Spectrum Technologies) coupled with a datalogger (CR5000, Campbell Scientific Inc.) installed at a location near the center of the field. Daily precipitation was calculated by summing the number of recorded instrument trips for each day and multiplying by the rainfall depth for each trip using MATLAB software (MathWorks, 2011).

Data processing and statistics

All data processing (except for daily rainfall calculation), graphing procedures, and statistics were performed with R software (R Core Team, 2011).

The binomial distribution was applied to the results of the hotspot identification procedure to test the hypothesis that some chamber locations have a higher occurrence of hotspots, and to test the hypothesis that hotspots occur more frequently at certain times of the year. Once identified, hotspots were grouped by chamber and by date, and the number of hotspots in the most extreme examples of each grouping were used for the hypothesis tests. The binomial distribution is presented in Eq. 2, it is a discrete probability distribution that describes the probability of observing a specific outcome in a sequence of trials where each trial is considered either a success or a failure (Chin, 2006).

$$f(n) = \frac{N!}{n!(N-n)!} p^n (1-p)^{N-n} \qquad \text{Eq. 2}$$

In Eq. 2, *f(n)* is the probability of observing *n* successes in *N* trials, each trial with a probability of success *p*. The probability of observing *n*-or-more successes can then be calculated by summing the probabilities for observing each of the outcomes with *n*-or-more successes, Eq. 3.

$$P(x_i \geq x_n) = \sum_{x_i \geq x_n}^{x_N} f(x_i) \qquad \text{Eq. 3}$$

To evaluate the alternative hypothesis that some chamber locations have a higher occurrence of hotspots, a two-step process was used to test the null hypothesis that hotspots occur at random chamber locations for each treatment. Similarly, we used this two-step approach to evaluate the hypothesis that hotspots occur more frequently during specific times of the year by testing the null hypothesis that hotspots occur randomly in time. The calculations for these hypothesis tests using the binomial distribution are presented with additional details in appendix B.

To calculate average emission rates from datasets of chamber flux observations that were often skewed, we used the method of moments (arithmetic mean). While some alternative methods have been suggested to estimate population parameters for skewed sample distributions more accurately (Parkin, et al., 1988), these methods offer very little improvement over the method of moments in the circumstances of this research. In addition, frequency distributions of spatially distributed N_2O flux have been shown to lack true log-normality (Yates, et al., 2006). The method of moments is a robust approach that performs relatively well in a variety of applications, it was shown to be unbiased and does not underestimate the population mean for skewed sample distributions (Parkin, et al., 1988).

Results

Hotspot occurrence and contribution to emissions

Hotspots were observed in all treatments and throughout most of the study, but the magnitude of hotspot emissions was greatest in the months of May, June, July and August (Figs. 2.1-2.6). The relative contribution of the hotspots (compared to the background) was highly variable by date and was poorly correlated to the magnitude of background emissions. In addition, there was not a clear relationship of hotspot occurrence, or of relative contribution, with time since fertilizer application (Fig. 2.7).

Table 2.2 summarizes the occurrence of hotspots and their contribution to emissions. Greater numbers of hotspots were observed in the fertilized treatments, and the proportion of chambers with at least one hotspot was also higher in the fertilized treatments. Hotspot occurrence increased in all treatments in 2014 compared to the previous year (Table 2.2), but this may be due to the different observation schedule for the two years, which in 2014 was tailored to focus on post-fertilization events. It is striking that although the frequency of hotspots and

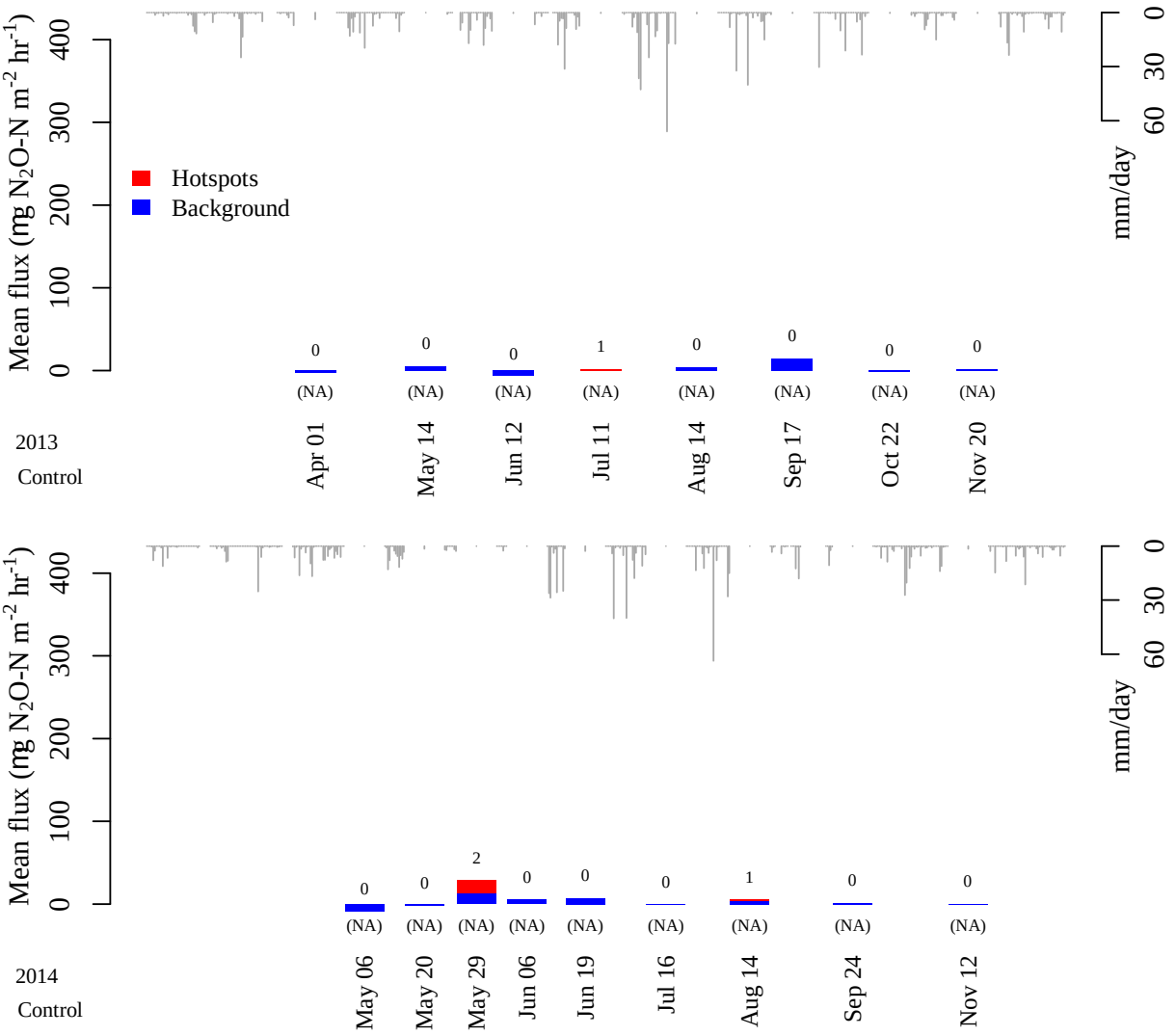

Figure 2.1: Barplots showing the contribution of hotspots to mean N_2O emissions in the Control treatment in years 2013 and 2014. Overall bar height indicates the magnitude of the mean emission rate, red and blue portions of each bar show the contribution of hotspots and background respectively. Numerals above each bar indicate the number of hotspots observed in the treatment on that date. Below each bar, the number of days elapsed since fertilizer application is indicated in parentheses ("NA" describes unfertilized treatments). Precipitation is also presented in the upper portion of each pane.

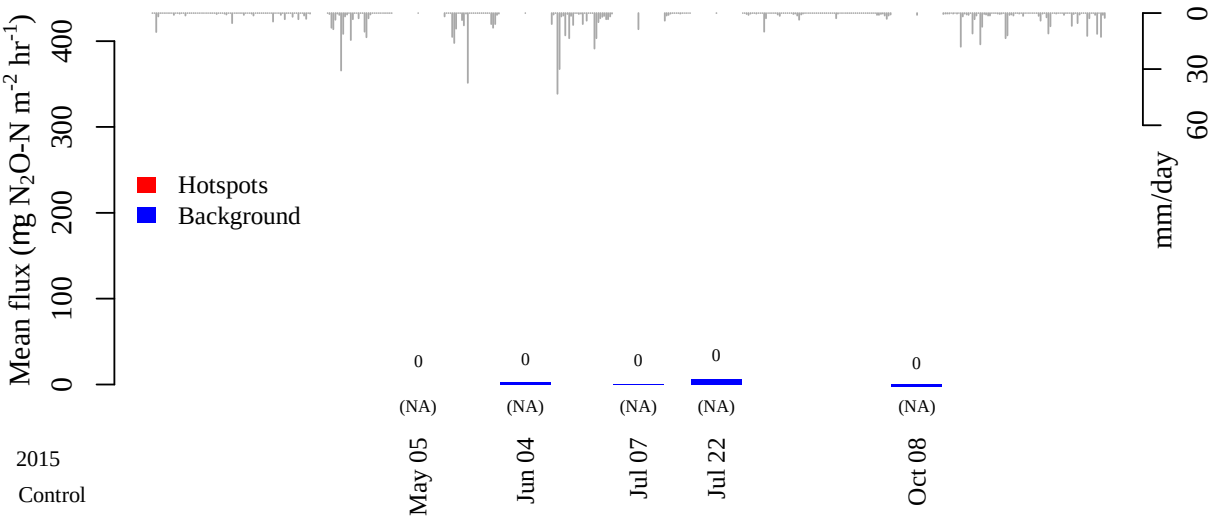

Figure 2.2: Barplots showing the contribution of hotspots to mean N_2O emissions in the Control treatment in year 2015. Overall bar height indicates the magnitude of the mean emission rate, red and blue portions of each bar show the contribution of hotspots and background respectively. Numerals above each bar indicate the number of hotspots observed in the treatment on that date. Below each bar, the number of days elapsed since fertilizer application is indicated in parentheses ("NA" describes unfertilized treatments). Precipitation is also presented in the upper portion of each pane.

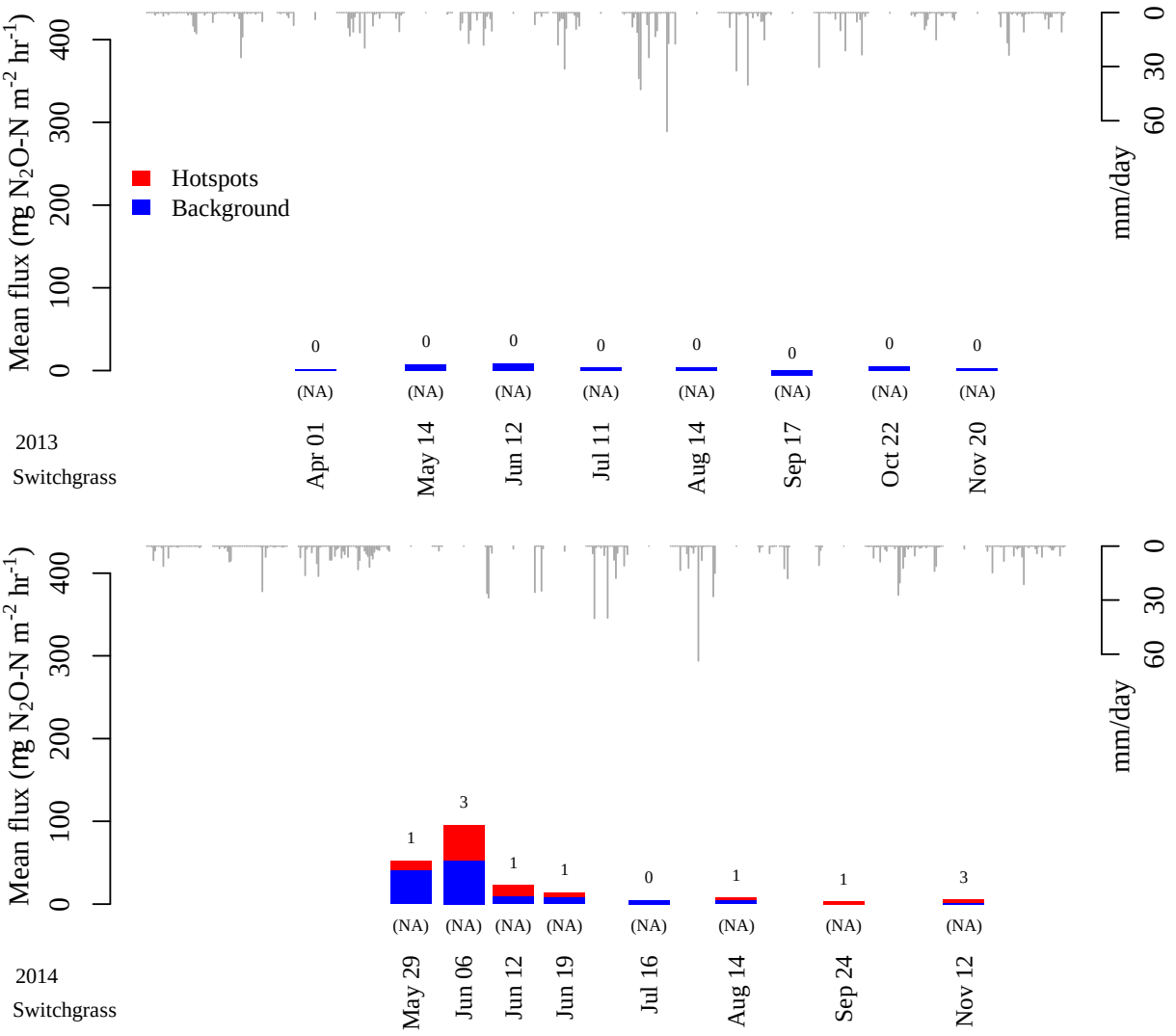

Figure 2.3: Barplots showing the contribution of hotspots to mean N_2O emissions in the unfertilized Switchgrass treatment in years 2013 and 2014. Overall bar height indicates the magnitude of the mean emission rate, red and blue portions of each bar show the contribution of hotspots and background respectively. Numerals above each bar indicate the number of hotspots observed in the treatment on that date. Below each bar, the number of days elapsed since fertilizer application is indicated in parentheses ("NA" describes unfertilized treatments). Precipitation is also presented in the upper portion of each pane.

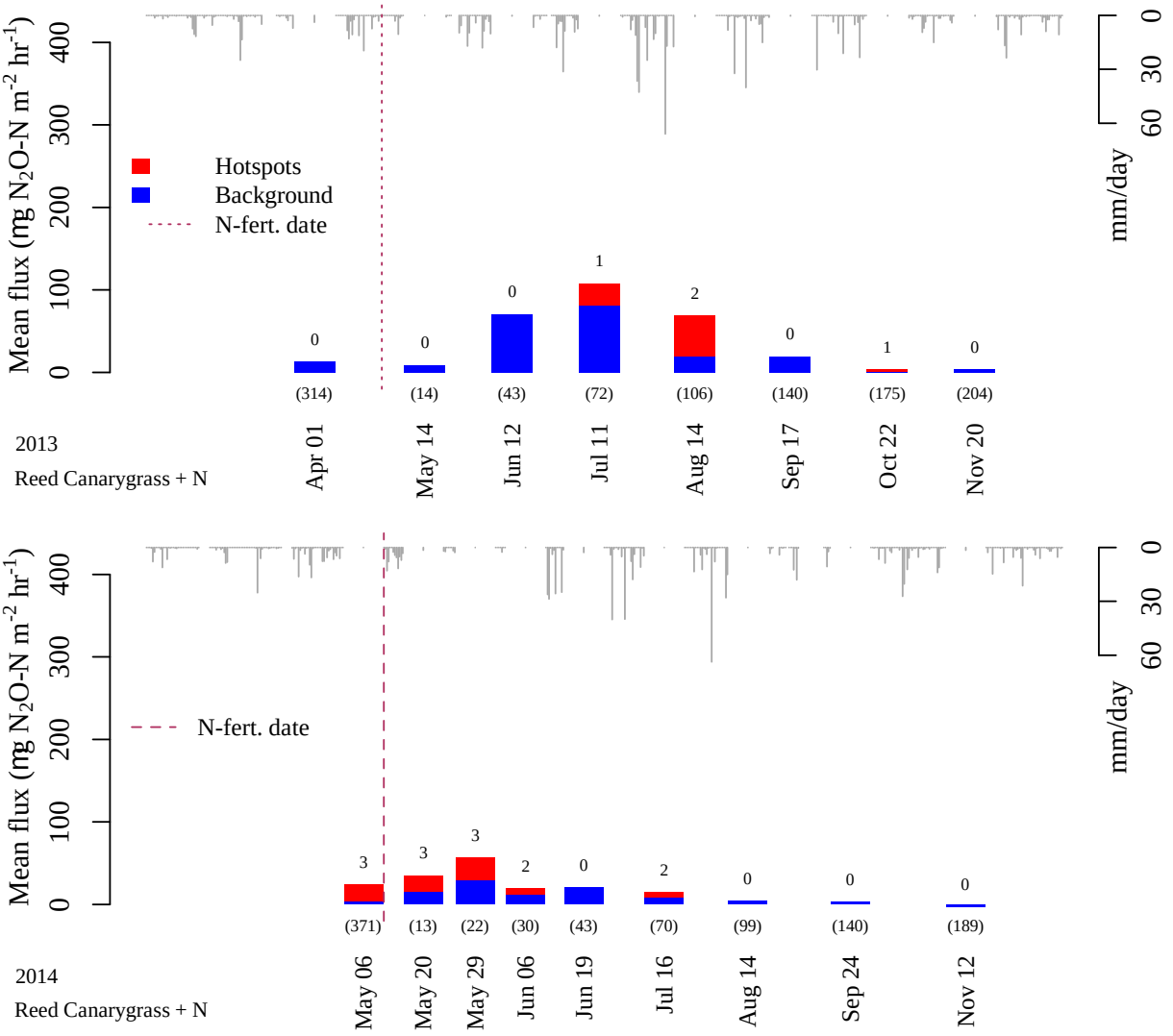

Figure 2.4: Barplots showing the contribution of hotspots to mean N_2O emissions in the Reed Canarygrass + N treatment in years 2013 and 2014. Overall bar height indicates the magnitude of the mean emission rate, red and blue portions of each bar show the contribution of hotspots and background respectively. Numerals above each bar indicate the number of hotspots observed in the treatment on that date. Below each bar, the number of days elapsed since fertilizer application is indicated in parentheses. Maroon dotted and dashed lines indicate dates of fertilizer application. Precipitation is also presented in the upper portion of each pane.

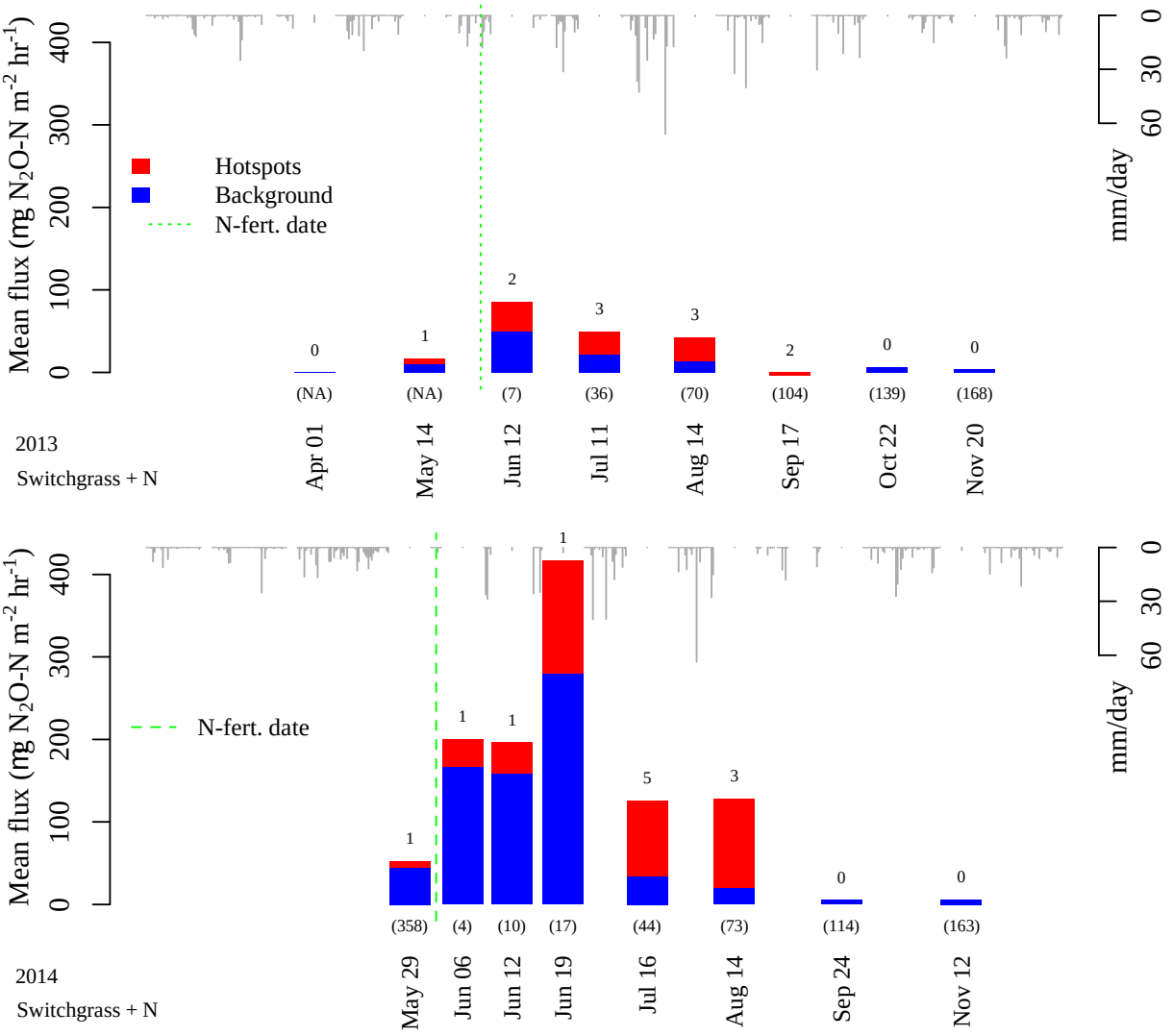

Figure 2.5: Barplots showing the contribution of hotspots to mean N_2O emissions in the Switchgrass + N treatment in years 2013 and 2014. Overall bar height indicates the magnitude of the mean emission rate, red and blue portions of each bar show the contribution of hotspots and background respectively. Numerals above each bar indicate the number of hotspots observed in the treatment on that date. Below each bar, the number of days elapsed since fertilizer application is indicated in parentheses. Green dotted and dashed lines indicate dates of fertilizer application. Precipitation is also presented in the upper portion of each pane.

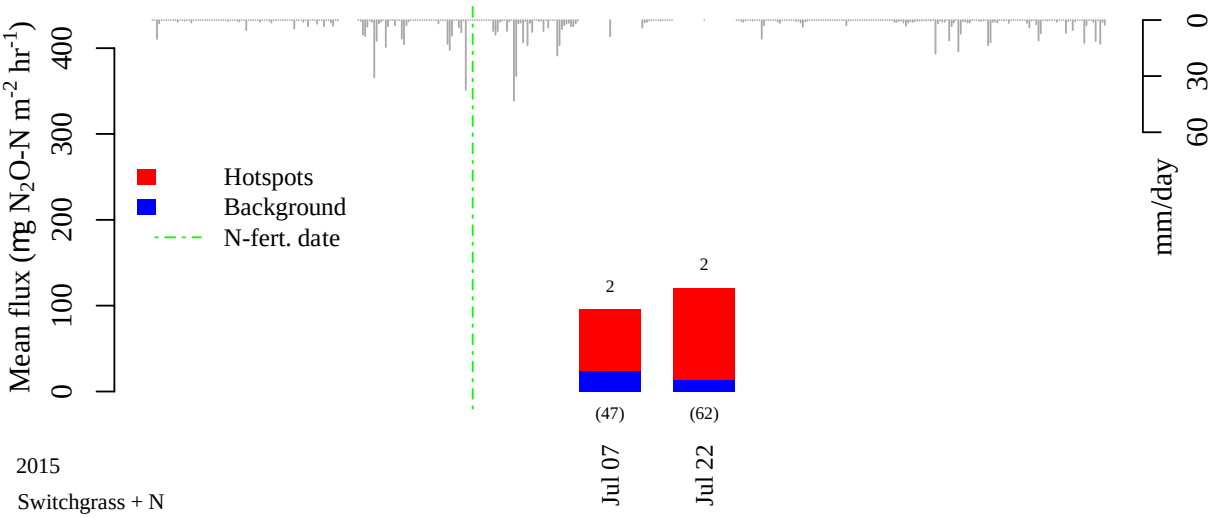

Figure 2.6: Barplots showing the contribution of hotspots to mean N_2O emissions in the Switchgrass + N treatment in year 2015. Overall bar height indicates the magnitude of the mean emission rate, red and blue portions of each bar show the contribution of hotspots and background respectively. Numerals above each bar indicate the number of hotspots observed in the treatment on that date. Below each bar, the number of days elapsed since fertilizer application is indicated in parentheses. Green dotted and dashed lines indicate dates of fertilizer application. Precipitation is also presented in the upper portion of each pane.

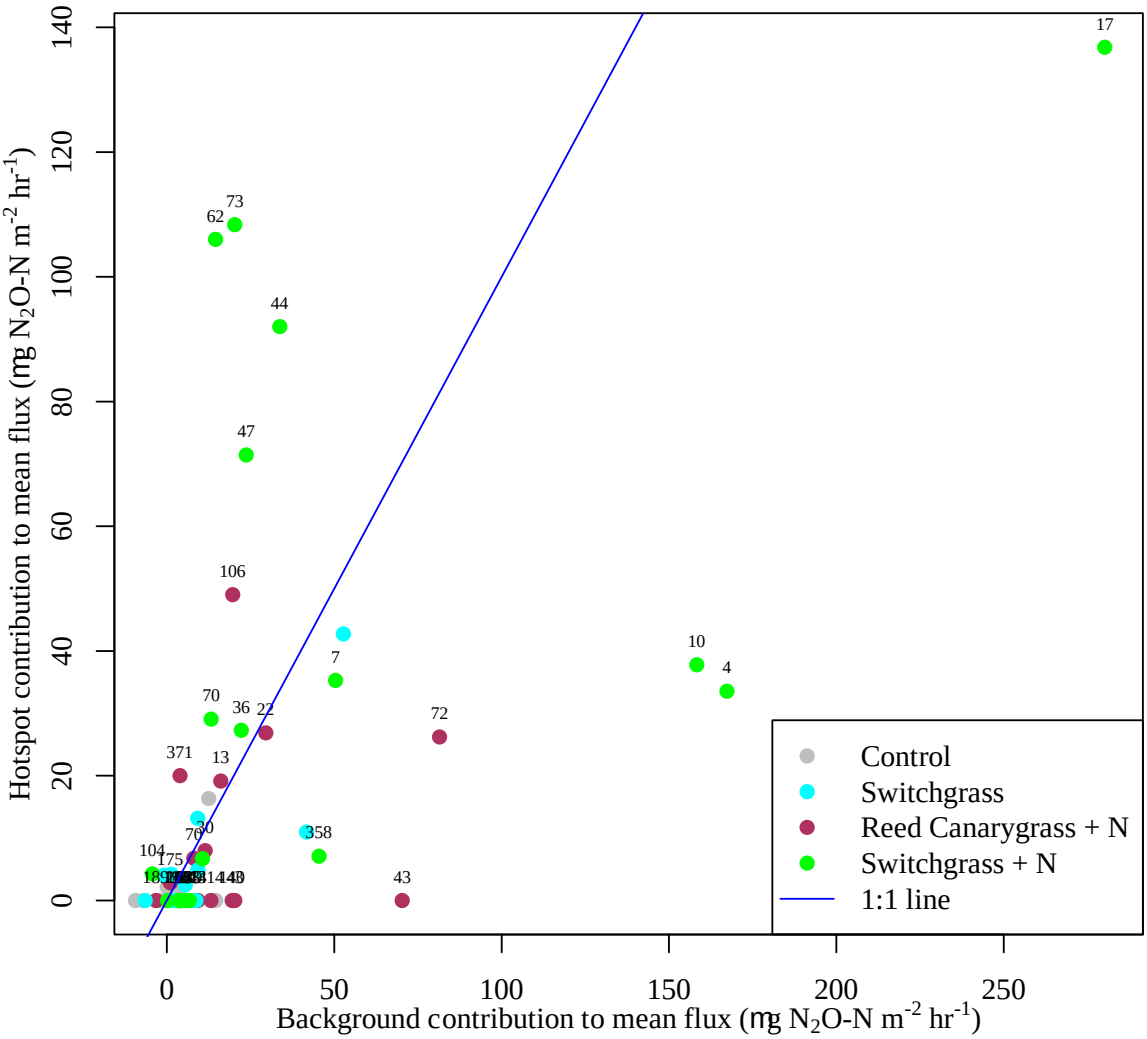

Figure 2.7: Plot showing irregular relationship between the magnitude of background N_2O emissions (X axis) and hotspot emissions (Y axis). Numerals above each plotted point indicate number of days elapsed since the last fertilizer application. The blue 1:1 line divides instances where the total emissions were dominated by hotspots from instances where emissions were dominated by the background.

Table 2.2: N_2O hotspot occurrence and contribution to total emission for each treatment during years 2013 and 2014. (Additionally, in year 2015, 4 hotspots were observed in the Switchgrass + N treatment, the other treatments were not monitored in 2015. Results from 2015 are not included in the table.)

Treatment	No. of hotspots (2013, 2014)	No. of hotspots (2013)	No. of hotspots (2014)	No. of chambers monitored	% of chambers w/ hotspots	% of total emissions from hotspots
Control	4	1	3	30	13% (4)	38.1%
Switchgrass	11	0	11	30	23% (7)	35.4%
Reed canarygrass + N	17	4	13	30	40% (12)	34.3%
Switchgrass + N	23	11	12	30	43% (13)	39.1%

number of unique chambers exhibiting hotspot activity varied widely between treatments, the contribution of hotspots was between 34.3% and 39.1% of the total emissions for all treatments (Table 2.2). Across all treatments in years 2013 and 2014 combined, only 2.9% of all chamber observations were hotspots.

Precipitation, soil moisture, groundwater depth, and temperature trends

Rainfall was fairly consistent and frequent during the study period and there was not a clear relationship between rainfall and hotspot occurrence or magnitude (Figs. 2.1-2.6); significant hotspot activity occurred in fertilized treatments shortly after rainfall (Fig. 2.5: August 14 2013 and August 14 2014) and during dry periods (Fig. 2.6: July 22 2015. Fig. 2.4: June 6 2014), and at times was also absent following precipitation events (Fig. 2.4: June 19 2014).

Soil moisture was fairly stable during the study period (Figs. 2.8,2.9), with a notable decrease in soil moisture in late spring (i.e. May 14 2013 and June 6 2014). Mean soil moisture in years 2013 and 2014 was 59.8% and 59.9% WFPS respectively. The control was generally wetter than the other treatments (Fig. 2.8). The average groundwater depth across all observed subplots varied from 10 cm to 90 cm, and followed similar seasonal trends in years 2013 and 2014 (Fig. 2.8).

In all years and all treatments, soil temperature followed a clear annual trend; warmer temperatures in summer months with cooler temperatures in spring and fall (Figs. 2.10,2.11). Peak mean soil temperature was 25.0, 27.6, and 27.7 °C on July 11 2013, June 19 2014, and July 22 2015 respectively. The Reed Canarygrass + N treatment was consistently cooler than the other treatments (Fig. 2.10) which could be attributed to more complete canopy closure due to rapid establishment and growth.

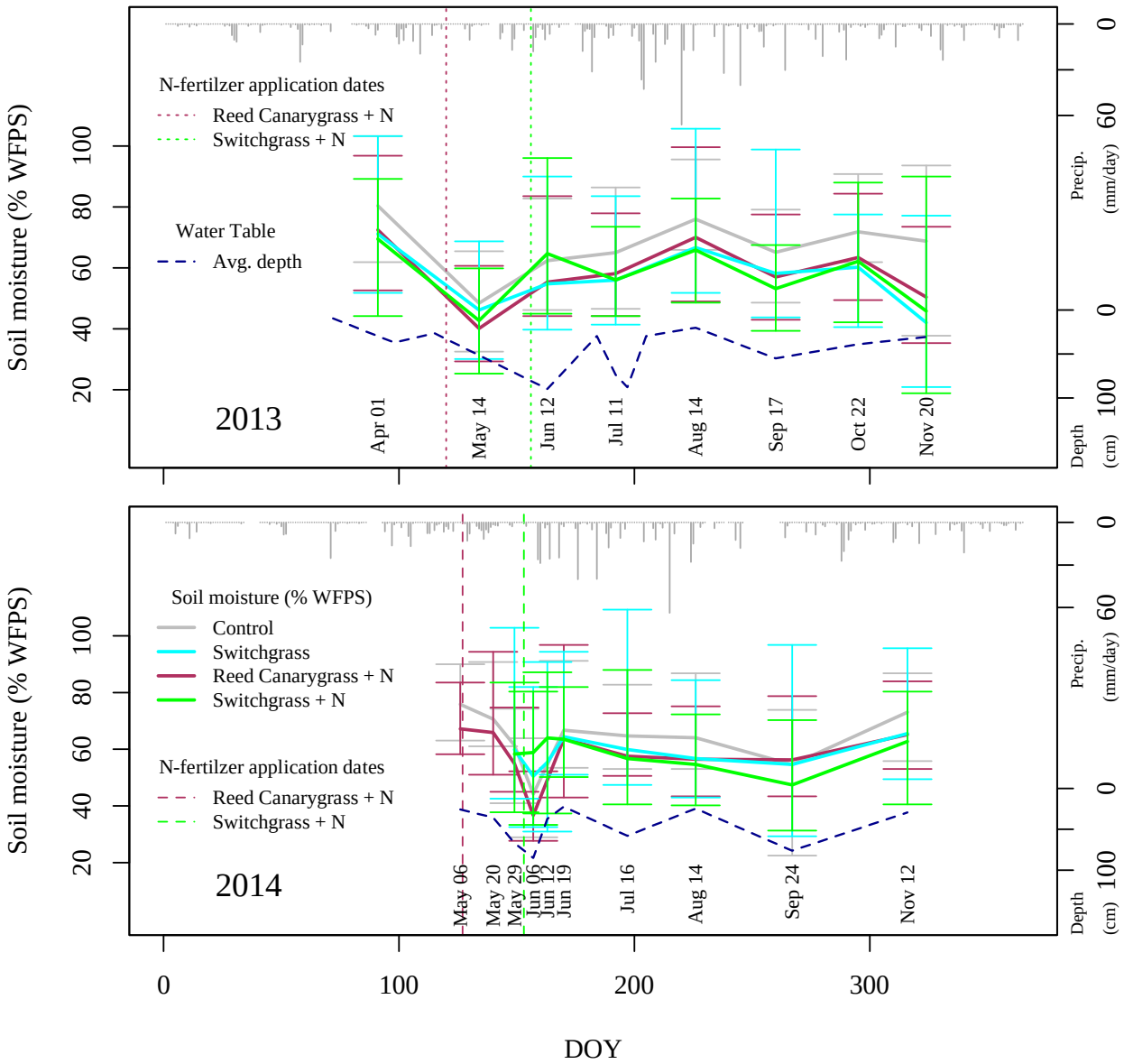

Figure 2.8: Soil moisture (% WFPS) for each treatment, precipitation (mm/day), and average groundwater depth (cm) at the research site for years 2013 and 2014. Colored solid lines indicate soil moisture with whiskers to convey the range of variation in soil moisture for a treatment on a given date. Grey bars represent precipitation and dashed blue lines indicate groundwater depth below the soil surface. Maroon dotted and dashed lines show dates of fertilizer application in the Reed Canarygrass + N treatment. Green dotted and dashed lines show dates of fertilizer application in the Switchgrass + N treatment.

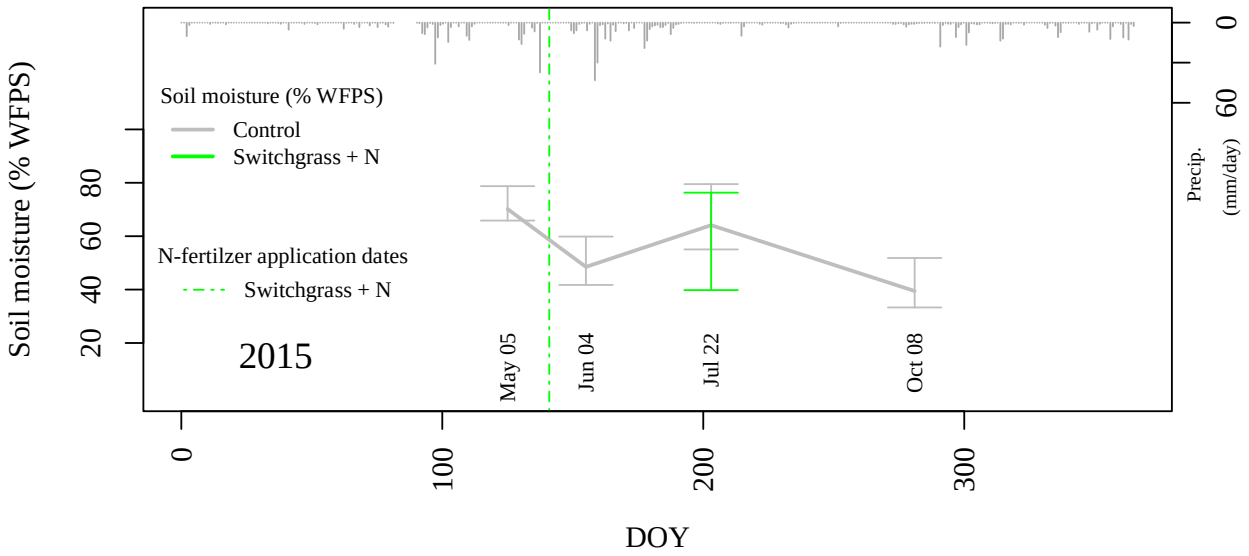

Figure 2.9: Soil moisture (% WFPS) for the Control and Switchgrass + N treatments, and precipitation at the research site for year 2015. Whiskers indicate the range of variation in soil moisture for a treatment on a given date. The green dot-dash line indicates dates of fertilizer application in the Switchgrass + N treatment.

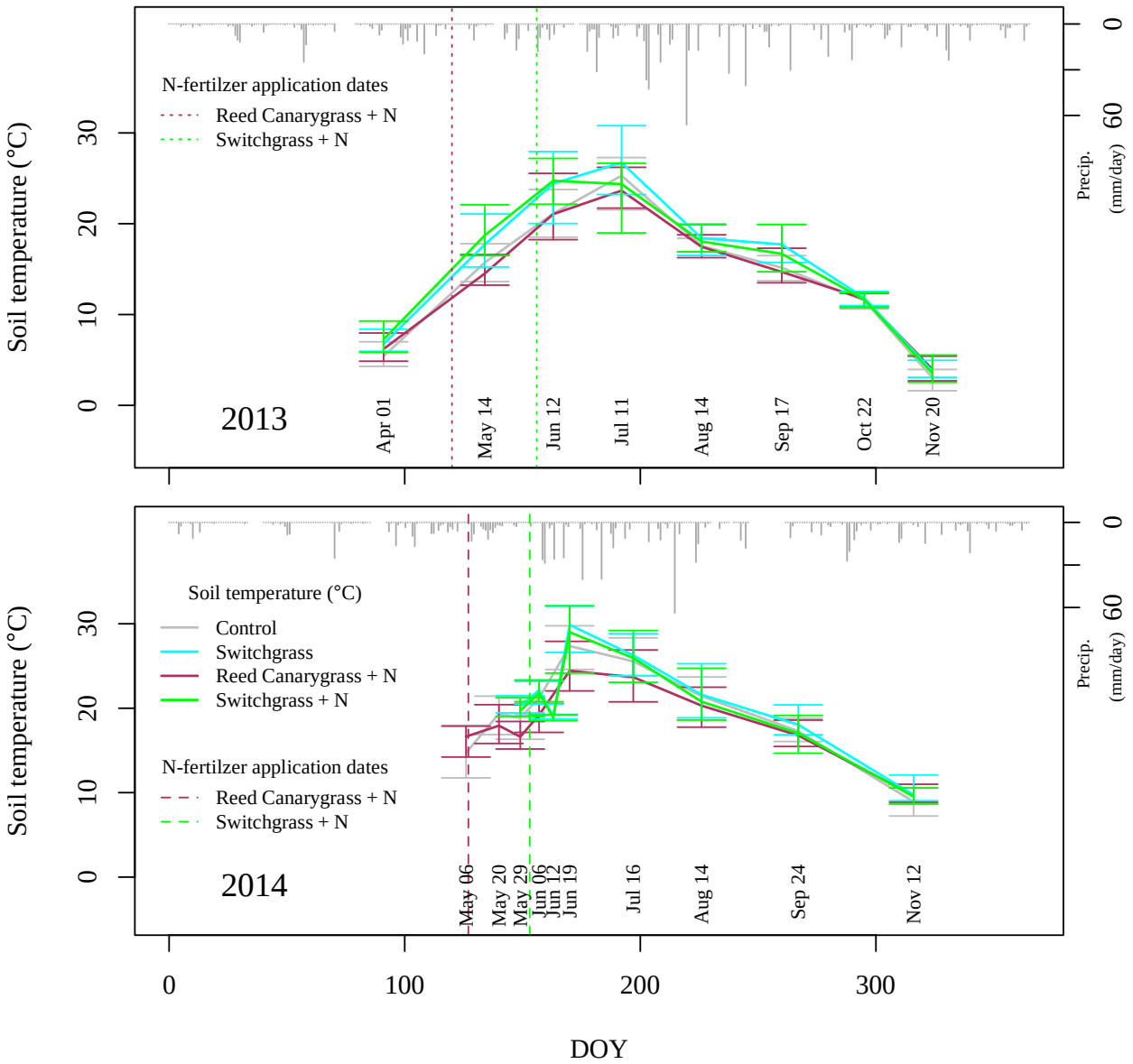

Figure 2.10: Soil temperature (°C) for each treatment, and precipitation at the research site for years 2013 and 2014. Whiskers indicate the range of variation in soil temperature for a treatment on a given date. Maroon dotted and dashed lines indicate dates of fertilizer application in the Reed Canarygrass + N treatment. Green dotted and dashed lines indicate dates of fertilizer application in the Switchgrass + N treatment.

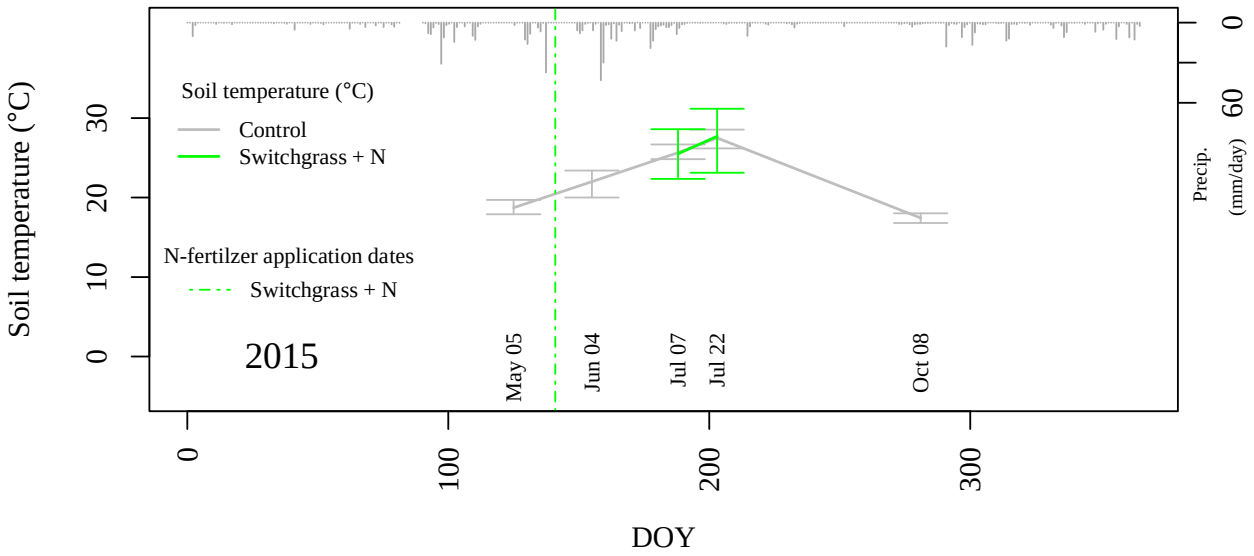

Figure 2.11: Soil temperature (°C) for the Control and Switchgrass + N treatments, and precipitation at the research site for year 2015. Whiskers indicate the range of variation in soil temperature for a treatment on a given date. The green dot-dash line indicates dates of fertilizer application in the Switchgrass + N treatment.

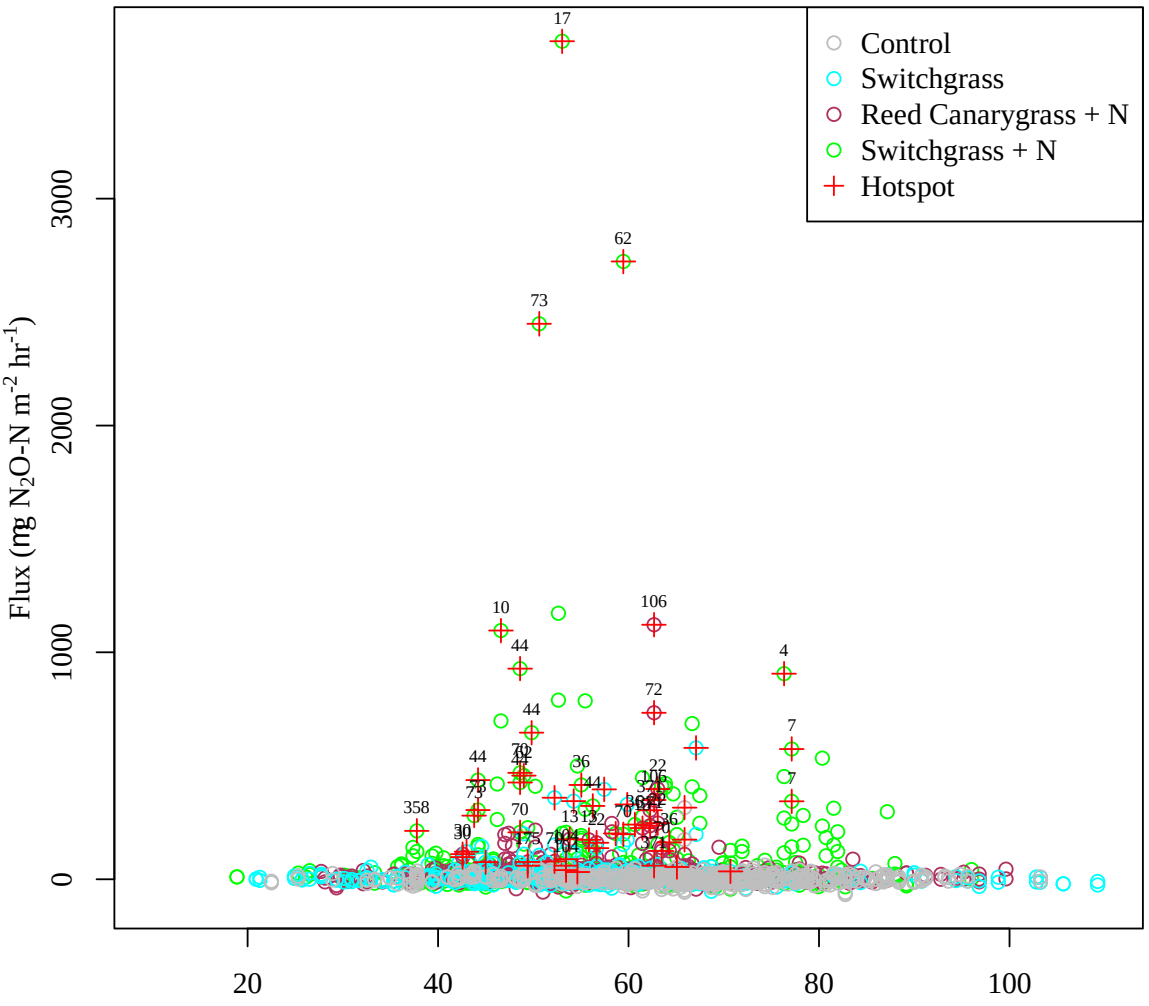

Numerals above points indicate days elapsed since N-fertilizer application.

Figure 2.12: The relationship between chamber N_2O flux and soil moisture (% WFPS) is plotted above for each treatment in years 2013-2015. Chamber observations that were statistically identified as hotspots are marked with a red cross. Numerals above points indicate days elapsed since fertilizer application, if applicable.

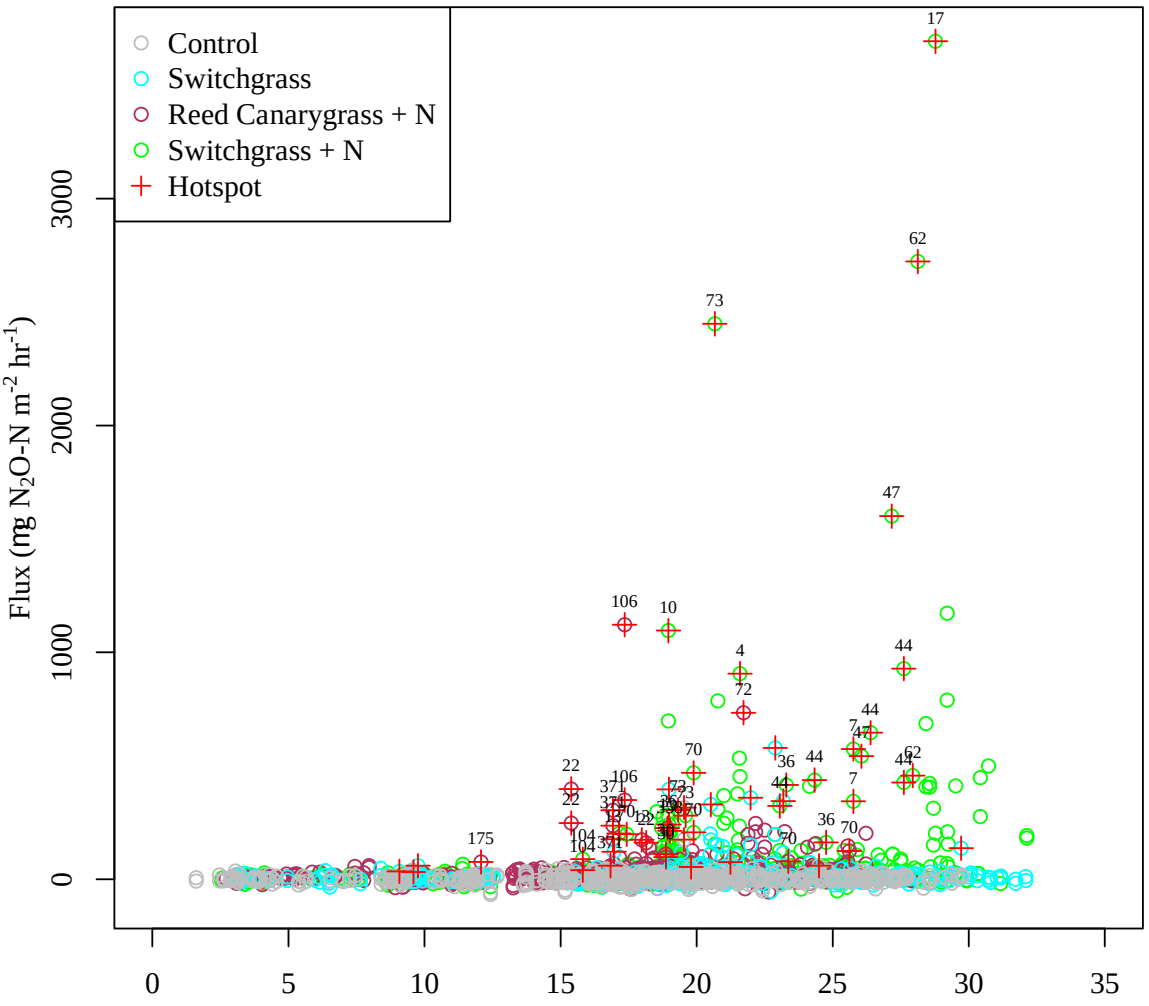

Numerals above points indicate days elapsed since N-fertilizer application.

Figure 2.13: The relationship between chamber N_2O flux and soil temperature (°C) is plotted above for each treatment in years 2013-2015. Chamber observations that were statistically identified as hotspots are marked with a red cross. Numerals above points indicate days elapsed since fertilizer application, if applicable.

Soil conditions at hotspots

The occurrence and magnitude of hotspot emission showed a strong dependency on localized soil moisture conditions (Fig. 2.12). In this study, the hotspot of largest instantaneous flux was observed under conditions of 53.0% WFPS in the Switchgrass + N treatment on June 19 2014. About this maximum, the magnitude of hotspot emissions appears to decrease symmetrically in either direction, following a more-or-less bell (or Gaussian)-shaped distribution with respect to soil moisture (Fig. 2.12). Overall, hotspots occurred only within the range of soil moisture between 37.8% and 77.1% WFPS (Fig. 2.12). Localized soil temperature also had a strong effect on hotspot occurrence and magnitude (Fig. 2.13). Hotspots were observed only at soil temperatures above 9.1 °C and the hotspot of greatest flux magnitude occurred at 28.8 °C, near the upper limit of soil temperature observations (Fig. 2.13). In contrast to soil moisture (Fig. 2.12), the distribution of hotspot magnitude around this maximum does not appear symmetric (Fig. 2.13). Excluding four low-magnitude, late season hotspots that occurred late in the season on November 12 2014 and October 22 2013, all hotspot activity was observed at soil temperatures greater than 15.0 °C (Fig. 2.13). Generally, we found that soils supporting hotspot activity were at moisture levels between about 40% and 80% WFPS, and temperatures above 15 °C (Fig. 2.14).

In the driest and wettest subplots (as determined from the ranking of long-term soil moisture at each subplot), we examined the effect of soil moisture dynamics on hotspot occurrence by plotting flux observations as a function of departure from the average soil moisture for the subplot. Figure 2.15 shows hotspot occurrence in the wettest and driest quintiles for the Reed canarygrass + N and Switchgrass + N treatments. In the Reed canarygrass + N treatment, hotspots occurred in the driest areas only when they were wetter than usual, while in

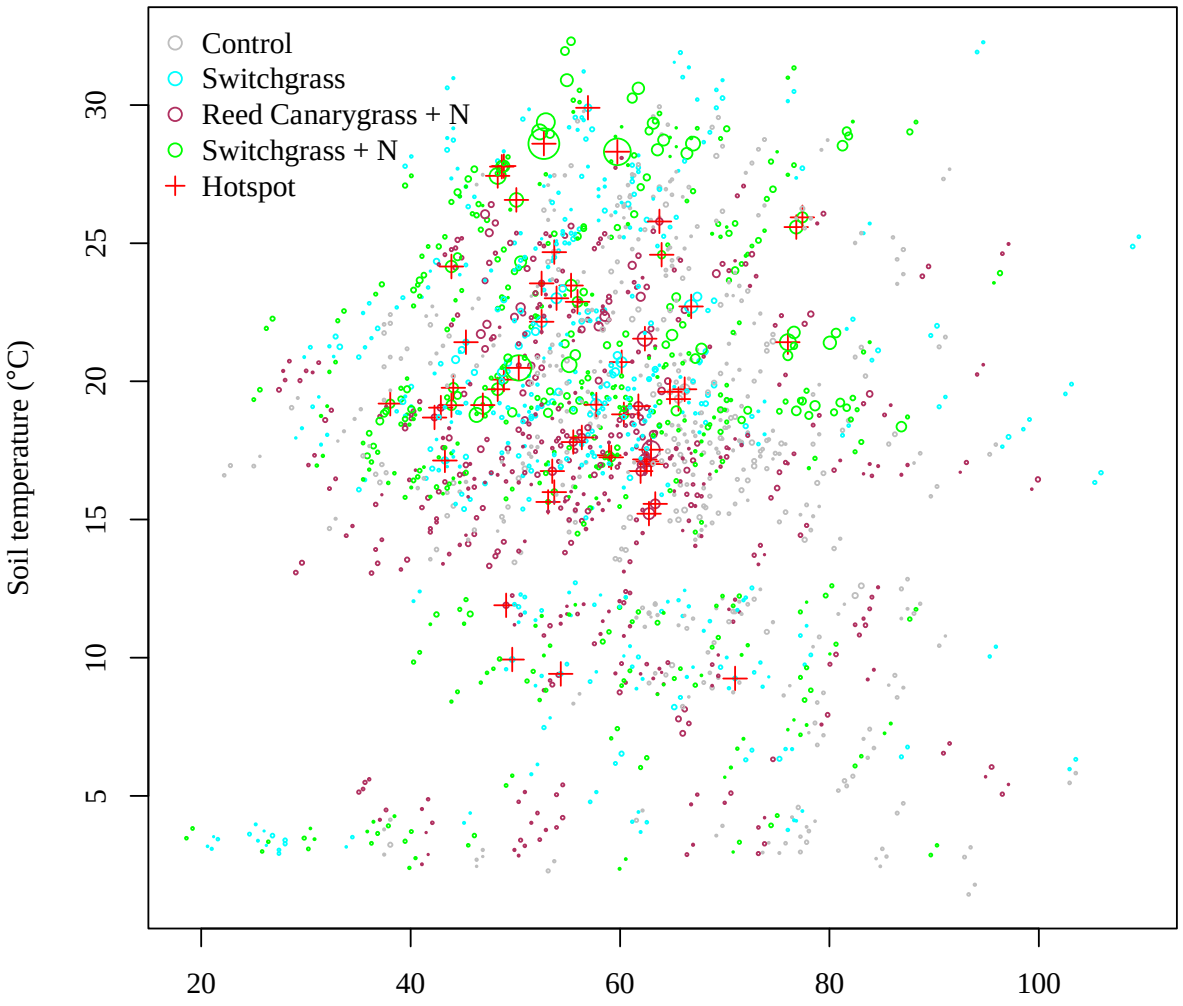

Figure 2.14: Plot showing the nexus of soil moisture (% WFPS) and soil temperature (°C) where increased N_2O emissions occur for each treatment for years 2013-2015. Statistically identified hotspot observations are marked with a red cross. The size of circular points indicates flux magnitude. X and Y coordinates were perturbed by a fraction of a unit to separate coincident points.

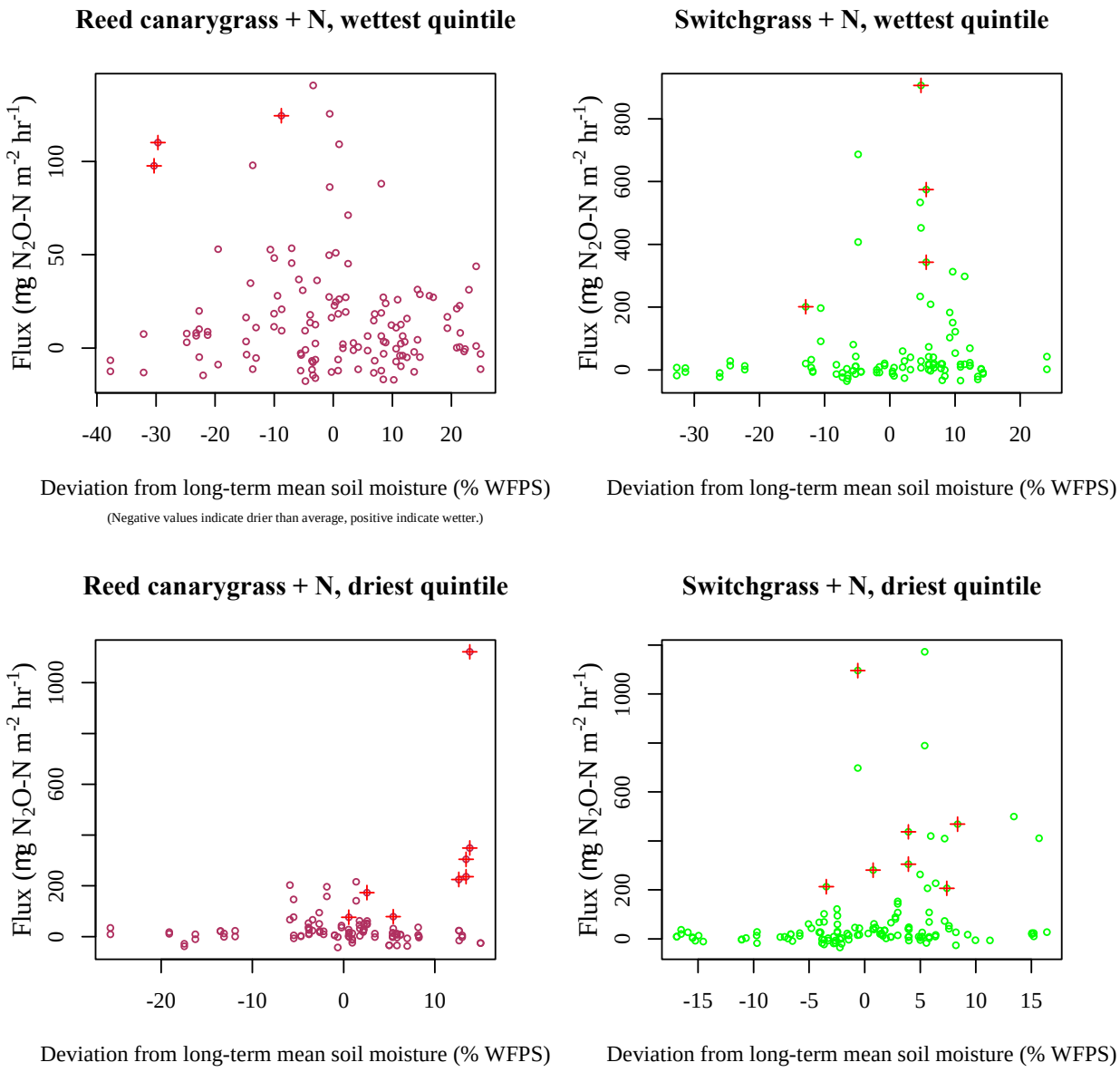

Figure 2.15: Plots showing magnitude of N_2O fluxes and hotspots in relation to deviation from long-term mean soil moisture at the chamber location. Negative deviation values indicate that conditions were drier than usual, and positive deviation values indicate that conditions were wetter than usual. Wettest quintiles are shown in upper panes, driest quintiles in lower panes, with Reed canarygrass + N on the left and Switchgrass + N on the right. Circular points indicate background flux observations, red crosses indicate hotspots.

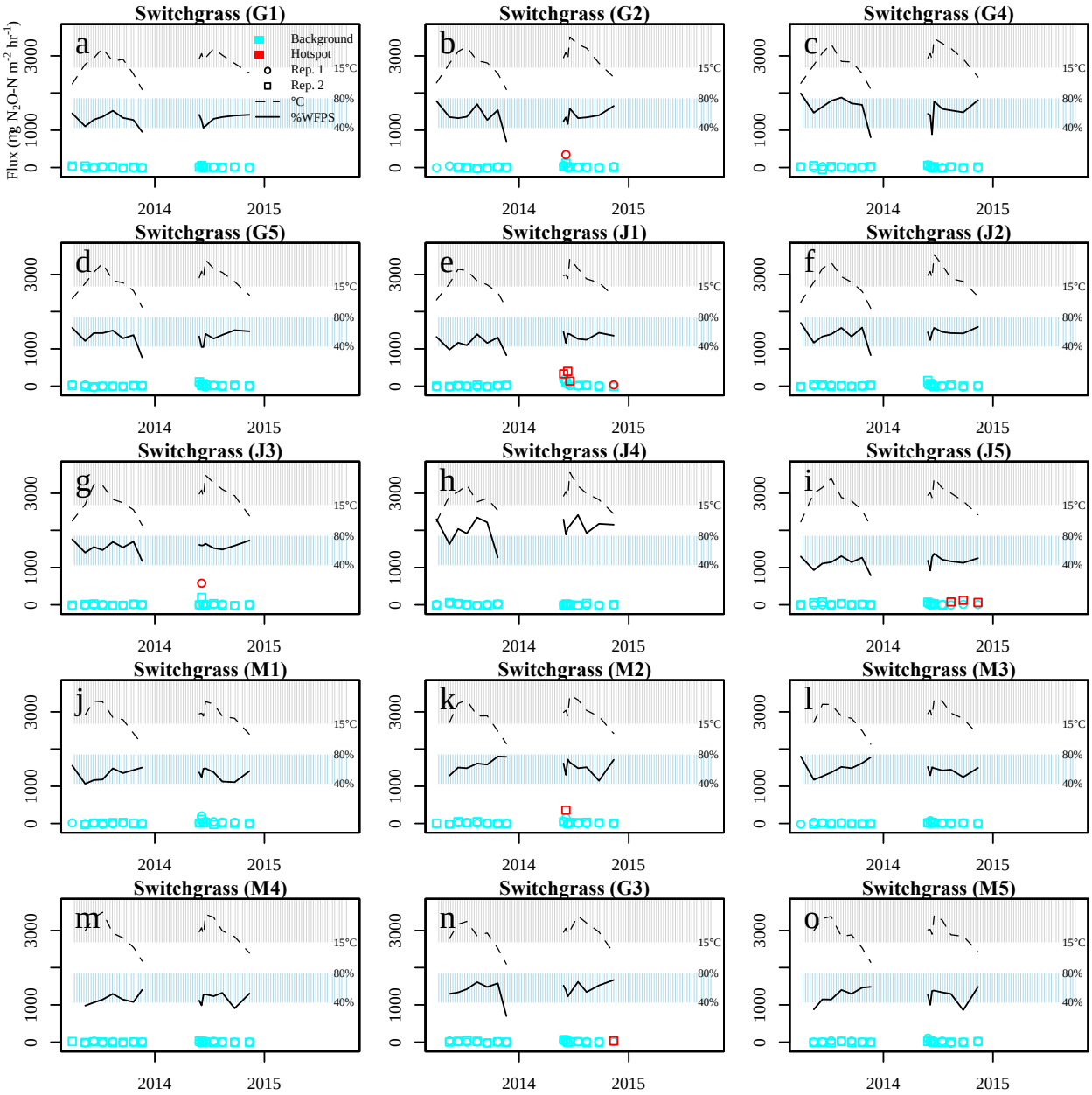

Figure 2.16: Time series of N_2O flux observations at individual static chambers in the unfertilized Switchgrass treatment for years 2013-2014, organized by subplot. Instances of hotspots are indicated in red. Dashed black lines indicate local soil temperature and grey shading indicates temperatures greater that 15°C. Solid black lines indicate local soil moisture and blue shading indicates WFPS between 40% and 80%.

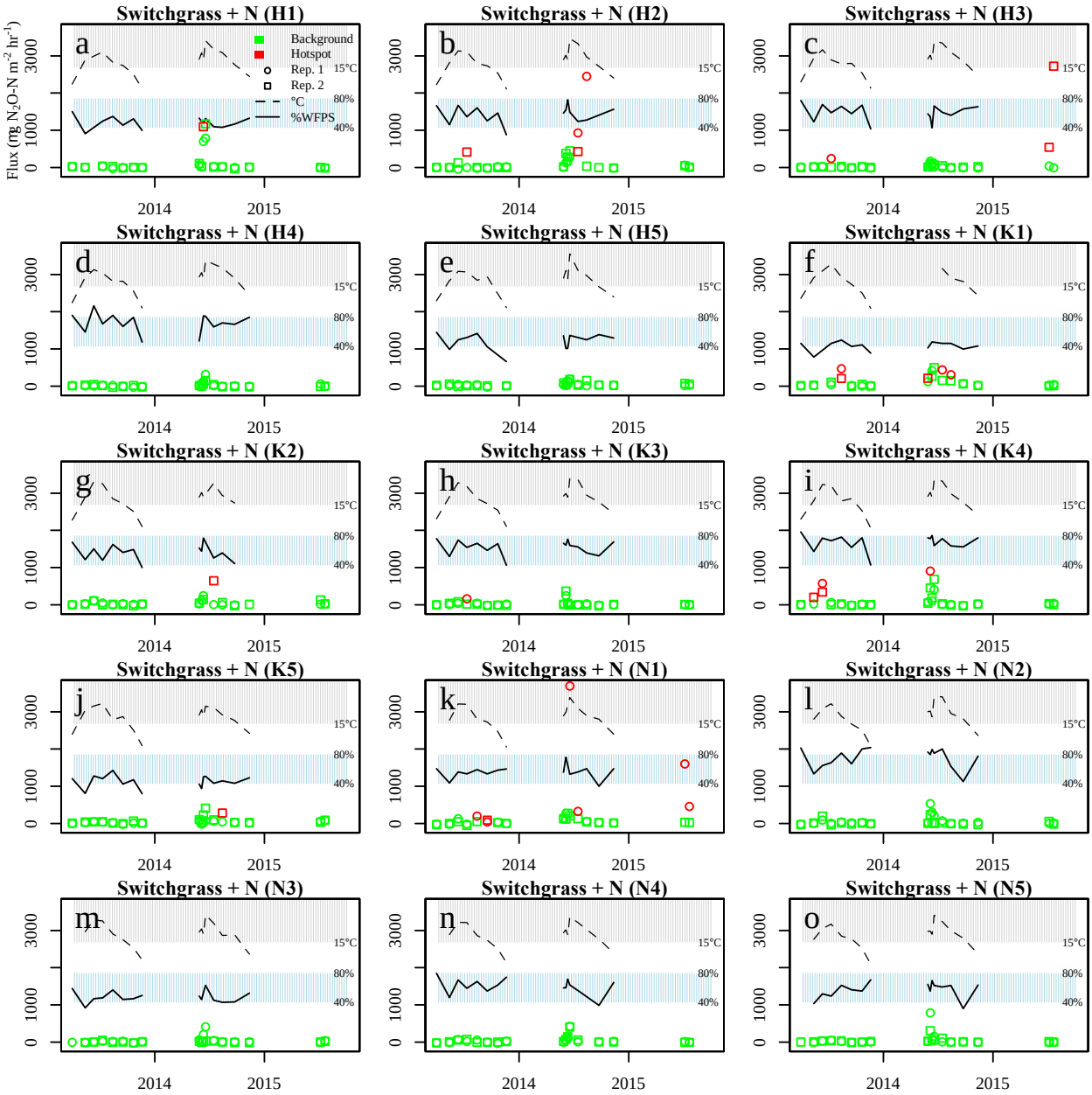

Figure 2.17: Time series of N_2O flux observations at individual static chambers in the Switchgrass + N treatment for years 2013-2015, organized by subplot. Instances of hotspots are indicated in red. Dashed black lines indicate local soil temperature and grey shading indicates temperatures greater that 15°C. Solid black lines indicate local soil moisture and blue shading indicates WFPS between 40% and 80%.

the wet areas in the same treatment, hotspots were observed only when conditions were drier than usual. However, this same trend was not as apparent in the Switchgrass + N treatment, and overall, hotspots were observed under conditions that were both drier and wetter than usual.

Hotspot clusters in space and time

All hotspot occurrences were organized by treatment and aggregated by subplot (Figs. 2.16-2.17, Figs. S2.1,S2.2) and by date (Figs. 2.1-2.6), and the most extreme clusters were identified in each case. The Switchgrass + N treatment produced the most hotspots in this study and provided the best opportunity to test statistical hypotheses with regard to hotspot clustering.

In the Switchgrass + N treatment, the chamber with the greatest number of hotspot observations during the study period (called "N1-1": Fig. 2.17k) exhibited 6 hotspots in 18 observations. We used the binomial distribution (see appendix B: Text S2.1) to show that if the null hypothesis (that hotspots occur randomly in space) is correct, the chance in this study of observing one-or-more chambers with 6-or-more hotspots is approximately 0.006 (see appendix B: Table S2.1, Table S2.2). In addition to being a frequently active hotspot, this chamber also produced the single highest magnitude flux observed in this entire study (3694.0 μg N_2O-N m^{-2} hr^{-1}) (Fig. 2.17k). In the unfertilized Switchgrass treatment, clustering was observed at two chambers that each yielded three hotspots (called "J1-2" and "J5-2", Fig. 2.16e, 2.16i) in 16 observations. In this case, if the null hypothesis is correct, the chance of observing 2-or-more chambers each with 3-or-more hotspots is 0.014 (see appendix B: Table S2.3, Table S2.4). These results show that in the Switchgrass and Switchgrass + N treatments, there is statistical evidence to reject the null hypothesis and accept the alternative hypothesis that hotspots do not occur randomly in space, but tend to be more frequent at some areas of the soil surface. (In the Control

and Reed Canarygrass + N treatments there was not sufficient statistical evidence to reject the null hypothesis).

In the Switchgrass + N treatment, the observation date with the greatest number of hotspots was July 16 2014 with 5 hotspots (Fig. 2.5). The binomial distribution was used to test the null hypothesis that hotspots occurred randomly in time during the study period (see appendix B: Text S2.1). The results show that the chance in this study of one or more observation dates yielding 5 or more hotspots is approximately 0.28 if the null hypothesis is correct (see appendix B: Table S2.5, Table S2.6). It follows that there is insufficient statistical evidence to reject this null hypothesis, as this cluster of 5 hotspots on a single date can be explained by chance.

Discussion

Hotspot significance and effect of treatment

Hotspots accounted for only 2.9% of flux observations yet contributed between 34.3% and 39.1% of the total emissions in this study (Table 2.2). A report by Van den Heuvel, et al. (2009) indicates that in a study of a riparian buffer zone in the Eastern Netherlands using chambers each covering an area 0.31m^2, hotspots representing 4% of the observation area produced 33% of summer N_2O emissions, proportions very similar to our results despite our use of somewhat smaller chambers (0.07 m^2). Both studies show that hotspots contribute greatly and disproportionately to overall emissions despite their relatively limited occurrence, and incorporating the N_2O hotspot phenomenon in models and inventories is critical in order to produce accurate estimates of N_2O emissions from these landscapes.

In the control treatment where hotspot occurrence was the lowest, hotspots still played a large role in determining total emissions (Table 2.2). The Switchgrass + N treatment had the

most frequent and highest magnitude hotspots (Table 2.2 and Figs. 2.5,2.6), and hotspots in this cropping system may have a greater impact on emission of N_2O, and present more effective mitigation opportunities. It seems logical that nitrogen fertilizer application in both the Switchgrass + N and Reed Canarygrass + N treatments increased hotspot frequency (Table 2.2) compared to the control (rather than tillage or crop species), and this indicates the importance of nitrogen input as a key factor in hotspot formation. When nitrogen fertilizer was applied to the Switchgrass + N and Reed Canarygrass + N treatments, nitrogen limitation was eased and more hotspots developed.

Soil temperature and soil moisture

Soil temperature and soil moisture were seen to govern the occurrence of hotspots; hotspots were only observed within well-defined ranges of moisture and temperature (Figs. 2.12-2.14). However, within those ranges, there remained wide discrepancies between the flux rates of hotspots and the background (Figs 2.12-2.14 and Figs. 2.16,2.17, Figs. S2.1,S2.2), and this research was not able to explain the wide variation in flux rates from soils within the observed window of optimum N_2O emission conditions. Clearly there are additional factors which control the activity of hotspots that were not assessed in this study. Such factors could include spatial variation in pH, heterogeneous distribution of N-fertilizer, decomposable carbon substrate (Groffman, et al., 2009), or microbial community, and influx of dissolved nitrate (NO_3) due to subsurface or overland hydrologic flow paths (McClain, et al., 2003). However, the strong relationship between soil moisture and background and hotspot N_2O emissions (Fig. 2.12) supports the assertion that the combination of hydrologic models that accurately simulate soil moisture conditions via lateral moisture fluxes with process-based biogeochemical models could improve our ability to predict the spatial distribution of hotspots (Groffman, et al., 2009).

The contrasting shapes of the response of N_2O hotspot flux magnitude to soil temperature and to soil moisture is noteworthy. Flux rates appear to increase rather suddenly with soil temperature (Fig. 2.13), while the response to soil moisture resembles a "bell-shaped" or Gaussian curve (Fig. 2.12) that has been observed in other studies (Dunmola, et al., 2010, Rabot, et al., 2014). The non-linear limit of hotspot flux magnitude in response to soil temperature could be an indication of the effect of a thermally induced increase in soil respiration on oxygen depletion in soil pores (Ball, et al., 1997, Smith, et al., 1998), further enhancing anaerobic denitrification and thus N_2O production rates, in addition to a thermally induced increase in denitrifier kinetics. However, the effect of soil moisture status on the magnitude of N_2O hotspot flux follows a very different pattern than that of soil temperature (Figs. 2.12,2.13). Flux rates clearly decline as soil moisture levels exceed the optimum of 53.0% WFPS (Fig. 2.12). This trend could be explained by two counteracting influences of soil moisture; on one hand, anaerobicity in water filled pores (Bateman and Baggs, 2005) increases the total volume of soil pore space potentially harboring denitrification and thus production of N_2O, but it also reduces the opportunity for N_2O to escape the soil matrix (Ball, et al., 1997) and reach the atmosphere before being further reduced to N_2 (Li, 2007, Rabot, et al., 2014). High soil moisture and anoxic conditions also slows the production of NO_3 by nitrification and could diminish NO_3 availability. The optimum emission rate at 53.0% WFPS observed here (Fig. 2.12), could indicate a balance of the bidirectional influence of anaerobicity on N_2O genesis and on diffusion potential. Many process based models, the DNDC model for example, appears to incorporate a diffusion mechanism, thus capturing the combined effect of soil moisture on N_2O genesis and diffusion (Giltrap, et al., 2010).

Soil structure and texture can also influence air permeability and gas diffusivity and interact with the parameters of soil temperature and soil moisture as described above (Ball, et al., 1997). Models of terrestrial carbon and nitrogen cycling are often sensitive to soil texture (Groffman, et al., 2009). Generally, in aerobic conditions (< 60% WFPS (Bateman and Baggs, 2005, Hellebrand, et al., 2008, Yates, et al., 2006)), nitrification dominates production of N_2O. In temperate climates, the threshold of transition between dominance of nitrification and of denitrification as a N_2O source is thought to lie between 60% and 80% WFPS (Bateman and Baggs, 2005). Dunmola, et al. (2010), found that N_2O emission from a calcareous glacial till in Manitoba, Canada occurred within a limited range of 50% to 80% WFPS, and the optimum soil moisture level for N_2O emission is thought to be around 60% to 70% WFPS (Bateman and Baggs (2005) observed maximum N_2O emission at 70% WFPS on a brown earth silt loam soil). In this study however, emissions of N_2O occurred at slightly lower soil moisture conditions, in the range of about 40% to 80% WFPS with the maximum hotspot emission observed at 53.0% WFPS (Fig. 2.12). In addition, when soil moisture exceeded 53.0% WFPS, hotspot fluxes and emissions in general were lower (especially for soil moisture > 60% WFPS), as explained by the effect of soil moisture on air permeability. Thus in this study, N_2O emissions appear to occur at slightly lower WFPS (drier conditions) than reported in the literature, but do not occur below 40% WFPS where nitrification is thought to be dominant. We hypothesize that due to this pattern, nitrification was not a significant source of N_2O at the study site, and denitrification was the source of most of the N_2O emissions and N_2O hotspots. The occurrence of presumptive denitrification at low WFPS (40% to 50%) (Fig. 2.12) could be attributed to the fine texture of the silt-loam soils at the study site which are expected to have low air permeability, and could contribute to O_2 limitation in relatively dry conditions.

While rainfall events have been shown to be an important factor in the occurrence of hot-moments (Hellebrand, et al., 2008, Van Kessel, et al., 1993), the low temporal frequency of static chamber observations in this study hindered attempts to link hotspot appearance with specific precipitation events. We found some evidence that hotspots (and elevated emissions) can occur during wetting and drying periods (Fig. 2.15), and this is consistent with the findings of Rabot, et al. (2014) who observed emission peaks from soil columns during both wetting and drying events. The results shown in Fig. 2.15 also suggest that the direction of soil moisture dynamics affect N_2O emissions from wet and dry areas of the field differently.

Hot-moments have been shown to be important in determining overall emissions and these are better represented by process-based models which can accommodate high resolution meteorological conditions (Groffman, et al., 2009). The low-resolution of spatial data is considered a major impediment in process based modeling that seeks to estimate emissions of N_2O from large areas where the level of hotspot activity is unknown. A better understanding of the role that hotspot emissions play during hot-moments could be a step forward in incorporating the hotspot phenomenon in process based models that are able to simulate hot-moments.

Temporal and spatial occurrence

The results of this study provide evidence that hotspots of N_2O emission are prone to spatial clustering (i.e. Fig. 2.17k), meaning that hotspots are likely to be sustained or recur at specific locations within the field. Results show that the high frequency of hotspot recurrence at one chamber (called "N1-1") in the Switchgrass + N treatment (Fig. 2.17k) is unlikely to be due to chance (see appendix B: Text S2.1, Table S2.1, Table S2.2). In addition, in the unfertilized Switchgrass treatment, two chambers (Fig. 2.16e, 2.16i) were seen to have recurrence that was also unlikely due to chance (see appendix B: Text S2.1, Table S2.3, Table S2.4). Furthermore,

the most active chamber ("N1-1") also produced the highest magnitude flux of the entire study (Fig. 2.17k), and all three of these chambers had hotspots on consecutive sampling dates (Fig. 2.16e, 2.16i and Fig. 2.17k). These findings could support the hypothesis that the location of hotspots can be determined by preferential hydrologic flow paths that transport reactants to a consistent location (McClain, et al., 2003). Hydrologic flow paths are determined by relatively static attributes such as soil hydraulic conductivity, and depth to restrictive layer, and their consistency could explain the hotspot stationarity observed here. Additionally, studies by Corre, et al. (1996) and Van Kessel, et al. (1993) also imply temporal stability of spatial patterns of N_2O emission, explained as a function of topography. Post-hoc investigation of the most active chamber ("N1-1", Fig. 2.17k) revealed that it had been situated directly over a vigorous switchgrass tussock with a pronounced root ball, suggesting that the individual plant and/or associated exudates may have promoted increased rates of microbial activity, and high rates of N_2O emission from its root zone. Future research efforts may be able to further explain the drivers of hotspot formation by carefully investigating co-occurring anomalies in other drivers of denitrification at the precise location of chamber "N1-1".

The binomial hypothesis test to investigate the temporal occurrence of hotspots did not prove fruitful in showing that hotspot frequency varied by observation date (see appendix B: Text S2.1, Table S2.5, Table S2.6). However, there was a correlation between hotspot flux and soil temperature (Fig. 2.13), and this is also visible in Fig. 2.18 and Fig. 2.19. The seasonal trend in emissions (related to soil temperature) is especially pronounced in the fertilized plots (Fig. 2.19), but the trend is not as visible in the unfertilized plots (Fig. 2.18). Since soil temperature itself clearly followed a seasonal trend (Figs. 2.10,2.11), a seasonal effect on hotspot contribution becomes evident in Fig. 2.19. In other studies, a seasonal trend in general and hotspot N_2O

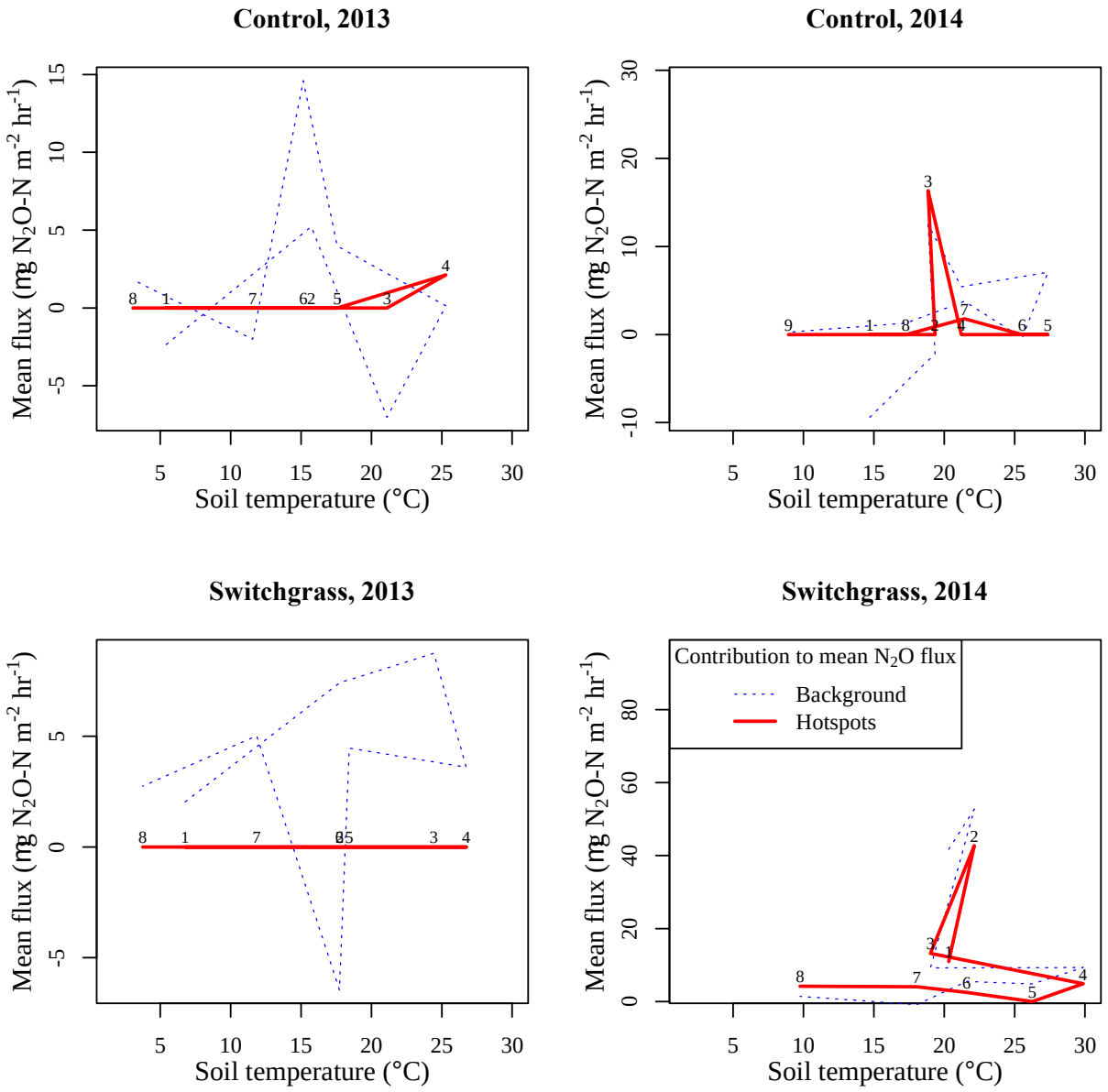

Figure 2.18: Plots showing relationship between soil temperature and hotspot contribution to mean N_2O emissions for the Control and unfertilized Switchgrass treatments in years 2013 and 2014. Solid red lines indicate hotspot contribution to the mean N_2O emissions and dotted blue lines indicates the background contribution. Black numerals just above each red line indicate sequence of observation dates as the growing season progressed in each case.

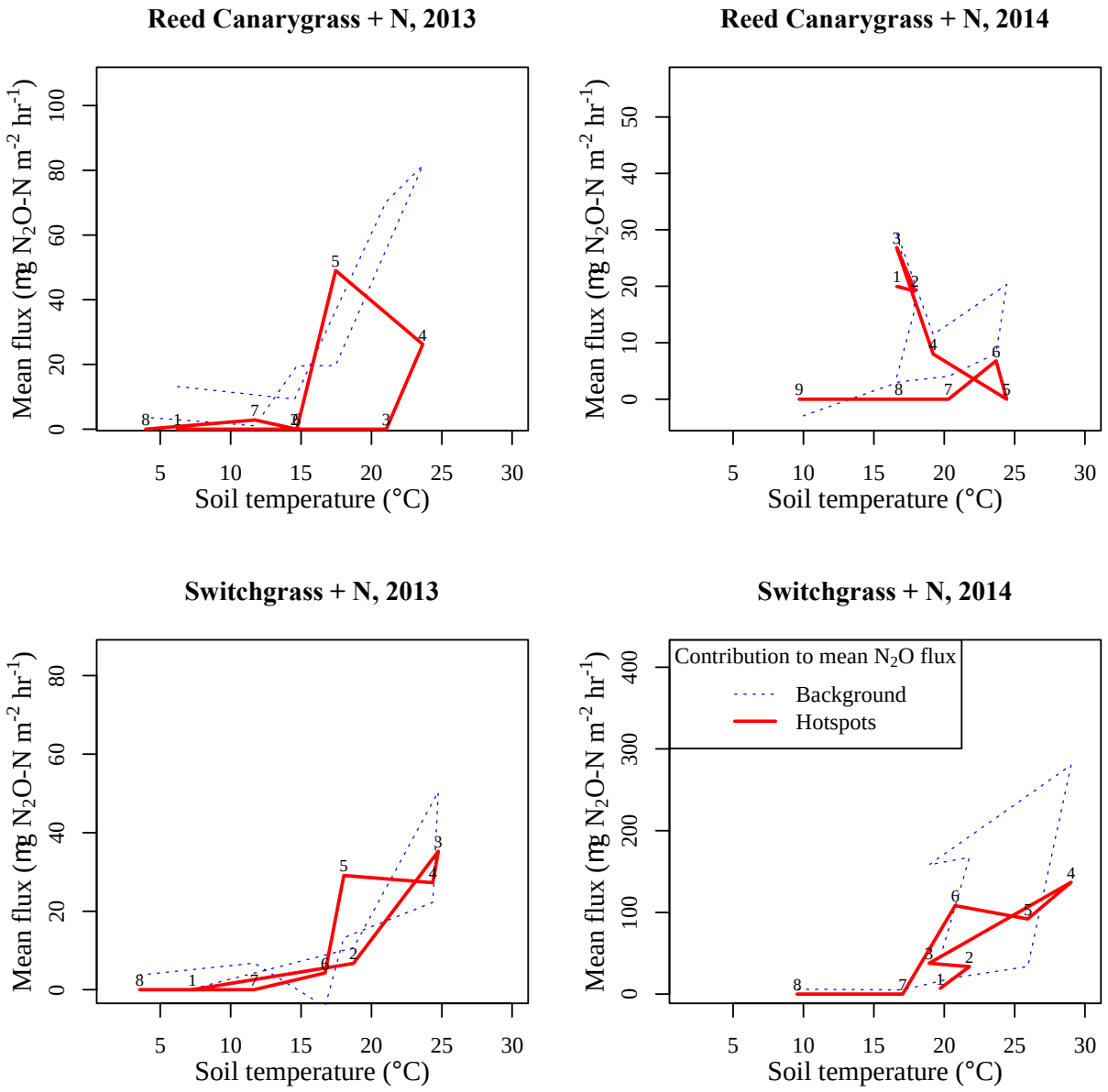

Figure 2.19: Plots showing relationship between soil temperature and hotspot contribution to mean N_2O emissions for the Reed Canarygrass + N and Switchgrass + N treatments in years 2013 and 2014. Solid red lines indicate hotspot contribution to the mean N_2O emissions and dotted blue lines indicates the background contribution. Black numerals just above each red line indicate sequence of observation dates as the growing season progressed in each case.

emissions has been reported (Brumme, et al., 1999, Christensen, et al., 1990, Corre, et al., 1996, Dunmola, et al., 2010, Hellebrand, et al., 2008), often correlating with soil temperature (However, the coincident timing of N-fertilizer application with rising temperature could be a confounding factor). In this study, we observed that as soil temperature increases to a maximum in the middle of the growing season, hotspot emissions also increase, and as soil temperature declines in late summer and autumn, hotspot emissions decrease. This pattern is clear in three out of four instances of the fertilized treatments (Fig. 2.19). In 2014, the Reed Canarygrass + N treatment followed a different pattern that somewhat obscured the trend in seasonality (Fig. 2.4, Fig. 2.19). Here, we see significant contribution from hotspots early in the season, and hotspot contribution was not sustained as soil temperature continued to rise. (This behavior is also evident in the unfertilized Switchgrass treatment in the same year, shown in Fig. 2.3). It is not clear what caused the two contrasting seasonal patterns, but perhaps nitrogen losses were substantial, or nitrogen uptake by the crop was rapid in the Reed canarygrass + N in 2014.

Conclusion

This study revealed that field scale N_2O emission hotspots are an important phenomenon with respect to overall emissions from perennial grasses on wet silt loam soils. We showed that in both fertilized and unfertilized cropping systems, hotspots contributed more than $1/3^{rd}$ of the total observed growing season emissions. The frequency of hotspot occurrence was affected by the practice of nitrogen fertilizer application. Soil moisture and soil temperature also governed the occurrence and magnitude of hotspots; hotspots were observed between approximately 40% and 80% WFPS and at temperatures greater than 15 °C, and N_2O hotspot emissions peaked at 53.0% WFPS and 28.8 °C. Hotspot and background N_2O emission was attributed to denitrification rather than nitrification because of the lack of emissions from dry soils, suggesting

that denitrification was the dominant source of N_2O at the study site, even at soil moisture levels between 40% and 50% WFPS, which was explained by the fine texture of the soil contributing to O_2 scarcity. Hotspots were clustered spatially, indicating that stationary underlying physical processes play a role in determining hotspot formation. N_2O emissions from hotspots generally increased during summer months when soil temperature was warmest, with lower emissions observed during spring and autumn.

Nitrogen fertilizer addition, soil moisture, and soil temperature are factors that are incorporated into process-based models used to simulate or predict emissions of N_2O, and this research supports the validity of such a mechanistic framework. However, these three factors alone did not explain the inconsistencies in hotspot occurrence. Further investigation that explores the effect of soil temperature on N_2O hotspots and emissions should seek to decouple the roles of temperature and nitrogen availability as they commonly co-vary in agricultural soils when N-fertilizer is applied in the spring or early summer. Future research could explore the impact of other drivers (i.e. pH, DOC) that are used in mechanistic models to determine N_2O emission, especially investigation into the spatial structure of their variability, and the manner in which hotspots co-vary with interactions of driver variability.

Works cited

Ambus, P. 1998. Nitrous oxide production by denitrification and nitrification in temperate forest, grassland and agricultural soils. European Journal of Soil Science 49: 495-502.

Ball, B.C., G.W. Horgan, H. Clayton and J.P. Parker. 1997. Spatial variability of nitrous oxide fluxes and controlling soil and topographic properties. Journal of environmental quality 26: 1399-1409.

Barton, L., B. Wolf, D. Rowlings, C. Scheer, R. Kiese, P. Grace, et al. 2015. Sampling frequency affects estimates of annual nitrous oxide fluxes. Scientific reports 5.

Bateman, E. and E. Baggs. 2005. Contributions of nitrification and denitrification to N2O emissions from soils at different water-filled pore space. Biology and Fertility of Soils 41: 379-388.

Bessou, C., F. Ferchaud, B. Gabrielle and B. Mary. 2011. Biofuels, greenhouse gases and climate change. A review. Agronomy for Sustainable Development 31: 1-79. doi:10.1051/agro/2009039.

Brumme, R., W. Borken and S. Finke. 1999. Hierarchical control on nitrous oxide emission in forest ecosystems. Global Biogeochemical Cycles 13: 1137-1148.

Chin, D.A. 2006. Water-Resources Engineering. 2nd ed. Prentice Hall.

Christensen, S., S. Simkins and J.M. Tiedje. 1990. Spatial variation in denitrification: dependency of activity centers on the soil environment. Soil Sci Soc Am J 54: 1608-1613.

Corre, M.D., C. van Kessel and D.J. Pennock. 1996. Landscape and seasonal patterns of nitrous oxide emissions in a semiarid region. Soil Sci Soc Am J 60: 1806-1815.

Dunmola, A.S., M. Tenuta, A.P. Moulin, P. Yapa and D.A. Lobb. 2010. Pattern of greenhouse gas emission from a Prairie Pothole agricultural landscape in Manitoba, Canada. Canadian Journal of Soil Science 90: 243-256.

Giltrap, D.L., C. Li and S. Saggar. 2010. DNDC: A process-based model of greenhouse gas fluxes from agricultural soils. Agriculture, Ecosystems & Environment 136: 292-300.

Groffman, P.M., K. Butterbach-Bahl, R.W. Fulweiler, A.J. Gold, J.L. Morse, E.K. Stander, et al. 2009. Challenges to incorporating spatially and temporally explicit phenomena (hotspots and hot moments) in denitrification models. Biogeochemistry 93: 49-77.

Hellebrand, H.J., V. Scholz and J. Kern. 2008. Fertiliser induced nitrous oxide emissions during energy crop cultivation on loamy sand soils. Atmos Environ 42: 8403-8411.

Kester, R.A., M.E. Meijer, J.A. Libochant, W. De Boer and H.J. Laanbroek. 1997. Contribution of nitrification and denitrification to the NO and N 2 O emissions of an acid forest soil, a river sediment and a fertilized grassland soil. Soil Biology and Biochemistry 29: 1655-1664.

Li, C. 2007. Quantifying greenhouse gas emissions from soils: Scientific basis and modeling approach. Soil Science and Plant Nutrition 53: 344-352. doi:10.1111/j.1747-0765.2007.00133.x.

MathWorks, I.T. 2011. MATLAB. The MathWorks Inc., Natick, Massachusetts.

McClain, M.E., E.W. Boyer, C.L. Dent, S.E. Gergel, N.B. Grimm, P.M. Groffman, et al. 2003. Biogeochemical hot spots and hot moments at the interface of terrestrial and aquatic ecosystems. Ecosystems 6: 301-312.

Parkin, T., J. Meisinger, J. Starr, S. Chester and J. Robinson. 1988. Evaluation of statistical estimation methods for lognormally distributed variables. Soil Sci Soc Am J 52: 323-329.

Parkin, T.B. 1987. Soil microsites as a source of denitrification variability. Soil Sci Soc Am J 51: 1194-1199.

Parkin, T.B. and R.T. Venterea. 2010. Sampling Protocols. Chapter 3. Chamber-Based Trace Gas Flux Measurements. Sampling Protocols. R.F. Follett, editor.: p. 3-1 to 3-39.

R Core Team. 2011. R: A language and environment for statistical computing. R Foundation for Statistical Computing, Vienna, Austria.

Rabot, E., C. Hénault and I. Cousin. 2014. Temporal Variability of Nitrous Oxide Emissionsby Soils as Affected by Hydric History. Soil Sci Soc Am J 78: 434-444.

Rees, R., J. Augustin, G. Alberti, B. Ball, P. Boeckx, A. Cantarel, et al. 2013. Nitrous oxide emissions from European agriculture: an analysis of variability and drivers of emissions from field experiments. Biogeosciences 10: 2671-2682.

Rütting, T., D. Huygens, P. Boeckx, J. Staelens and L. Klemedtsson. 2013. Increased fungal dominance in N2O emission hotspots along a natural pH gradient in organic forest soil. Biology and Fertility of Soils 49: 715-721.

Schelde, K., P. Cellier, T. Bertolini, T. Dalgaard, T. Weidinger, M. Theobald, et al. 2012. Spatial and temporal variability of nitrous oxide emissions in a mixed farming landscape of Denmark. Biogeosciences 9: 2989-3002.

Smith, K.A., P.E. Thomson, H. Clayton, I.P. McTaggart and F. Conen. 1998. Effects of temperature, water content and nitrogen fertilisation on emissions of nitrous oxide by soils. Atmos Environ 32: 3301-3309. doi:Doi 10.1016/S1352-2310(97)00492-5.

Van den Heuvel, R., M. Hefting, N. Tan, M. Jetten and J. Verhoeven. 2009. N 2 O emission hotspots at different spatial scales and governing factors for small scale hotspots. Science of the Total Environment 407: 2325-2332.

Van Kessel, C., D. Pennock and R. Farrell. 1993. Seasonal variations in denitrification and nitrous oxide evolution at the landscape scale. Soil Sci Soc Am J 57: 988-995.

Yanai, J., T. Sawamoto, T. Oe, K. Kusa, K. Yamakawa, K. Sakamoto, et al. 2003. Spatial variability of nitrous oxide emissions and their soil-related determining factors in an agricultural field. Journal of environmental quality 32: 1965-1977.

Yates, T., B. Si, R. Farrell and D. Pennock. 2006. Probability distribution and spatial dependence of nitrous oxide emission. Soil Sci Soc Am J 70: 753-762.

CHAPTER 3

Chamber and eddy covariance measurements of nitrous oxide compared over heterogeneous grasses[‡]

[‡]Authors: Cedric W. Mason, Cathelijne R. Stoof, Brian K. Richards, Jon Warland, Christine L. Goodale, Tammo S. Steenhuis

Introduction

The greenhouse gas nitrous oxide (N_2O) is produced within Earth's soils and transmitted by diffusion (Ambus, 1998) and turbulent mixing to the atmosphere where it contributes to climate change. Nitrous oxide is a particularly potent greenhouse gas that has an estimated 100-year global warming potential 298 times that of CO_2 (Forster, 2007). In addition to constituting 6% of anthropogenic radiative forcing (Davidson, 2009), N_2O is the primary anthropogenic pollutant causing the destruction of stratospheric ozone (Conrad, 1996, Ravishankara, 2009). Agricultural soils are a primary source of N_2O emission (U.S., 2013) due to inputs of nitrogen fertilizer and manure (Davidson, 2009), but the microbial processes of nitrification and denitrification that mediate the production of N_2O (Li, 2007, Reay, et al., 2012), and their coupling with environmental factors that control release into the atmosphere, are complex and not well understood (Bessou, et al., 2011, Dunmola, et al., 2010). N_2O emissions can be estimated by employing emission factors or mechanistic models, but such efforts are hampered by high uncertainties (Davidson, 2009, Groffman, et al., 2009). However, these methods of estimating emissions can be improved and validated by comparing to lab and field measurements of nitrous oxide emission (Beheydt, et al., 2007). In addition, direct observation of emissions can inform N_2O mitigation strategies. As such, measuring emissions of nitrous oxide from various ecosystems is critical to furthering an understanding of the processes involved, and quantifying emissions at larger scales.

Enclosed chambers and micrometeorological techniques are two approaches that are commonly used to observe and quantify N_2O (and other trace gas) emission rates from land surface areas, and each method has its own advantages and disadvantages. Chamber-based monitoring of small ($< 1m^2$) patches is relatively cheap, effective, and adaptable to complex

terrains (Parkin and Venterea, 2010, Wang, et al., 2013). Multiple chambers can be deployed simultaneously to study spatial variation in flux rates over wider areas (Jones, et al., 2011), but they can disturb soil, vegetation, and the microenvironment, thus causing biased results (Parkin and Venterea, 2010). Over large areas and long time periods, low resolution sampling designs may miss short bursts (hot-moments) or small patches (hotspots) of high emissions (McClain, et al., 2003). In contrast, micrometeorological approaches, such as the eddy covariance method (Burba and Anderson, 2010), can provide unintrusive, temporally continuous flux measurements over large integrated areas (0.01 km^2 – 1 km^2 (Burba and Anderson, 2010, Jones, et al., 2011, Wang, et al., 2013)), such as agricultural fields (Molodovskaya, et al., 2011). The eddy covariance method is the most direct way of measuring flux (Burba and Anderson, 2010). However, the eddy covariance method requires expensive high-performance instruments, is computationally demanding, and stipulates many assumptions such as fully developed turbulence conditions, and a uniform horizontal upwind source area (Burba and Anderson, 2010, Jones, et al., 2011, Molodovskaya, et al., 2012, Wang, et al., 2013). The footprint concept is used to link a defined area of an emitting surface to a micrometeorological flux measurement. For an eddy covariance measurement of a heterogeneous surface, the signal depends on the location and size of its footprint (Schmid, 2002), and establishing the source area for measurements via a footprint model is useful for accurate upscaling (Vesala, et al., 2008, Zhao, et al., 2014).

Neither the chamber nor the eddy covariance method can resolve emission sources much smaller than the area being measured unless heterogeneity of the source area is extremely simplified (see Molodovskaya, et al. (2011)). This is especially problematic for the eddy covariance method because the source area is typically much larger than the study plot scale at which management practices are investigated, and as a result it is not helpful in determining

localized emission sources (Molodovskaya, et al., 2011). Hence, assessing emissions at scales other than those at which they are actually measured is problematic, particularly for nitrous oxide given the wide variability in emission rates, both temporally and spatially. There is evidence that spatial variability of N_2O emission is high through a range of scales and highest at smaller scales (Ambus and Christensen, 1994, Parkin, 1987, Van den Heuvel, et al., 2009). Intermediate scale (as opposed to microsite or landscape scale) N_2O emission hotspots on the order of 1m were reported by Van den Heuvel, et al. (2009) and denitrification hotspots on the order of 1-2m have also been reported (McClain, et al., 2003). Spatial variability on this scale due to environmental factors or agricultural management practices is well suited to study by chambers of similar size. However, without complete chamber coverage, ecosystem or treatment scale emissions based on such sampling designs can fail to include coverage of hotspots (McClain, et al., 2003) or other important elements of spatial variability (Parkin and Venterea, 2010), leading to inaccurate results when individual chamber flux rates are averaged. Furthermore, when static chambers are used, the temporal resolution of measurement is typically very low, and this can also produce errors when observed emission rates are assumed to apply during interim periods during which significant changes in emission rates may actually occur; hot-moments have been widely documented (Molodovskaya, et al., 2012, Wagner-Riddle, et al., 2007). Using chambers, Parkin (2008) showed that a measurement frequency of 3d resulted in cumulative estimates that were within 10% of the actual cumulative flux, whereas a measurement interval of 21 days yielded results that were +60% to – 40% of the actual cumulative flux.

While the chamber method has been shown to be flawed because of disturbance to the physical environment (discussed previously), Mosier, et al. (1996) suggests that uncertainty in upscaled emission estimates is largely due to the diverse combinations of physical and biological

factors which control gas fluxes and produce patterns of high spatial and temporal variability that are difficult to capture with chambers. A strategy that has been employed to overcome this problem is to verify upscaled chamber emission estimates with a whole-system measurement, such as eddy covariance (McClain, et al., 2003, Wang, et al., 2013). In this way static chambers can be used to investigate small scale variation in flux and the impact of management and environmental factors, and the efficacy of the sampling design can be assessed with eddy covariance. The primary purpose of this study is to apply the eddy covariance method to verify the accuracy of emission estimates that were derived from linear interpolation of concurrent chamber observations over a heterogeneously managed land surface, particularly in determining the degree to which the chamber-based studies and resulting emission estimates are fully representative of N_2O emissions from their respective cropping system despite incomplete temporal and spatial coverage. The second objective of this study is to evaluate the performance of the chamber method and the eddy covariance method when measuring nitrous oxide emissions from a heterogeneous field of perennial grass.

Methods

Site description, field layout, and treatments

A relatively flat field in Ithaca, NY (N 42° 28.20', W 76° 25.94') was chosen as the site for this study, particularly because the seasonally wet silt loam soils are well suited to production of perennial grass bioenergy crops in the native temperate climate (Stoof, et al., 2014). The prevailing winds at the site were from the Northwestern and Southern directions, although a good deal of variation in direction and wind speed was observed (Fig. 3.1) (R Core Team, 2011, Ropkins, 2012). An area of the field, covering approximately 6.5 ha was surveyed and demarcated into 16 adjacent study plots of approximately 0.4 ha each. These adjacent plots were

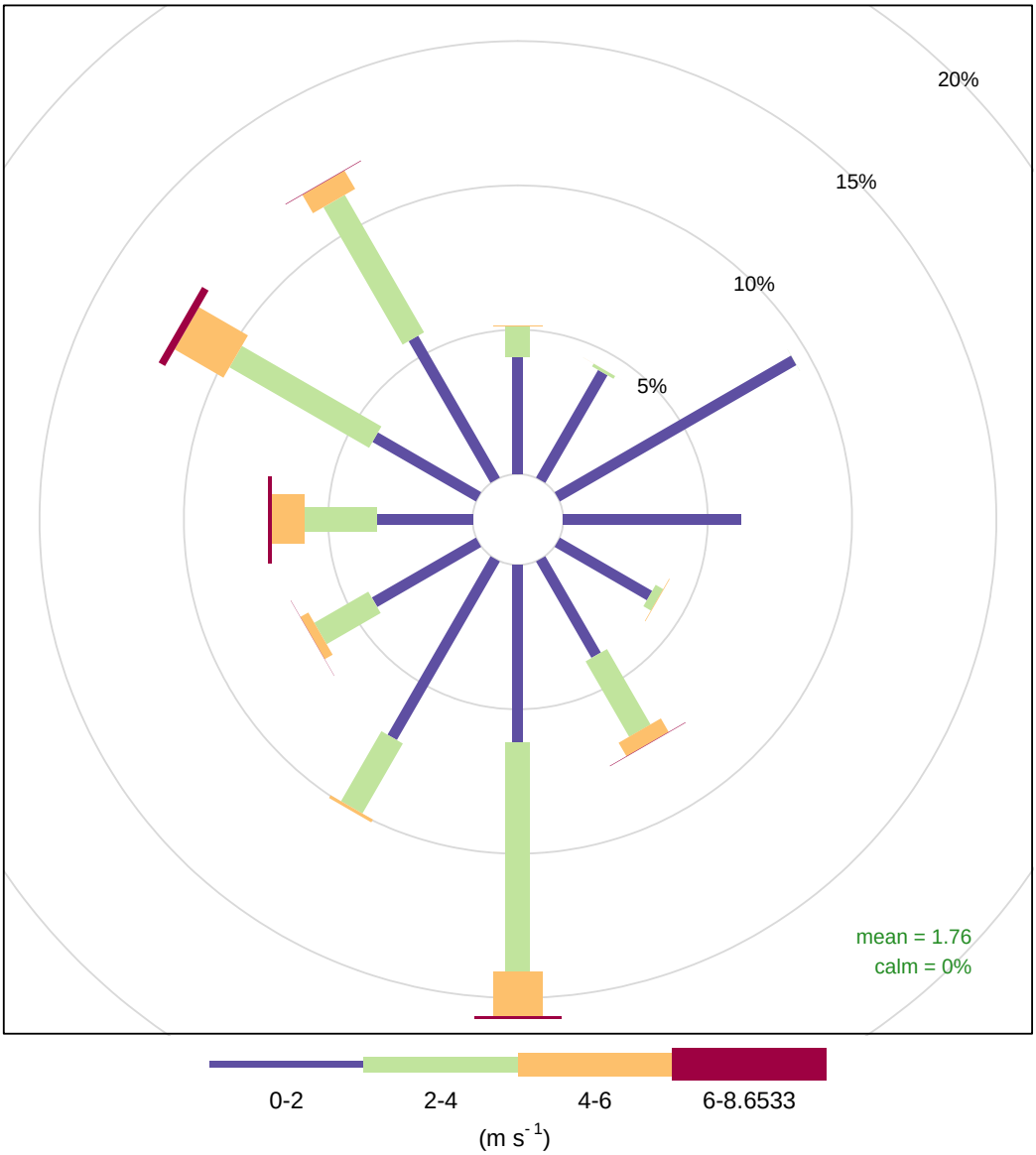

Figure 3.1: Wind rose of all wind data collected at the perennial grass research field during years 2012 to 2015.

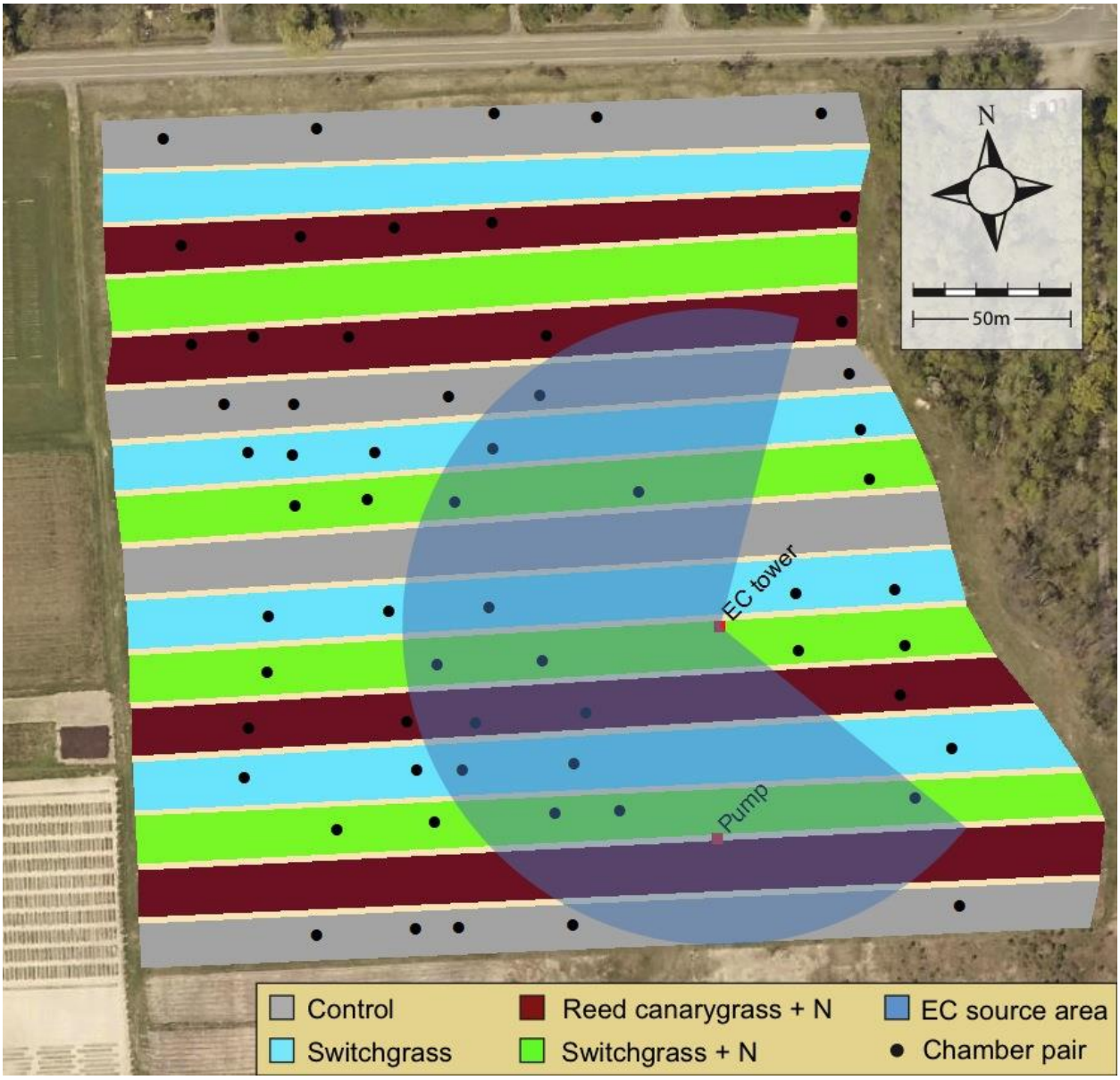

Figure 3.2: Map showing arrangement of the Control (grey), unfertilized Switchgrass (cyan), Reed canarygrass + N (maroon), and Switchgrass + N (green) research plots and access lanes (beige), as well as locations of subplots where pairs of chambers were situated (black dots) for measurement of local N_2O flux rates, and locations of the eddy covariance tower and pump (red squares) and the eddy covariance signal source area (transparent blue).

each in the shape of a strip 14.6m wide and extending about 200m along the East-West axis of the study area. In addition, access lanes 1.8m wide separated the plots. Four plots (strips) were assigned to each of four different treatments; these were all placed in random order across the study area, and managed accordingly (Fig. 3.2). The treatments were 1) an undisturbed control that consisted of the native forbs and grasses that pre-existed at the site, 2) unfertilized switchgrass (*Panicum virgatum*), 3) N-fertilized reed canarygrass (*Phalaris arundinaceae*), and 4) N-fertilized switchgrass (*Panicum virgatum*). All treatments except the control were established in the summer of year 2011 by sequentially mowing, applying glyphosate herbicide, tilling, and seeding with the respective crop. Standard annual practices in the fertilized and unfertilized Switchgrass plots included mid-spring glyphosate herbicide application to reduce weed competition with the late emerging, warm-season Switchgrass plants. All fertilized plots received 75 kg-N ha^{-1} annually as ammonium sulfate ($(NH_4)_2SO_4$) in a single application that occurred in mid-spring in the Reed canarygrass + N, plots and late-spring in the fertilized Switchgrass + N plots, although the Switchgrass + N treatment did not receive fertilizer in year 2012. In all plots except the control, grass crops were mowed and removed from the field in mid-autumn by conventional mechanized farm machinery typically used for grass forage crops. Crops were mowed but not removed from the field in autumn of 2012 due to low yields. Access lanes were typically mowed several times each summer to facilitate foot traffic, but were never tilled, or treated with fertilizer or herbicide.

Eddy covariance measurements

The core eddy covariance instrumentation consisted of a 3D-Sonic Anemometer (CSAT3D, Campbell Scientific Inc.) mounted at a height 3.05m above the soil surface with the head (-X direction) oriented due West, a tunable diode laser trace gas analyzer (TGA100A,

Campbell Scientific Inc.), and a datalogger (CR5000, Campbell Scientific Inc.). The sample intake port for the closed-path trace gas analyzer was positioned at the same elevation as the anemometer, approximately 9cm due East of the anemometer's sensors. Air samples were drawn from the intake port under the pull of a rotary vane vacuum pump (RB0021, Busch USA) and traveled at a rate of 18 L min^{-1} within a ~5m long transfer tube (I.D. 3.2mm) through a 10μm particulate filter (changed monthly) and a diffusive dryer (PD1000 Perma Pure) that removed moisture from the air sample. A small portion of the flow (3L min^{-1}) was purged, leaving a flow rate of 15L min^{-1} through the analyzer's sample cell. The time for air to travel from the intake port, through the filter, drier, and associated tubing, and register at the analyzer's detector (i.e. the lag time of the analyzer with respect to the anemometer) was determined to be 0.7s, measured using the timed response to a release of N_2O standard gas tracer at the inlet port. Concentration of N_2O of the air within the sample cell was measured at the 2205 cm^{-1} laser absorption line with a direct current of 757 mA, and calibrated with a standard reference gas (2000 ppm N_2O, balance N_2, Airgas, Inc., Cinnaminson, NJ) at a flow rate of 10 mL min^{-1}. A laser operating temperature of 89.3 K was maintained using a liquid nitrogen dewar, and the complete analyzer was housed within a case with a stabilized environment of 36°C. Measurements of 3-dimentional wind velocity and N_2O concentration were logged at 10Hz by the CR5000 datalogger and recorded on a compact flash card that was exchanged at regular intervals for data transfer and archiving.

The high-frequency binary data files from the CR 5000 datalogger were converted to Ascii text files using LoggerNet software (LoggerNet 3.4.1, Campbell Scientific Inc.), and these large text files were subsequently split into many separate files (one file for each 30-minute segment) using MATLAB software (MATLAB 7.12.0, The Mathworks Inc.). N_2O fluxes for

each 30-minute period were calculated from the covariance of the high-frequency (10Hz) vertical wind velocity and N_2O concentration measurements using EddyPro software (EddyPro 5.2.1, LI-COR Inc.). High frequency measurements of wind velocity and N_2O concentration that were outside a plausible range, or triggered a diagnostic error, were excluded, and 30-minute periods that were missing more than 5 minutes of data were subsequently discarded (16% missing sample allowance). Flux calculations were performed using the linear detrending method, double axis rotation for tilt correction, a constant time lag of 0.7 s (determined experimentally), and density fluctuations were corrected using the method of Ibrom, et al. (2007) for closed path analyzers. The maximum acceptable consecutive outliers in the high-frequency anemometer and N_2O concentration measurements was 3, and half-hour periods exhibiting any spikes were not used. The quality of each 30-minute flux value was rated using the 3-tier approach of Foken, et al. (2004), and fluxes that were not deemed acceptable for general analysis (i.e. annual budgets) using this criteria were dropped from the dataset.

Eddy covariance flux values were removed for periods during which equipment (such as the vacuum pump and the electrical power source) was being serviced, repaired, or functioning improperly. Times during which the laser dewar was refilled with Liquid N_2 were also removed, and padded with preceding and recovery times of 1 and 4 hr respectively. If the pressure within the sample cell was not within the normal operating range of 40 to 60 mb, the corresponding half-hour eddy covariance flux values were discarded. Additionally, we used only daytime half-hour eddy covariance flux values that corresponded with an average wind speed > 1.5 m s^{-1} and average friction velocity (u^*) > 0.1 m s^{-1}.

For the purpose of comparing the eddy covariance measurements to chamber based emission estimates, the remaining half-hour eddy covariance fluxes were used to construct two

data sets representing two separate time periods during which regular chamber observations had also been made. The two time periods were from July 11, 2013 to November 20, 2013, and from May 29, 2014 to September 24, 2014. During these two periods, the frequency of chamber measurements was regular, and the eddy covariance data was more-or-less continuous without interruption due to instrumental issues. Eddy covariance fluxes that occurred outside of these time periods were not used for comparison to the chamber observations, and vice-versa. Exploratory analysis of the remaining half-hour eddy covariance N_2O fluxes revealed that the flux values were normally distributed. We calculated the mean flux ($\bar{x}_f$) and its associated standard error (Eq. 1) from the half-hour eddy covariance measurements separately for the two comparison periods.

$$SE_{\bar{x}_f} = \frac{s}{\sqrt{n}} \qquad \text{Eq. 1}$$

In Eq. 1, *s* is the sample standard deviation (an estimate of the population standard deviation, σ), and *n* is the sample size (the number of final half-hour flux values in each period) (Boas, 1983). The 95% confidence interval for the mean flux ($\bar{x}_f$) was calculated for each period by multiplying the standard error by 1.96.

Defining the source area of eddy covariance measurement

Wind speed and direction, and thus the footprint of an eddy covariance measurement, shifts rapidly, extensively, and unpredictably, but micrometeorological researchers can exert some control over the source area of eddy covariance measurements by carefully choosing the instrument's location and height in consideration of anticipated wind speed and direction, and surface roughness. Because the height of the anemometer and air sample intake port was approximately 3m, the 100:1 rule-of-thumb (Burba and Anderson, 2010) suggests that the range of the fetch was about 300m, this distance extends quite significantly beyond the boundaries of

the research plots of interest. We used the footprint estimation feature of the EddyPro software to calculate footprint metrics for each half-hour of eddy covariance data using the model of Kljun, et al. (2004). In conditions where the assumptions of Kljun's model were not valid, the model of Kormann and Meixner (2001) was used instead. The canopy height was assumed to be a constant value at 0.75 m, the displacement height was 0.5 m, and the surface roughness was 0.11 m. By discriminately choosing half-hour flux values based on its associated footprint metrics, we were able to construct a dataset that represented a moldable long-term source area shape that covered a small subset of the area within the general fetch radius (300m). With this approach, we assumed that variations in footprint location and dimension due changes in meteorology and crop height would average out over the longer study period, and that the long term source area for the eddy covariance measurement was adequately represented by the basic partial circle shape.

In defining the long-term source area for the eddy covariance observation, we sought to 1) maximize the amount of useable data and thus actual surface area of the source area, while also 2) restricting the source area exclusively to the research plots, because there were other agricultural activities, as well as road traffic, very close to the plot boundaries. 3) Satisfying the assumptions of eddy covariance also entails ensuring that the source area is on level ground, and that the tower structure anchoring the meteorological instruments does not interfere with air currents reaching the sensors. We also sought to 4) maximize the eddy covariance signal by defining a source area that included as much of the fertilized research plots as possible. Thus we defined the source area as a partial circle of a certain radius centered at the eddy covariance tower location. Metrics of the source area were determined using Geographic Information System (GIS) software (ArcMap 10.1, Esri Inc.). Geographical coordinates of the plot and lane boundaries within the field were established using a hand held Global Positioning System (GPS)

unit (GPSmap 60CSx, Garmin) and uploaded to the GIS software. By overlaying the source area shape onto a map of the study plots, we calculated the fraction of the total source area shape that covered each treatment or other land use.

Chamber observations

Manually operated chambers each covering $0.07m^2$ were used to monitor local N_2O soil fluxes from each treatment at approximately monthly intervals during the growing season in years 2013 and 2014. Within 3 out of 4 plots for each treatment, 30 chambers were permanently installed across a range of soil moisture conditions (Fig. 3.2), and thus were distributed fairly evenly throughout the study area with equal representation for each treatment. Chamber coverage within the research plots was approximately 0.013% of the total area. Teams of researchers operated the chambers, commencing measurement at midday, with deployments lasting 30 minutes. An N_2O flux rate for each chamber location was calculated by observing the rate of change in N_2O concentration (determined by gas chromatography) within the chamber headspace during deployment. Additional details describing these chamber observations and results are described in Chapter 1.

Upscaling the chamber flux measurements in time and space

Two separate time periods were used for the comparison of N_2O emissions from the chamber fluxes and the eddy covariance measurements. The two time periods were from July 11, 2013 to November 20, 2013, and from May 29, 2014 to September 24, 2014. During these two periods, the frequency of chamber measurements was regular, and the eddy covariance data was more-or-less continuous without interruption due to instrumental issues. Eddy covariance measurements and chamber observations that occurred outside of these two time intervals were

excluded from the comparison, ensuring that emission estimates from each method were simultaneous.

We used GIS software (ArcMap 10.1, Esri Inc.) to analyze the representation of each treatment within the eddy covariance source area, and thus determine the contribution of each treatment towards the point-source eddy covariance measurement. The proportional representation of each treatment within the source area was used to weight the chamber-based emission estimates for the different treatments in order to construct a composite N_2O emission estimate for the source area. Because chamber observations were not made in the access lanes that separated the plots in the field, and because the management of the lanes was very similar to the management of the control plots, the lanes were assumed to have the same emissions as the control, and thus the control was weighted more heavily to compensate for the contribution of the lanes.

On each date of chamber observation used for the comparison to eddy covariance, an ensemble of plausible mean N_2O flux was calculated for the source area using a bootstrapping procedure similar to the one described in chapter 1. This was achieved by simulating a sample pool for each treatment (typically $n = 30$) on each chamber observation date by drawing randomly with replacement from the population of flux values that were actually observed for that treatment on that date. The resulting flux averages from the four pools corresponding to each treatment then were themselves averaged according to the weights indicated by the source area composition analysis, resulting in an estimate of the average N_2O flux rate for the source area shape. This was repeated 10,000 times, in turn producing an ensemble of plausible source area emissions for each date of chamber observation.

Using linear interpolation, a cumulative N_2O emission estimate was calculated for the source area using a random value from the ensemble of plausible source area emission for each observation date, and this was repeated 10,000 times, finally producing an ensemble of cumulative emission estimates for the source area during the two comparison periods. These were then divided by the duration of the respective comparison period, resulting in an ensemble of mean emission rates that was used to estimate the overall average emission rate and associated confidence interval for the source area during each comparison period.

The entire chamber upscaling procedure is conceptually and mathematically equivalent to taking the properly weighted average of the final cumulative emission rates of the four treatments in years 2013 and 2014 from chapter 1, but over slightly shorter time periods that were restricted to allow comparison of the eddy covariance and chamber methods. Our approach in this research is somewhat in contrast to the more direct comparison by Molodovskaya, et al. (2011) whereby each chamber measurement was weighted by its source area contribution that was determined by the distance from the eddy covariance tower according to the model of Schuepp, et al. (1990). However, given the relatively sparse chamber coverage in this study, our approach (first upscaling the chambers to the treatment scale, then the treatments to the eddy covariance source area) has the following advantages: A) it accounts for the contribution of broad portions of the source area that, due to the constraints of the overall experimental design, were not directly observed with chambers but certainly contributed substantially to the eddy covariance signal. These portions include the access lanes, and two plots that were not studied with chambers (Fig. 3.2). B) Fewer chambers would be used in the direct comparison, whereas all the chamber locations could be used in our approach. This is important given the high spatial variability of N_2O emissions. Spatial dependence of N_2O has been shown to be "moderate to

weak" (Yates, et al., 2006), and the dimensions of intermediate scale hotspots are thought to be on the order of only a few meters (McClain, et al., 2003, Van den Heuvel, et al., 2009). This suggests that emissions at locations within the source area that were not monitored with chambers (and were not very close to other chambers), are as likely to be correlated with distant chamber fluxes that were not within the source area as they are to be correlated with chambers within the broad source area. Given the high spatial variability of N_2O emissions, using greater numbers of chambers gives more certain estimates of fluxes from unmonitored locations within the source area if the environmental conditions were similar. C) The application of the footprint model assumes constant wind speed and direction over 30 minutes, and it assumes that locations outside the footprint threshold boundary do not contribute to the eddy covariance signal. These assumptions are false in this study. Thus it is a practical certainty that locations outside of the defined footprint boundaries contributed to some extent to the eddy covariance measurement.

Results

Analysis of the eddy covariance source area

Because of the position and orientation of the eddy covariance tower within the field, we excluded the angles between 20° and 130° (clockwise from magnetic North) in which directions there was uneven surface topography, and this also excluded wind conditions associated with interference from the eddy covariance tower. In choosing the radius of the partial circle shape representing the source area, we investigated some trends in the footprint metrics calculated for each half-hour flux value by the EddyPro software. Histograms showed that the 90% cumulative flux threshold for the footprint was rarely more than 100m from the eddy covariance tower, the peak source area was mostly closer than 30m from the tower, and the offset (the initial 1% of the cumulative flux) was on the order of 10m or less (Appendix C, Fig. S3.1). Using a maximum

possible radius of the source area shape, for example one that stretched from the eddy covariance tower to the Western or Northern study boundary, would require excluding data associated with wind from the South (which was the second most active wind source direction according to the wind rose for the site (Fig. 3.1, Appendix C Fig. S3.2)) in order to prevent the source area from extending beyond the study plots and this would result in considerable loss of data. In addition there was little to be gained from using a larger source area radius because most of the footprint was almost always less than 100m from the tower (Appendix C, Fig. S3.1). The offset (distance to initial 1% of the cumulative flux) was generally small, and sometimes negative, and was not removed from the source area shape.

Under these considerations, we chose a source area that covered a radius of 97.5m (the distance from the eddy covariance tower to the Southern boundary) from the eddy covariance tower, excluding angles from 20 to 130 degrees (Fig. 3.2). In addition, this smaller radius ensured that the outer fringe of the source area (90% to 100% cumulative flux) also was mostly within the boundaries of the study area, reducing the undesired influence of other activities nearby. This shape ensured that 1) many half-hour flux values could be used to determine emissions 2) the source area was almost exclusively over study plots, 3) the assumptions of the eddy covariance method were satisfied, and 4) a substantial fraction of the point source eddy covariance measurement represented fertilized treatments. Accordingly, we only used half-hour eddy covariance flux values for which the 90% cumulative flux threshold of the footprint was less than or equal to 97.5m and the average wind source direction was not between 20° and 130°. Although the pump was located to the south of the eddy covariance tower and was often upwind (Fig. 3.1, Fig. 3.2), the contribution of the expelled calibration sample to the measured flux was assumed to be insignificant because of the low rate (10 mL min^{-1}), the low concentration of N_2O

Table 3.1: Composition of eddy covariance source area, and resulting weights used to upscale chamber-based treatment averages of N_2O emission. The weight used to upscale the Control incorporates the contribution of the lanes to the source area.

	Control	Switchgrass	Reed Canarygrass + N	Switchgrass + N	Lane	Total
% of source area	18.3%	24.9%	21.6%	24.4%	10.8%	100.0%
Weight in upscaled chambers	0.291	0.249	0.216	0.244	NA	1.0

(2000 ppm), and the location (the pump was approximately 66m from the tower, nowhere near the footprint peak, see Appendix C Fig. S3.1). The average contribution of the expelled N_2O standard calibration gas to the measured eddy covariance signal was estimated to be 0.07 μg N_2O-N m^{-2} hr^{-1}.

This partial circle shaped source area (Fig. 3.2) was calculated to cover a surface area totaling 20,740 m^2. We used GIS software (ArcMap 10.1, Esri Inc.) to analyze the representation of each treatment within the source area, and thus the contribution of each treatment towards the point-source eddy covariance measurement. The analysis revealed that the treatments comprised variable fractions of the source area, and that the lanes (from which fluxes of N_2O were not observed with static chambers) comprised a significant portion as well (Table 3.1).

Chamber N_2O flux observations

Nitrous oxide flux values resulting from the static chamber observations generally followed a seasonal trend, with increased emissions during summer months. The distribution of flux rates was positively skewed and ranged from -57.1 to 3694.0 μg N_2O-N m^{-2} hr^{-1} (Fig. 3.3A). The instantaneous upscaled chamber estimates of the N_2O emission rate of the source area based on the weighted average of the different treatments (Table 3.1) ranged from a minimum of -0.4 μg N_2O-N m^{-2} hr^{-1} on September 24, 2014 to a maximum of 185.2 μg N_2O-N m^{-2} hr^{-1} on June 19, 2014 (Fig. 3.3B). Linear interpolation of the chamber-based emission estimates indicated that the average N_2O emission rate of the source area for the period from July 11, 2013 to November 20, 2013 was 14.7 μg N_2O-N m^{-2} hr^{-1} (range of uncertainty: 10.2 to 20.4 μg N_2O-N m^{-2} hr^{-1}), and during the period from May 29, 2014 to September 24, 2014 the average emission rate was 46.8 μg N_2O-N m^{-2} hr^{-1} (range of uncertainty: 32.1 to 66.0 μg N_2O-N m^{-2} hr^{-1}) (Fig. 3.3B). The average emission rate estimated from the chambers was higher during the comparison period of

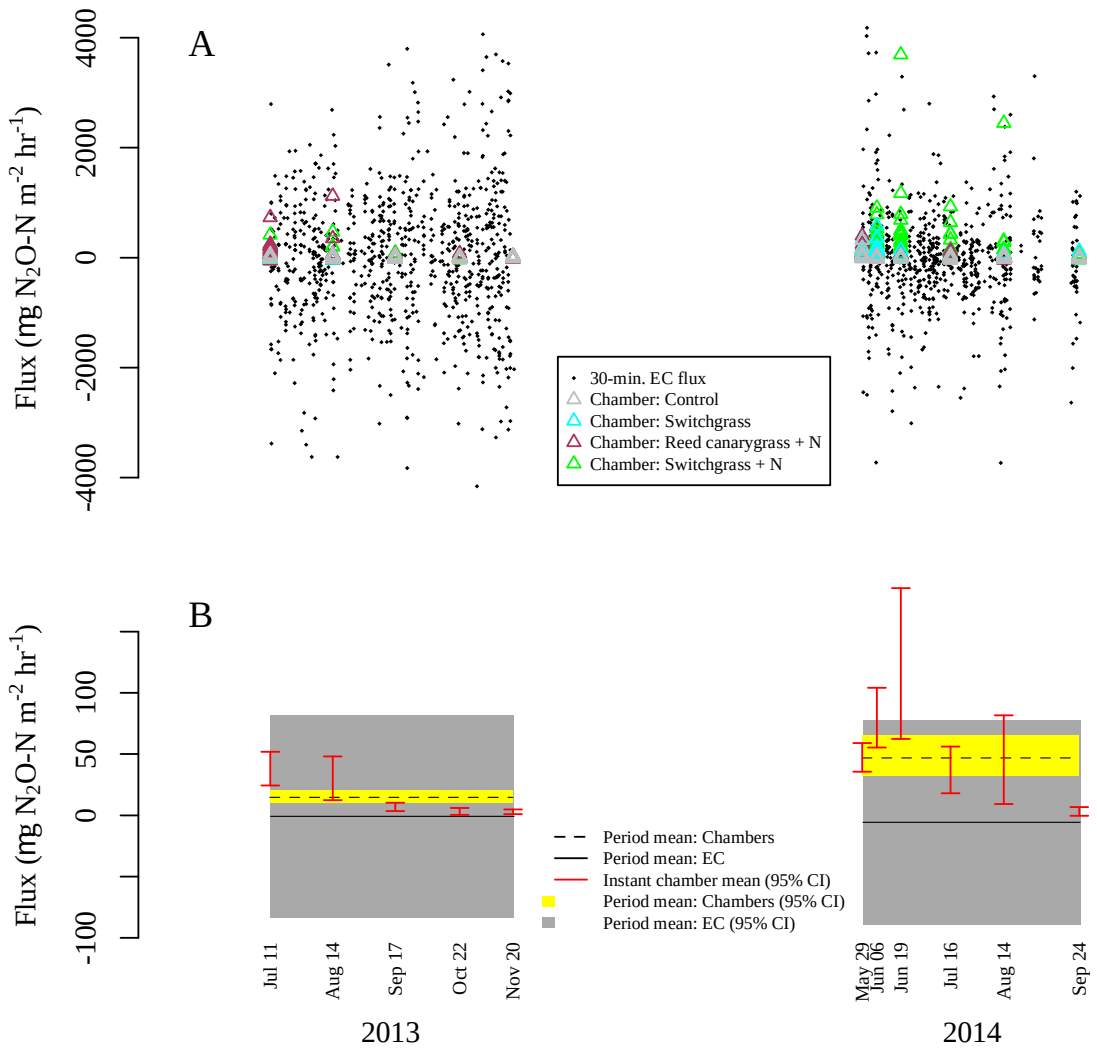

Figure 3.3: Plots of N_2O emissions as determined by the eddy covariance and chamber methods. Half-hour eddy covariance (black diamonds) and instantaneous chamber measurements (triangles) are presented in the upper pane (A). In the lower pane (B), spatially upscaled chamber estimates are represented by red confidence intervals (95%) along with linearly interpolated averages from chambers (yellow with dotted line), and average eddy covariance measurements (grey with sold black line) for each comparison period.

year 2014 than it was for the comparison period of year 2013, but the two periods spanned slightly different times of the year.

Eddy covariance N_2O flux observations

Half-hour eddy covariance flux values were approximately normally distributed and ranged from a minimum of -5547.0 μg N_2O-N m^{-2} hr^{-1} to a maximum of 5320.0 μg N_2O-N m^{-2} hr^{-1} (Fig. 3.3A). The mean N_2O emission rate from the eddy covariance measurements for the period from July 11, 2013 to November 20, 2013 was -0.8 μg N_2O-N m^{-2} hr^{-1} (range of uncertainty: -83.5 to 81.9 μg N_2O-N m^{-2} hr^{-1}), and for the period from May 29, 2014 to September 24, 2014 the average N_2O emission rate was -5.7 μg N_2O-N m^{-2} hr^{-1} (range of uncertainty: -89.0 to 77.5 μg N_2O-N m^{-2} hr^{-1}) (Fig. 3.3B). There was not a discernable signal, or any emission peaks (hot-moments), apparent in the sequence of half-hour eddy covariance flux measurements.

Discussion

Magnitude of emissions

Nitrous oxide fluxes from agricultural soils have been observed to vary widely in magnitude. Molodovskaya, et al. (2012) reported that measured emissions from fertilized cropland fall in a range from 0.7 to 51.8 mg N_2O-N m^{-2} d^{-1} (29.2 to 2158.3 μg N_2O-N m^{-2} hr^{-1}). Wang, et al. (2013) determined mean emission rates of 19.7 μg N m^{-2} hr^{-1} and 39.8 μg N m^{-2} hr^{-1} from a fertilized (75 kg N ha^{-2} yr^{-1}) cotton field in Northern China over a full year using chambers and eddy covariance respectively. Wagner-Riddle (1997) reported micrometeorology based estimates of annual N_2O emissions from agricultural land in temperate Guelph, Canada: 0 to 0.5 kg N ha^{-1} yr^{-1} (0 to 5.7 μg N_2O-N m^{-2} hr^{-1}) from bluegrass, and 5.7 to 7.4 kg N ha^{-1} yr^{-1} (65.1 to 84.5 μg N_2O-N m^{-2} hr^{-1}) from manure fertilized fallow. Considering that our upscaled

estimates for the two periods represent a roughly 50/50 combination of fertilized and unfertilized soils, and that the periods over which we estimated emissions were less than a full year (but spanned both high and background emission periods), our chamber-based results (14.7 and 46.8 μg N_2O-N m^{-2} hr^{-1} in periods for 2013 and 2014 respectively) align quite well with these reported values. Our estimated N_2O emission rates from the eddy covariance rate are considerably lower (-0.8 and -5.7 μg N_2O-N m^{-2} hr^{-1} in periods for 2013 and 2014 respectively), but the relatively high level of uncertainty in the eddy covariance averages accommodates our chamber-based estimates (Fig. 3.3B). Generally speaking, our chamber-based estimates suggest that the overall N_2O emission rate of the eddy covariance source area was near the lower end of the range of reported values for agricultural emissions. This was likely due to the high influence of unfertilized soils on the eddy covariance measurement (54%), and also the relatively low nitrogen loading (75 kg-N ha^{-1} yr^{-1}) rate of the fertilized treatments that comprised the complementary 46% of the signal.

Uncertainty of eddy covariance measurement

Quantifying low-level N_2O emission rates with micrometeorological methods is challenging. Wang, et al. (2013) concluded that the application of eddy covariance during low emission periods produces uncertain results, and was unable to calculate a lag time via covariance maximization during such periods. The study of Wang, et al. (2013) produced estimates of the detection limit for their eddy covariance measurements (using similar instrumentation as our study) on the order of 37.6 μg N m^{-2} hr^{-1} for a 30-minute averaging period. Jones, et al. (2011) estimated the detection limit for a 30-minute period with their similar eddy covariance instrumentation to be between 11 and 33.6 ng N_2O-N m^{-2} s^{-1} (between 39.6 and 121.0 μg N_2O-N m^{-2} hr^{-1}). Using identical instrumentation as our study, Molodovskaya, et al.

(2011) reported a detection limit for a 30-minute averaging interval of at least 3 μg N_2O-N m^{-2} hr^{-1}, yet produced half-hour flux values during low emission periods that varied to approximately the same extent as in our study (see Fig. 3.3A), a range that greatly exceeds all of these reported detection limit estimates. A possible explanation for the wide variability of the eddy covariance measurements in this study is random error due to a single measurement point and finite sampling period. Very large variability has been demonstrated in 30-minute N_2O fluxes, particularly at levels close to the instrumental detection limit (Wang, et al., 2013), and these could be due to statistical random errors. Interestingly, Wang, et al. (2013) calculated random uncertainties in 30-minute flux observations to be about +/- 600 μg N m^{-2} hr^{-1}, which greatly exceeds the related estimate of the instrumental detection limit (37.6 μg N m^{-2} hr^{-1}). In our study, the maximum instantaneous source area emission estimate from the upscaled chambers was only 185.2 μg N_2O-N m^{-2} hr^{-1} (Fig. 3.3B), and if the high random uncertainty in half hour eddy covariance measurements reported by Wang, et al. (2013) is a factor in our eddy covariance measurements, this implies that the source area emissions never dominated the eddy covariance measurements, and this explains the lack of a clear eddy covariance signal. In an effort to reduce the magnitude of the uncertainty, we averaged the eddy covariance flux values over longer periods, and indeed this reduced the uncertainty, but not to the extent that it was reduced below the magnitude of expected source area emissions as indicated by the chambers for the same period.

The symmetry of positive and negative half-hour eddy covariance flux values that were observed in this study, coupled with the absence of substantial N_2O uptake (negative flux values) in the chamber observations (Fig. 3.3A), also suggests that in our case the random error in half-hour eddy covariance values was quite large. In addition to the influence of random error and

measurement detection limits discussed above, misrepresentative measurements can arise due to other uncompensated factors such as separation of anemometer and analyzer measurements, and damping of fluctuations in the sampling line (Burba and Anderson, 2010, Jones, et al., 2011), besides laser noise that contributes to the theoretical detection limit. Given the relatively low-level of emissions assumed in our study, and the relatively wide span of our normally distributed half-hour eddy covariance flux values, we believe that the source area emissions were generally below the method detection limit of our eddy covariance measurements.

Comparison of eddy covariance and chamber estimates of N_2O emission

It has been noted that closed chambers are preferred for observing N_2O emission because accumulation of small amounts of the trace gas in chamber headspace results in lower detection limits compared to micrometeorological methods (Barton, et al., 2015). Studies comparing chamber and eddy covariance measurements of N_2O are quite limited, especially long term studies (Wang, et al., 2013), and have shown mixed results. While Jones, et al. (2011) found that eddy covariance fluxes were 70% of the fluxes from chambers, Wang, et al. (2013) found higher emissions estimates from eddy covariance (17-20%). We observed lower emissions using the eddy covariance method than for the chamber method, but found basic agreement between the two methods because the chamber based estimate was entirely within the range of uncertainty of the eddy covariance estimate for both comparison periods (Fig. 3.3B).

While our findings suggest basic agreement between the two methods, the divergence of the estimates from chambers and eddy covariance could be due to several distinct elements of the full upscaling procedure. For example, chamber bias due to barometric pumping, soil disturbance, mid-day sampling bias due to diurnal fluctuation in N_2O production rates, as well as spatial interpolation, and linear interpolation over time, could all have contributed independently

to artificially higher chamber-based estimates in this study. Due to reduction of the covariance signal from physical aspects of the instrumentation, underestimation of eddy covariance measurements is more likely than overestimation (Jones, et al., 2011), and this could explain the low eddy covariance based emission estimates in our study.

Because overall emissions were quite low in the context of general agricultural N_2O emission rates, and the signal of the eddy covariance was associated with high uncertainty, probably due to random error, it would be somewhat futile to attempt to tease apart the contribution of each possible source of error in the overall difference between chamber and eddy covariance estimates. In our case, limitations of the eddy covariance data prohibited instantaneous comparison of chamber-based and eddy covariance based estimates of the source area emissions which would have removed the uncertainty due to the linear interpolation approach to temporal upscaling. In addition, heterogeneity of the source area coupled with simplification of the footprint and source area undoubtedly contributed to some degree to the divergence of the two methods in our case. While we conclude general agreement between the two methods and the processes used to upscale them to comparable spatial scales and time frames, specific elements of the measurement and upscaling approach are best investigated and evaluated under conditions of high emissions.

However, because spatial and temporal heterogeneity of the physical and biological factors that drive emissions are thought to be the primary cause of divergence of estimates from each method (Mosier, et al., 1996), the results of this study give some weight to assumptions of validity with respect to the efficacy of spatial coverage with chambers, and temporal averaging technique (linear interpolation) that was used to produce estimates of cumulative emissions of each treatment using chamber measurements of N_2O in this study, and in Chapter 1.

Conclusion

The eddy covariance based N_2O emission estimates did not contradict emissions estimates from closed chambers when compared over extended periods. Both the eddy covariance and chamber observations indicated that overall emissions were relatively low in magnitude, and we conclude that chambers provide more accurate and useful estimates of N_2O emissions in such conditions. The frequency distribution of half-hour eddy covariance measurements was fairly normally distributed, and this indicates an absence of short bursts of high N_2O emissions (hot-moments) during the periods of observation. However, spring-thaw events were not monitored in this study, and should be included to produce accurate and reliable annual emission estimates.

Estimates of N_2O emissions from a wide area based on small, widely spaced chambers, were within the range of uncertainty for estimates based on eddy covariance, and this suggests that the spatial and temporal chamber sampling design that we used adequately captured heterogeneity, including any hotspots and hot-moments, in N_2O emission rates from the study area. The heterogeneous source area that was studied provided a good opportunity to investigate spatial upscaling techniques, and we suggest that heterogeneous source areas can be useful in studying micrometeorological footprint models.

Works cited

Ambus, P. 1998. Nitrous oxide production by denitrification and nitrification in temperate forest, grassland and agricultural soils. European Journal of Soil Science 49: 495-502.

Ambus, P. and S. Christensen. 1994. Measurement of N2O emission from a fertilized grassland: an analysis of spatial variability. Journal of Geophysical Research: Atmospheres 99: 16549-16555.

Barton, L., B. Wolf, D. Rowlings, C. Scheer, R. Kiese, P. Grace, et al. 2015. Sampling frequency affects estimates of annual nitrous oxide fluxes. Scientific reports 5.

Beheydt, D., P. Boeckx, S. Sleutel, C. Li and O. Van Cleemput. 2007. Validation of DNDC for 22 long-term N 2 O field emission measurements. Atmos Environ 41: 6196-6211.

Bessou, C., F. Ferchaud, B. Gabrielle and B. Mary. 2011. Biofuels, greenhouse gases and climate change. A review. Agronomy for Sustainable Development 31: 1-79. doi:10.1051/agro/2009039.

Boas, M.L. 1983. Mathematical Methods in the Physical Sciences John Wiley & Sons. Inc. Canada.

Burba, G. and D. Anderson. 2010. A brief practical guide to eddy covariance flux measurements: principles and workflow examples for scientific and industrial applicationsLi-Cor Biosciences.

Conrad, R. 1996. Soil microorganisms as controllers of atmospheric trace gases (H-2, CO, CH4, OCS, N2O, and NO). Microbiol Rev 60: 609-+.

Davidson, E.A. 2009. The contribution of manure and fertilizer nitrogen to atmospheric nitrous oxide since 1860. Nature Geoscience 2: 659-662.

Dunmola, A.S., M. Tenuta, A.P. Moulin, P. Yapa and D.A. Lobb. 2010. Pattern of greenhouse gas emission from a Prairie Pothole agricultural landscape in Manitoba, Canada. Canadian Journal of Soil Science 90: 243-256.

Foken, T., M. Göockede, M. Mauder, L. Mahrt, B. Amiro and W. Munger. 2004. Post-field data quality control. Handbook of micrometeorology. Springer. p. 181-208.

Forster, P., V. Ramaswamy, P. Artaxo, T. Berntsen, R. Betts, D.W. Fahey, J. Haywood, J. Lean, D.C. Lowe, G. Myhre, J. Nganga, R. Prinn, G. Raga, M. Schulz, R. Van Dorland. 2007. Changes in Atmospheric Constituents and in Radiative Forcing. In: Climate Change 2007: The Physical Science Basis. Contribution of Working Group I to the Fourth Assessment Report of the Intergovernmental Panel on Climate Change [Solomon, S., D. Qin, M. Manning, Z. Chen, M. Marquis, K.B. Averyt, M.Tignor and H.L. Miller (eds.)]. Cambridge University Press, Cambridge, United Kingdom and New York, NY, USA.

Groffman, P.M., K. Butterbach-Bahl, R.W. Fulweiler, A.J. Gold, J.L. Morse, E.K. Stander, et al. 2009. Challenges to incorporating spatially and temporally explicit phenomena (hotspots and hot moments) in denitrification models. Biogeochemistry 93: 49-77.

Ibrom, A., E. Dellwik, H. Flyvbjerg, N.O. Jensen and K. Pilegaard. 2007. Strong low-pass filtering effects on water vapour flux measurements with closed-path eddy correlation systems. Agricultural and forest meteorology 147: 140-156.

Jones, S., D. Famulari, C. Di Marco, E. Nemitz, U. Skiba, R. Rees, et al. 2011. Nitrous oxide emissions from managed grassland: a comparison of eddy covariance and static chamber measurements. Atmospheric Measurement Techniques 4: 2179-2194.

Kljun, N., P. Calanca, M. Rotach and H. Schmid. 2004. A simple parameterisation for flux footprint predictions. Boundary-Layer Meteorology 112: 503-523.

Kormann, R. and F.X. Meixner. 2001. An analytical footprint model for non-neutral stratification. Boundary-Layer Meteorology 99: 207-224.

Li, C. 2007. Quantifying greenhouse gas emissions from soils: Scientific basis and modeling approach. Soil Science and Plant Nutrition 53: 344-352. doi:10.1111/j.1747-0765.2007.00133.x.

MathWorks, I.T. 2011. MATLAB. The MathWorks Inc., Natick, Massachusetts.

McClain, M.E., E.W. Boyer, C.L. Dent, S.E. Gergel, N.B. Grimm, P.M. Groffman, et al. 2003. Biogeochemical hot spots and hot moments at the interface of terrestrial and aquatic ecosystems. Ecosystems 6: 301-312.

Molodovskaya, M., O. Singurindy, B.K. Richards, J. Warland, M.S. Johnson and T.S. Steenhuis. 2012. Temporal Variability of Nitrous Oxide from Fertilized Croplands: Hot Moment Analysis. Soil Sci Soc Am J 76: 1728-1740. doi:DOI 10.2136/sssaj2012.0039.

Molodovskaya, M., J. Warland, B.K. Richards, G. Oberg and T.S. Steenhuis. 2011. Nitrous oxide from heterogeneous agricultural landscapes: Source contribution analysis by eddy covariance and chambers. Soil Sci. Soc. Am. J. Soil Science Society of America Journal 75: 1829-1838.

Mosier, A., J. Duxbury, J. Freney, O. Heinemeyer and K. Minami. 1996. Nitrous oxide emissions from agricultural fields: Assessment, measurement and mitigation. Progress in nitrogen cycling studies. Springer. p. 589-602.

Parkin, T.B. 1987. Soil microsites as a source of denitrification variability. Soil Sci Soc Am J 51: 1194-1199.

Parkin, T.B. 2008. Effect of sampling frequency on estimates of cumulative nitrous oxide emissions. Journal of environmental quality 37: 1390-1395.

Parkin, T.B. and R.T. Venterea. 2010. Sampling Protocols. Chapter 3. Chamber-Based Trace Gas Flux Measurements. Sampling Protocols. R.F. Follett, editor.: p. 3-1 to 3-39.

R Core Team. 2011. R: A language and environment for statistical computing. R Foundation for Statistical Computing, Vienna, Austria.

Ravishankara, A. 2009. Nitrous oxide (N2O): The dominant ozone-depleting substance emitted in the 21st century. Science 326.

Reay, D.S., E.A. Davidson, K.A. Smith, P. Smith, J.M. Melillo, F. Dentener, et al. 2012. Global agriculture and nitrous oxide emissions. Nature Climate Change 2: 410-416.

Ropkins, D.C.a.K. 2012. openair.

Schmid, H.P. 2002. Footprint modeling for vegetation atmosphere exchange studies: a review and perspective. Agricultural and forest meteorology 113: 159-183.

Schuepp, P., M. Leclerc, J. MacPherson and R. Desjardins. 1990. Footprint prediction of scalar fluxes from analytical solutions of the diffusion equation. Boundary-Layer Meteorology 50: 355-373.

Stoof, C.R., B.K. Richards, P.B. Woodbury, E.S. Fabio, A.R. Brumbach, J. Cherney, et al. 2014. Untapped Potential: Opportunities and Challenges for Sustainable Bioenergy Production from Marginal Lands in the Northeast USA. BioEnergy Research. doi:10.1007/s12155-014-9515-8.

U.S., E.P.A. 2013. Global Mitigation of Non-CO2 Greenhouse Gases: 2010-2030. Office of Atmospheric Programs (6207J) Washington, DC 20005.

Van den Heuvel, R., M. Hefting, N. Tan, M. Jetten and J. Verhoeven. 2009. N 2 O emission hotspots at different spatial scales and governing factors for small scale hotspots. Science of the Total Environment 407: 2325-2332.

Vesala, T., N. Kljun, Ü. Rannik, J. Rinne, A. Sogachev, T. Markkanen, et al. 2008. Flux and concentration footprint modelling: State of the art. Environmental Pollution 152: 653-666.

Wagner-Riddle, C. 1997. Estimates of nitrous oxide emissions from agricultural fields over 28 months. Canadian journal of soil science 77.

Wagner-Riddle, C., A. Furon, N.L. Mclaughlin, I. Lee, J. Barbeau, S. Jayasundara, et al. 2007. Intensive measurement of nitrous oxide emissions from a corn-soybean-wheat rotation under two contrasting management systems over 5 years. Global Change Biol 13: 1722-1736. doi:DOI 10.1111/j.1365-2486.2007.01388.x.

Wang, K., X. Zheng, M. Pihlatie, T. Vesala, C. Liu, S. Haapanala, et al. 2013. Comparison between static chamber and tunable diode laser-based eddy covariance techniques for measuring nitrous oxide fluxes from a cotton field. Agricultural and forest meteorology 171: 9-19.

Yates, T., B. Si, R. Farrell and D. Pennock. 2006. Probability distribution and spatial dependence of nitrous oxide emission. Soil Sci Soc Am J 70: 753-762.

Zhao, J., X. Chen and A.M. Bao. 2014. Spatial representativeness of eddy covariance measurements using footprint analysis in arid areas. Environmental earth sciences 71: 1691-1697.

Appendix A

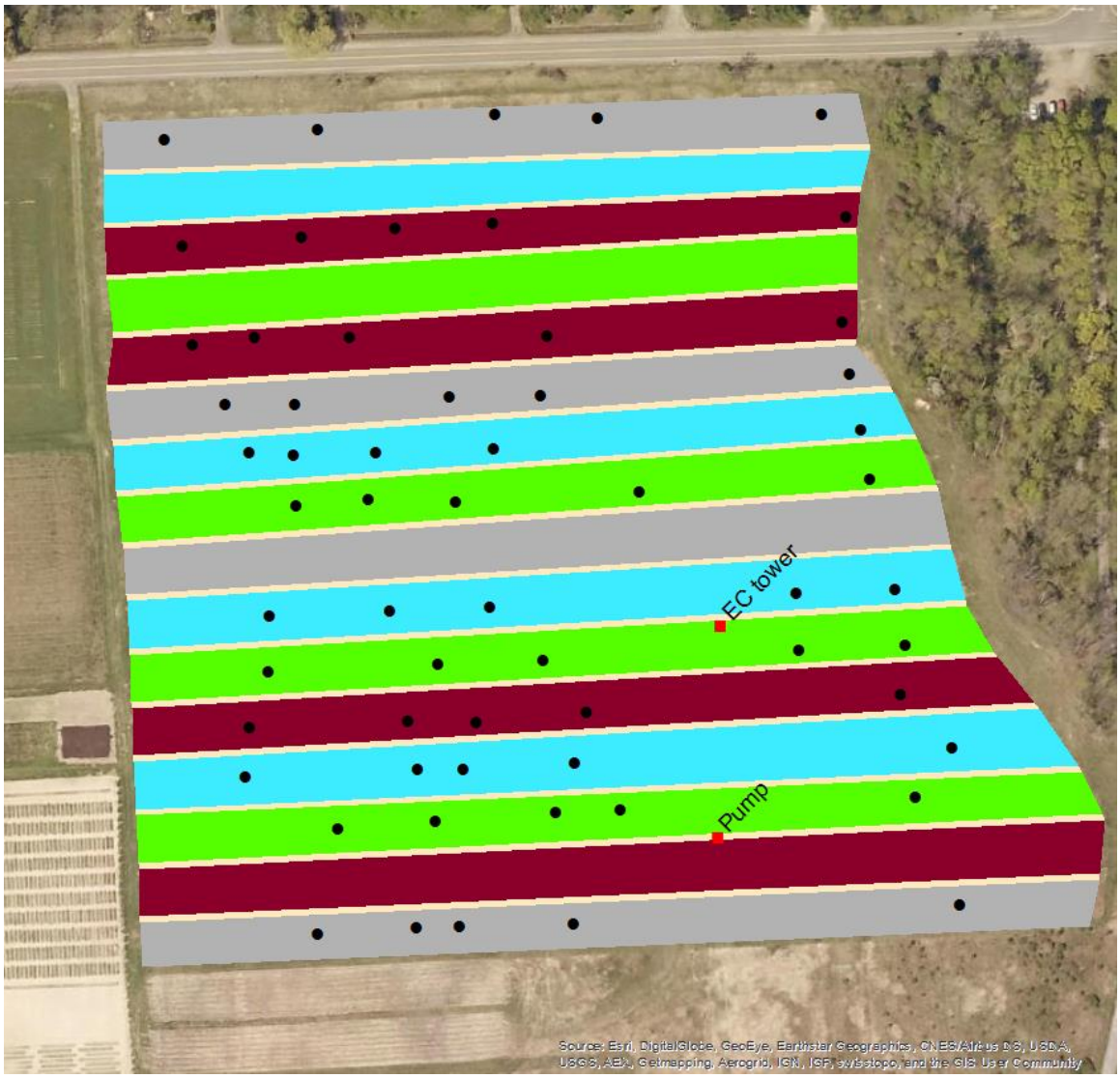

Figure S1.1: Image showing layout of treatments at the research site. Grey, cyan, maroon, and green horizontal strips represent Control, Switchgrass, Reed canarygrass + N, and Switchgrass + N treatments respectively. Black dots indicate locations of subplots where pairs of closed chambers were situated for monitoring of N_2O flux.

Table S1.1

Data used (white cells) for annual comparison of treatments				
Date	Control	Switchgrass	Reed canarygrass +N	Switchgrass +N
2013-04-01	✓	✓	314	✓
2013-05-14	✓	✓	14	✓
2013-06-12	✓	✓	43	7
2013-07-11	✓	✓	72	36
2013-08-14	✓	✓	106	70
2013-09-17	✓	✓	140	104
2013-10-22	✓	✓	175	139
2013-11-20	✓	✓	204	168
2014-05-06	✓		371	
2014-05-20	✓		13	
2014-05-29	✓	✓	22	358
2014-06-06	✓	✓	30	4
2014-06-12		✓		10
2014-06-19	✓	✓	43	17
2014-07-16	✓	✓	70	44
2014-08-14	✓	✓	99	73
2014-09-24	✓	✓	140	114
2014-11-12	✓	✓	189	163

Table S1.2

Data used for comparison of Control and Reed canarygrass + N				
Date	Control	Switchgrass	Reed canarygrass +N	Switchgrass +N
2013-04-01	✓	✓	314	✓
2013-05-14	✓	✓	14	✓
2013-06-12	✓	✓	43	7
2013-07-11	✓	✓	72	36
2013-08-14	✓	✓	106	70
2013-09-17	✓	✓	140	104
2013-10-22	✓	✓	175	139
2013-11-20	✓	✓	204	168
2014-05-06	✓		371	
2014-05-20	✓		13	
2014-05-29	✓	✓	22	358
2014-06-06	✓	✓	30	4
2014-06-12		✓		10
2014-06-19	✓	✓	43	17
2014-07-16	✓	✓	70	44
2014-08-14	✓	✓	99	73
2014-09-24	✓	✓	140	114
2014-11-12	✓	✓	189	163

Table S1.3

Data used for comparison of Switchgrass and Reed canarygrass + N				
Date	Control	Switchgrass	Reed canarygrass +N	Switchgrass +N
2013-04-01	✓	✓	314	✓
2013-05-14	✓	✓	14	✓
2013-06-12	✓	✓	43	7
2013-07-11	✓	✓	72	36
2013-08-14	✓	✓	106	70
2013-09-17	✓	✓	140	104
2013-10-22	✓	✓	175	139
2013-11-20	✓	✓	204	168
2014-05-06	✓		371	
2014-05-20	✓		13	
2014-05-29	✓	✓	22	358
2014-06-06	✓	✓	30	4
2014-06-12		✓		10
2014-06-19	✓	✓	43	17
2014-07-16	✓	✓	70	44
2014-08-14	✓	✓	99	73
2014-09-24	✓	✓	140	114
2014-11-12	✓	✓	189	163

Table S1.4

Data used for comparison of Switchgrass + N and Reed canarygrass + N				
Date	Control	Switchgrass	Reed canarygrass +N	Switchgrass +N
2013-04-01	✓	✓	314	✓
2013-05-14	✓	✓	14	✓
2013-06-12	✓	✓	43	7
2013-07-11	✓	✓	72	36
2013-08-14	✓	✓	106	70
2013-09-17	✓	✓	140	104
2013-10-22	✓	✓	175	139
2013-11-20	✓	✓	204	168
2014-05-06	✓		371	
2014-05-20	✓		13	
2014-05-29	✓	✓	22	358
2014-06-06	✓	✓	30	4
2014-06-12		✓		10
2014-06-19	✓	✓	43	17
2014-07-16	✓	✓	70	44
2014-08-14	✓	✓	99	73
2014-09-24	✓	✓	140	114
2014-11-12	✓	✓	189	163

Table S1.5

Data used for comparison of Switchgrass + N and Control				
Date	Control	Switchgrass	Reed canarygrass +N	Switchgrass +N
2013-04-01	✓	✓	314	✓
2013-05-14	✓	✓	14	✓
2013-06-12	✓	✓	43	7
2013-07-11	✓	✓	72	36
2013-08-14	✓	✓	106	70
2013-09-17	✓	✓	140	104
2013-10-22	✓	✓	175	139
2013-11-20	✓	✓	204	168
2014-05-06	✓		371	
2014-05-20	✓		13	
2014-05-29	✓	✓	22	358
2014-06-06	✓	✓	30	4
2014-06-12		✓		10
2014-06-19	✓	✓	43	17
2014-07-16	✓	✓	70	44
2014-08-14	✓	✓	99	73
2014-09-24	✓	✓	140	114
2014-11-12	✓	✓	189	163

Table S1.6

Data used for comparison of Switchgrass + N and Switchgrass				
Date	Control	Switchgrass	Reed canarygrass +N	Switchgrass +N
2013-04-01	✓	✓	314	✓
2013-05-14	✓	✓	14	✓
2013-06-12	✓	✓	43	7
2013-07-11	✓	✓	72	36
2013-08-14	✓	✓	106	70
2013-09-17	✓	✓	140	104
2013-10-22	✓	✓	175	139
2013-11-20	✓	✓	204	168
2014-05-06	✓		371	
2014-05-20	✓		13	
2014-05-29	✓	✓	22	358
2014-06-06	✓	✓	30	4
2014-06-12		✓		10
2014-06-19	✓	✓	43	17
2014-07-16	✓	✓	70	44
2014-08-14	✓	✓	99	73
2014-09-24	✓	✓	140	114
2014-11-12	✓	✓	189	163

Table S1.7

Data used for comparison of Switchgrass and Control				
Date	Control	Switchgrass	Reed canarygrass +N	Switchgrass +N
2013-04-01	✓	✓	314	✓
2013-05-14	✓	✓	14	✓
2013-06-12	✓	✓	43	7
2013-07-11	✓	✓	72	36
2013-08-14	✓	✓	106	70
2013-09-17	✓	✓	140	104
2013-10-22	✓	✓	175	139
2013-11-20	✓	✓	204	168
2014-05-06	✓		371	
2014-05-20	✓		13	
2014-05-29	✓	✓	22	358
2014-06-06	✓	✓	30	4
2014-06-12		✓		10
2014-06-19	✓	✓	43	17
2014-07-16	✓	✓	70	44
2014-08-14	✓	✓	99	73
2014-09-24	✓	✓	140	114
2014-11-12	✓	✓	189	163

```
#Calculate cumulative emissions
rm(list = ls())
maindir <- "/Users/Ced/Dropbox/Cedric's files/PhD/working/chamber_data/1_scripts"
#set working directory
setwd(maindir)

source("1_setup.R")
# main output data frame is "crc", includes ALL 2013-14 chamber data

#############################################################################
# setup data
#split into separate data frames for each year/treatment

crc.13.C <- crc[crc$date < "2014-01-01" & crc$treatment == "CONTROLL",]
crc.13.RC <- crc[crc$date < "2014-01-01" & crc$treatment == "RCG",]
crc.13.SG <- crc[crc$date < "2014-01-01" & crc$treatment == "SWG",]
crc.13.SGN <- crc[crc$date < "2014-01-01" & crc$treatment == "SWGN",]

crc.14.C <- crc[crc$date >= "2014-01-01" & crc$treatment == "CONTROLL",]
crc.14.RC <- crc[crc$date >= "2014-01-01" & crc$treatment == "RCG",]
crc.14.SG <- crc[crc$date >= "2014-01-01" & crc$treatment == "SWG",]
crc.14.SGN <- crc[crc$date >= "2014-01-01" & crc$treatment == "SWGN",]

datalist <- list(crc.13.C, crc.14.C, crc.13.SG, crc.14.SG, crc.13.RC, crc.14.RC, crc.13.SGN, crc.14.SGN)
#~~~~~~~~~~~~~~~~~~~~~~~~~~~~~~~~

out.df <- data.frame()

# "j" cycles through blocks of treatment/years
for (j in 1:length(datalist))
{
 #get dataset for treatment/yr
 tdata <- datalist[[j]]
 #get treatment
 treat <- unique(tdata$treatment)
 #get year
 year <- unique(format(tdata$date,"%Y"))
 #get dates
 dts <- unique(tdata$date)

 #split treatment/yr by campaign dates
 splitdate <- split(tdata, tdata$doy)

 #make new list with many bootstraped means for each date to draw from
 bootvals <- list()

 #cycle through dates for each year/treatment block
 for(s in 1:length(splitdate))
 {
  bootdata <- splitdate[[s]]$fluxL
  source("sub_bootstrap.R")
  #bootout.df$Poolmean is the vector to pull the means from for area under curve
  bootvals[[s]] <- bootout.df$Poolmean
 }
 names(bootvals) <- names(splitdate)

 #vector to recieve trial results
 Cumtrials <- c()
 NCumtrials <- 10000
 #cycle through many iterations of cumulative calculation
 for(r in 1:NCumtrials)
 {
```

```
    xpt <- c()
    ypt <- c()

    # fill in vectors with means and dates
    for(k in 1:length(bootvals))
    {
     # day of year
     xpt[k] <- as.numeric(names(bootvals[k]))

     # mean flux: instead of mean of data, use a bootstrapped mean

     ypt[k] <- sample(bootvals[[k]], 1, replace = TRUE)
    }

    #calculate cummulative value
    Trialsegs <- c()
    for(n in 1:length(xpt)-1)
    {
     doyS <- xpt[n]
     doyE <- xpt[n+1]
     AVperiod <- (ypt[n]+ypt[n+1])/2
     #"flux units are micrograms N2O-N m^-2 hr-1"
     duration <- (doyE - doyS)*24 #duration of period in hours

     Trialsegs[n] <- duration * AVperiod #units are micrograms N2O-N m^-2
    }

    Trialsum <- sum(Trialsegs)/1000 #units are miligrams N2O-N m^-2
    Cumtrials[r] <- Trialsum
  }

  #print info to output row
  out.df[j,1] <- year
  out.df[j,2] <- treat
  out.df[j,3] <- as.character(min(dts)) #start date
  out.df[j,4] <- as.character(max(dts)) #end date
  out.df[j,5] <- mean(Cumtrials) #mean of all cumulative trials (should closely match previous version)

  #establish confidence intervals for cumulative value
  tempQ <- quantile(Cumtrials, probs = c(0.025, 0.975))
  out.df[j,6] <- min(tempQ)
  out.df[j,7] <- max(tempQ)
  out.df[j,8] <- median(Cumtrials)
}

names(out.df) <- c("Year", "Treatment", "Start date", "End date", "Mean_cum", "CIlower", "CIupper", "Median")
```

```
# sub_bootstrap.R: sub-routine to calculate confidence intervals from bootstrapping of flux vector
#############################################################################
#data: vector of fluxL values is "bootdata"
fluxvec <- bootdata
#make loop to go through all dates
#define N, number of times for each trial
trials <- 10000
Cmax <- length(bootdata)

bootout.df <- data.frame()
tempout.df <- data.frame()

 #for each trial
 for (m in 1:trials)
 {
  #pull Cmax samples from the fluxvector, with replacement
  fluxpool <- sample(fluxvec, Cmax, replace = TRUE)
  #find mean of pool
  Poolmean <- mean(fluxpool)
  PoolN <- Cmax

  #print N
  tempout.df[m,1] <- PoolN
  #print iteration #
  tempout.df[m,2] <- m
  #print pool average
  tempout.df[m,3] <- Poolmean

 }

 bootout.df <- rbind(bootout.df, tempout.df)
 names(bootout.df) <- c("PoolN","iteration","Poolmean")
```

Appendix B

Text S2.1: Description of hypothesis tests using the binomial distribution function

The binomial distribution is a discrete probability distribution described by Eq. S1.

$$f(n) = \frac{N!}{n!(N-n)!} p^n (1-p)^{N-n} \qquad \text{Eq. S1}$$

In circumstances where the outcome of a single trial is considered either a success or a failure, the binomial distribution function is used to predict the likelihood of *n* successes in a sequence of *N* trials, where the probability of success for a single trial is given by *p*. In this research, the binomial distribution function was applied as follows to test the null hypotheses that a) "hotspots in this study occurred independently and randomly in space", and b) "hotspots in this study occurred independently and randomly in time". We focused on evaluating these hypotheses for the Switchgrass + N treatment because the occurrence of hotspots was found to be greatest in those plots, and the observations showed potential for meaningful statistical work.

a) Assuming that each chamber observation in this study is indeed independent and random in time and space, the overall probability of observing a hotspot in any single chamber observation is equal to the total number of hotspots divided by the number of observations for the treatment. In the case of the Switchgrass + N treatment for years 2013 - 2015, p = 27/521, or 0.052. The binomial distribution function (Eq. S1) was used to calculate the probability of observing each possible number of hotspots at a single chamber with 18 observations in all, thus the probability of *n* successes was calculated for n = 0 to 18 using Eq. S1. These results are presented in Table S2.1, column 2. The values from Table S2.1, column 2 were then used to calculate the probability of "*n*-or-more" hotspot occurrences for n = 0 to 18 by summing the probabilities from outcomes for *n* to N = 18 (Eq. S2).

$$P(x_i \geq x_n) = \sum_{x_i \geq x_n}^{x_N} f(x_i) \qquad \text{Eq. S2}$$

These results are presented in Table S2.1, column 3; The values indicate the probability of observing *n*-or-more hotspots at a single chamber location in 18 observations for the Switchgrass + N treatment.

The second step of this hypothesis test repeats the above process but applies the variables to different parameters. Here, we start with Eq. S1 and treat each set of 18 observations for a chamber as one independent event, with 30 chambers being observed for the treatment. Here, N is the number of chambers observed (30), p_k is the probability of observing k or more hotspots at a single chamber (values from Table S2.1, column 3), and n_c is the number of chambers showing k-or-more hotspots. Table S2.2, column 2 shows these results. Finally, the probability of observing n_c-or-more chambers with k-or-more hotspots is calculated by applying Eq. S2 to the values in Table S2.2, column 2, these results are presented in Table S2.2, column 3.

From Table S2.2, column 3, we see that in the Switchgrass + N treatment, the chance of observing 1-or-more chambers, each with 6-or-more hotspots (the actual outcome at chamber "N1-1") is about 0.006. This indicates that if the assumptions of spatial independence and randomness are true, the result at chamber "N1-1" is statistically unlikely, and this is grounds to reject the null hypothesis. Therefore, we conclude that the hotspot observations are not independent and random in space, and this implies that hotspots are prone to recurrence in some areas more than others. In the case of chamber "N1-1", we can conclude that the clustering of hotspot observations here are not due to chance, but to physically stationary biogeochemical processes that cause the soil to emit N_2O at considerably higher levels than the surrounding area for a longer period than the 30 minutes of a single chamber deployment.

This test of the null hypothesis was also shown to be false for the unfertilized Switchgrass treatment. For the unfertilized Switchgrass, the *p*-value for observing 2-or-more

chambers each with 3-or-more hotspots is 0.014 (See Table S2.3 and Table S2.4). In the Control and Reed canarygrass + N treatments, these statistical tests did not provide enough evidence to reject the null hypothesis.

b) A similar 2-step process was applied to the Switchgrass + N hotspot identification results to investigate whether hotspots occur randomly over the course of the growing season. In the first step, N = 30 (the number of chambers observed on each observation date), again p = 27/521, n was varied from 0 to N, and the probabilities for n-or-more successes (hotspots) were calculated to determine the probability of observing n-or-more hotspots on any single observation date. Then in the second step, the resulting values were used to calculate the probability of observing various numbers of campaigns with n-or-more hotspots. Here, N=18 (the number of observation dates), and p is taken as the values determined in step one for number of hotspots on a single date. The final results show that the probability of one-or-more campaigns with 5-or-more hotspots (the observation for Switchgrass + N on 2014-07-16) is approximately 0.28, which is not statistically significant. The results also show that the chance of producing 4-or-more campaigns each with 3-or-more hotspots (also an actual occurrence) is about 0.51, also not statistically significant.

Overall, these results strongly suggest that in the Switchgrass + N treatment, hotspots tend to occur more frequently in specific locations. The statistical results do not support the hypothesis that hotspots occur more frequently at specific times of the growing season. However, trends in the data suggest that hotspots may actually occur more frequently at specific times of the growing season, more research may be needed to show this statistically.

Sources:
Chin, David A., Water-Resources Engineering, 2nd Ed. Copyright 2006, Pearson Education , Inc.
Boas, M. L. (1983). Mathematical methods in the physical sciences, 2nd Ed.

Table S2.1: Results of the binomial distribution function for $N = 18$ and $p = 27/521$. The first column shows the number of successes (hotspots) n at one chamber location, the second column shows the chance of exactly n successes, and the third column shows the chance of n-or-more successes. Note that the p-value for 6-or-more hotspots is 0.0002.

n (hotspots)	*p*-value (for *n* hotspots)	*p*-value (for *n*-or-more hotspots)
0	0.383712601	1
1	0.377498631	0.616287399
2	0.175376389	0.238788768
3	0.051121862	0.063412379
4	0.010477912	0.012290517
5	0.001603502	0.001812605
6	0.000189888	0.000209103
7	1.78E-05	1.92E-05
8	1.34E-06	1.42E-06
9	8.12E-08	8.54E-08
10	3.99E-09	4.16E-09
11	1.59E-10	1.64E-10
12	5.06E-12	5.19E-12
13	1.28E-13	1.30E-13
14	2.49E-15	2.53E-15
15	3.63E-17	3.67E-17
16	3.72E-19	3.75E-19
17	2.39E-21	2.40E-21
18	7.27E-24	7.27E-24

Table S2.2: Results of the binomial distribution function for $N = 30$ chambers, $p = 0.0002$. The first column shows the number of chambers (n), the second column shows the chance of exactly n chambers with 6-or-more hotspots, and the third column shows the p-value for observing n-or-more chambers each with 6-or-more hotspots. Note that the p-value for observing 1-or-more chambers with 6-or-more hotspots is approximately 0.006.

n (number of chambers)	*p*-value for exactly *n* chambers with 6-or-more hotspots per chamber	*p*-value for *n*-or-more chambers with 6-or-more hotspots per chamber
0	0.993745904	1
1	0.00623515	0.006254096
2	1.89E-05	1.89E-05
3	3.69E-08	3.70E-08
4	5.21E-11	5.22E-11
5	5.67E-14	5.67E-14
6	4.94E-17	4.94E-17
7	3.54E-20	3.54E-20
8	2.13E-23	2.13E-23
9	1.09E-26	1.09E-26
10	4.78E-30	4.78E-30
11	1.82E-33	1.82E-33
12	6.02E-37	6.02E-37
13	1.74E-40	1.74E-40
14	4.43E-44	4.43E-44
15	9.88E-48	9.88E-48
16	1.94E-51	1.94E-51
17	3.34E-55	3.34E-55
18	5.04E-59	5.04E-59
19	6.66E-63	6.66E-63
20	7.66E-67	7.66E-67
21	7.63E-71	7.63E-71
22	6.52E-75	6.53E-75
23	4.75E-79	4.75E-79
24	2.90E-83	2.90E-83
25	1.45E-87	1.45E-87
26	5.85E-92	5.85E-92
27	1.81E-96	1.81E-96
28	4.06E-101	4.06E-101
29	5.85E-106	5.85E-106
30	4.08E-111	4.08E-111

Table S2.3: Results of the binomial distribution function for $N = 16$ and $p = 11/465$. The first column shows the number of successes (hotspots) n at one chamber location, the second column shows the chance of exactly n successes, and the third column shows the chance of n-or-more successes. Note that the p-value for 3 or more hotspots is 0.0059.

n (hotspots)	p-value (for n hotspots)	p-value (for n-or-more hotspots)
0	0.681783363	1
1	0.264303683	0.318216637
2	0.048028753	0.053912954
3	0.005430564	0.005884201
4	0.000427627	0.000453637
5	2.49E-05	2.60E-05
6	1.10E-06	1.14E-06
7	3.82E-08	3.93E-08
8	1.04E-09	1.06E-09
9	2.24E-11	2.28E-11
10	3.81E-13	3.86E-13
11	5.03E-15	5.08E-15
12	5.08E-17	5.12E-17
13	3.79E-19	3.81E-19
14	1.97E-21	1.97E-21
15	6.35E-24	6.36E-24
16	9.62E-27	9.62E-27

Table S2.4: Results of the binomial distribution function for $N = 30$ chambers, $p = 0.0059$. The first column shows the number of chambers (n), the second column shows the chance of exactly n chambers with 3-or-more hotspots, and the third column shows the p-value for observing n-or-more chambers each with 3-or-more hotspots. Note that the p-value for observing 2-or-more chambers with 3-or-more hotspots is approximately 0.014.

n (number of chambers)	*p*-value for exactly *n* chambers with 3-or-more hotspots per chamber	*p*-value for *n*-or-more chambers with 3-or-more hotspots per chamber
0	0.837740044	1
1	0.14875825	0.162259956
2	0.012767316	0.013501706
3	0.000705321	0.00073439
4	2.82E-05	2.91E-05
5	8.67E-07	8.89E-07
6	2.14E-08	2.18E-08
7	4.34E-10	4.42E-10
8	7.39E-12	7.50E-12
9	1.07E-13	1.08E-13
10	1.33E-15	1.34E-15
11	1.43E-17	1.44E-17
12	1.34E-19	1.35E-19
13	1.10E-21	1.11E-21
14	7.89E-24	7.94E-24
15	4.98E-26	5.01E-26
16	2.77E-28	2.78E-28
17	1.35E-30	1.35E-30
18	5.76E-33	5.78E-33
19	2.15E-35	2.16E-35
20	7.01E-38	7.03E-38
21	1.98E-40	1.98E-40
22	4.79E-43	4.80E-43
23	9.85E-46	9.87E-46
24	1.70E-48	1.70E-48
25	2.42E-51	2.42E-51
26	2.75E-54	2.75E-54
27	2.41E-57	2.41E-57
28	1.53E-60	1.53E-60
29	6.24E-64	6.25E-64
30	1.23E-67	1.23E-67

Table S2.5: Results of the binomial distribution function for $N = 30$, and $p = 27/521$. The first column shows the number of successes (hotspots) n during one campaign date, the second column shows the chance of exactly n successes, and the third column shows the chance of n-or-more successes. Note that the p-value for 5 or more hotspots is 0.018.

n (hotspots)	p-value (for n hotspots)	p-value (for n-or-more hotspots)
0	0.202617414	1
1	0.332226934	0.797382586
2	0.263293208	0.465155651
3	0.134311515	0.201862443
4	0.049551161	0.067550928
5	0.014082962	0.017999767
6	0.003207152	0.003916806
7	0.000600993	0.000709653
8	9.44E-05	0.00010866
9	1.26E-05	1.42E-05
10	1.45E-06	1.61E-06
11	1.44E-07	1.57E-07
12	1.25E-08	1.35E-08
13	9.42E-10	1.01E-09
14	6.25E-11	6.64E-11
15	3.65E-12	3.84E-12
16	1.87E-13	1.96E-13
17	8.41E-15	8.75E-15
18	3.32E-16	3.44E-16
19	1.15E-17	1.18E-17
20	3.44E-19	3.54E-19
21	8.97E-21	9.17E-21
22	2.00E-22	2.04E-22
23	3.81E-24	3.87E-24
24	6.08E-26	6.16E-26
25	7.97E-28	8.05E-28
26	8.38E-30	8.44E-30
27	6.78E-32	6.82E-32
28	3.97E-34	3.99E-34
29	1.50E-36	1.50E-36
30	2.73E-39	2.73E-39

Table S2.6: Results of the binomial distribution function for N=18 campaigns, p=0.018. The first column shows the number of campaigns (n), the second column shows the chance of exactly n campaigns with 5-or-more hotspots, and the third column shows the p-value for observing n-or-more campaigns each with 5-or-more hotspots. Note that the p-value for observing 1-or-more campaigns with 5-or-more hotspots is approximately 0.28.

n (number of campaigns)	*p*-value for exactly *n* campaigns with 5-or-more hotspots per campaign	*p*-value for *n*-or-more campaigns with 5-or-more hotspots per campaign
0	0.721121815	1
1	0.237923004	0.278878185
2	0.037068982	0.040955181
3	0.003623804	0.003886199
4	0.000249087	0.000262395
5	1.28E-05	1.33E-05
6	5.08E-07	5.24E-07
7	1.60E-08	1.64E-08
8	4.02E-10	4.10E-10
9	8.19E-12	8.33E-12
10	1.35E-13	1.37E-13
11	1.80E-15	1.82E-15
12	1.93E-17	1.94E-17
13	1.63E-19	1.64E-19
14	1.07E-21	1.07E-21
15	5.21E-24	5.23E-24
16	1.79E-26	1.80E-26
17	3.86E-29	3.87E-29
18	3.93E-32	3.93E-32

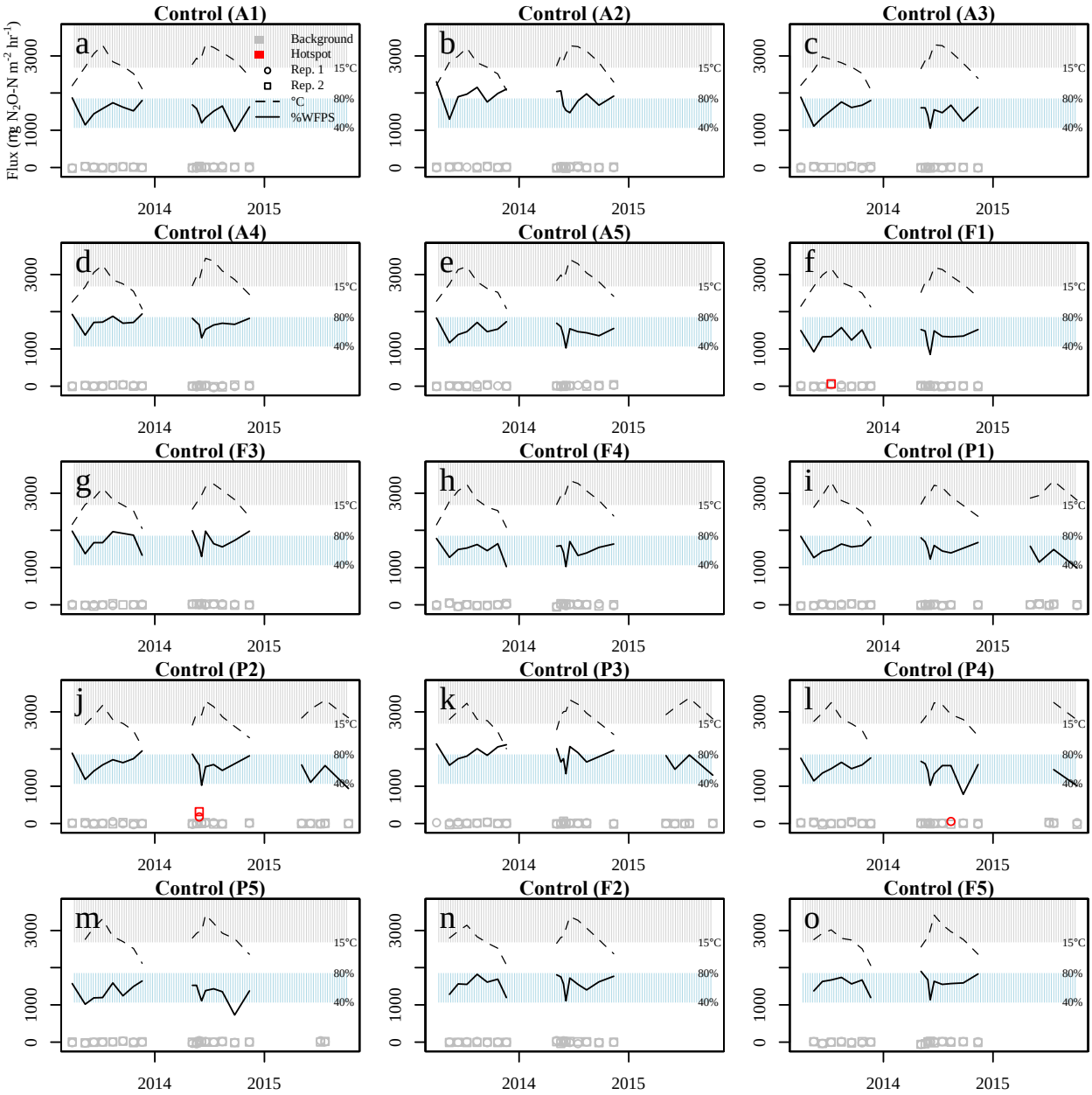

Figure S2.1: Time series of N_2O flux observations at individual static chambers in the Control treatment for years 2013-2015, organized by subplot. Instances of hotspots are indicated in red. Dashed black lines indicate local soil temperature and grey shading indicates temperatures greater that 15°C. Solid black lines indicate local soil moisture and blue shading indicates WFPS between 40% and 80 %.

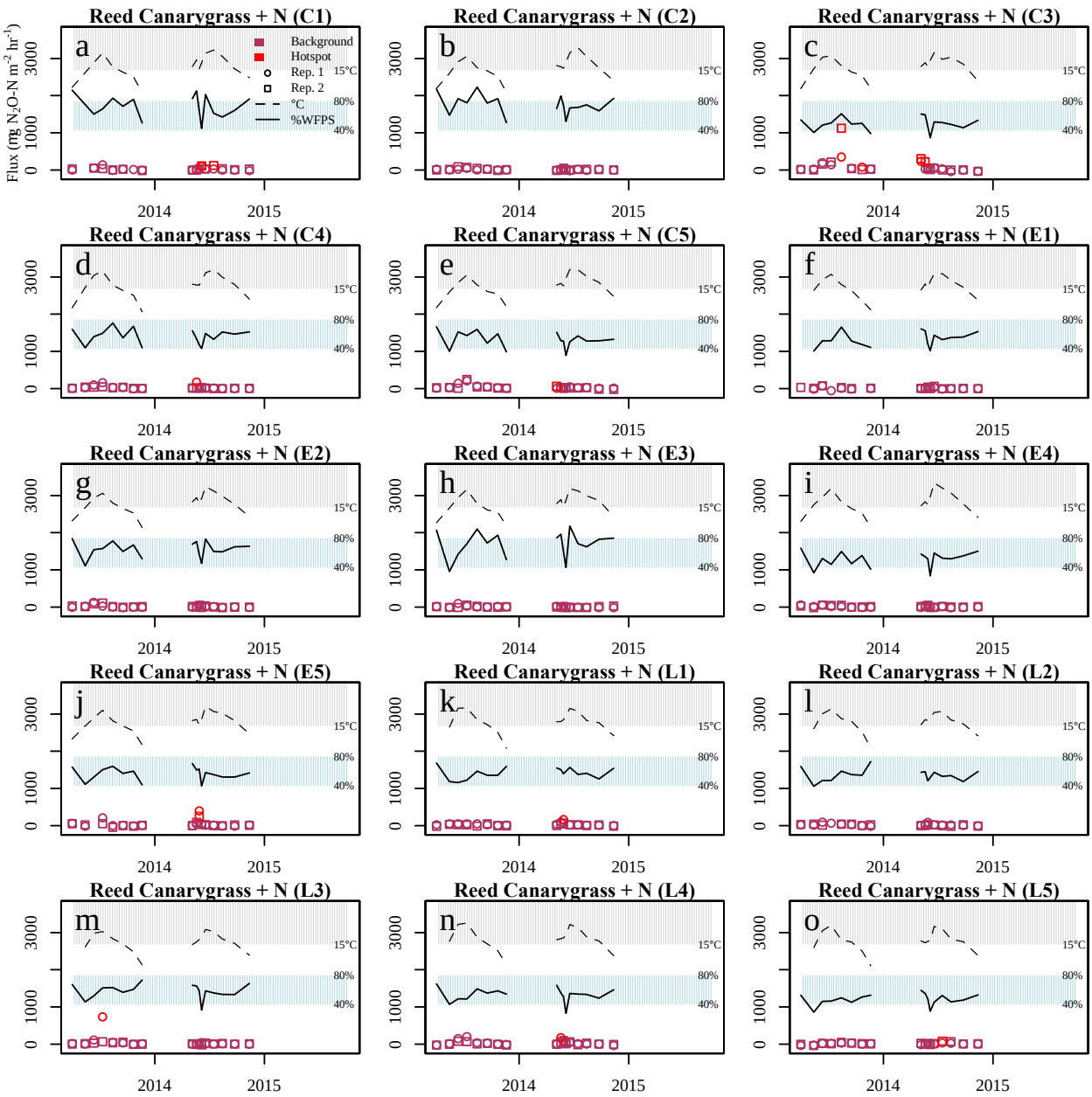

Figure S2.2: Time series of N_2O flux observations at individual static chambers in the Reed Canarygrass + N treatment for years 2013-2014, organized by subplot. Instances of hotspots are indicated in red. Dashed black lines indicate local soil temperature and grey shading indicates temperatures greater that 15°C. Solid black lines indicate local soil moisture and blue shading indicates WFPS between 40% and 80%.

Appendix C

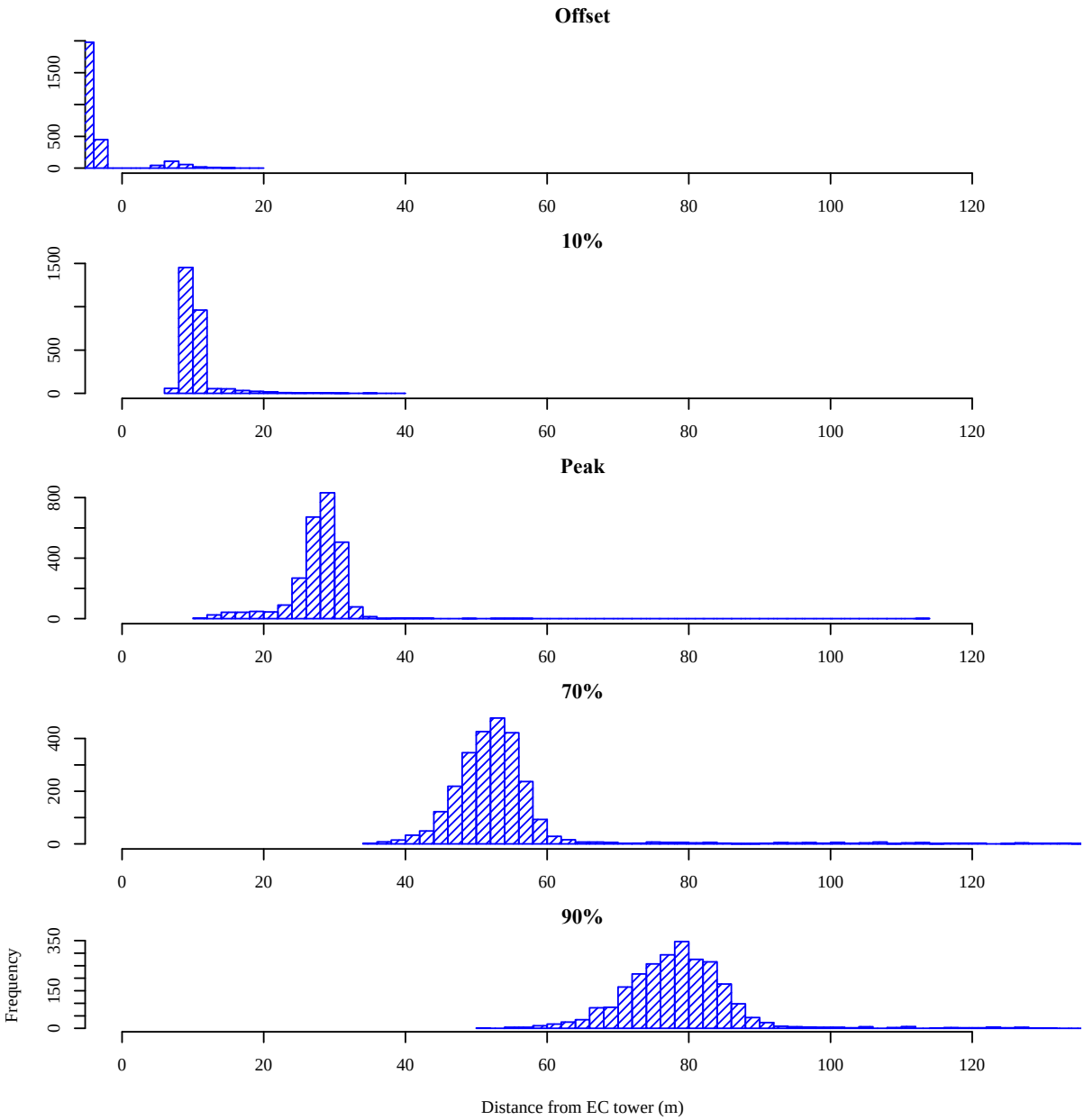

Figure S3.1: Histograms showing distributions of eddy covariance footprint threshold distances (m) from the eddy covariance tower for the footprint offset (1%), 10% threshold, peak, 70% threshold, and 90% threshold.

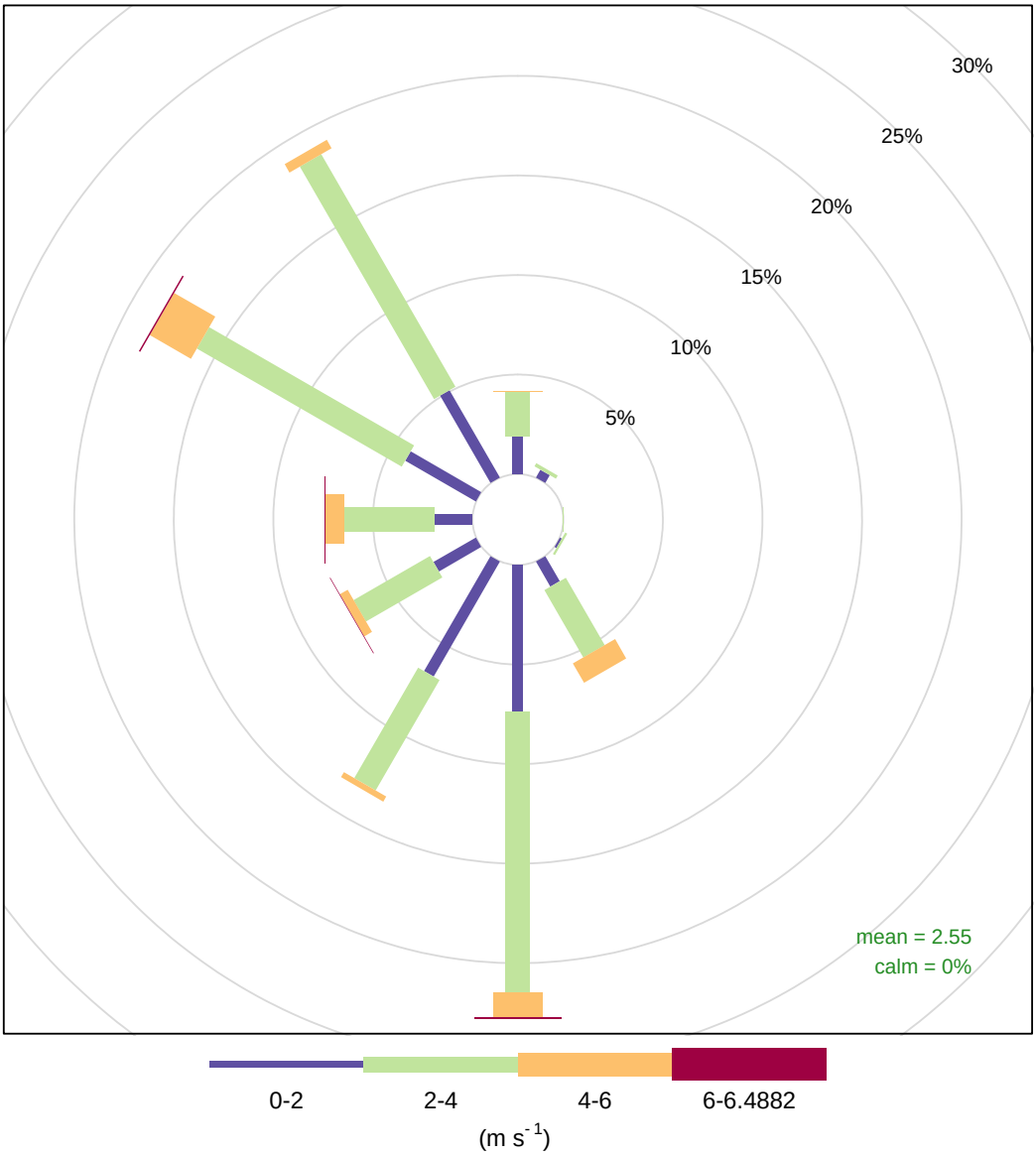

Figure S3.2: Wind rose showing trends in the wind at the research site for filtered (useable) eddy covariance data.

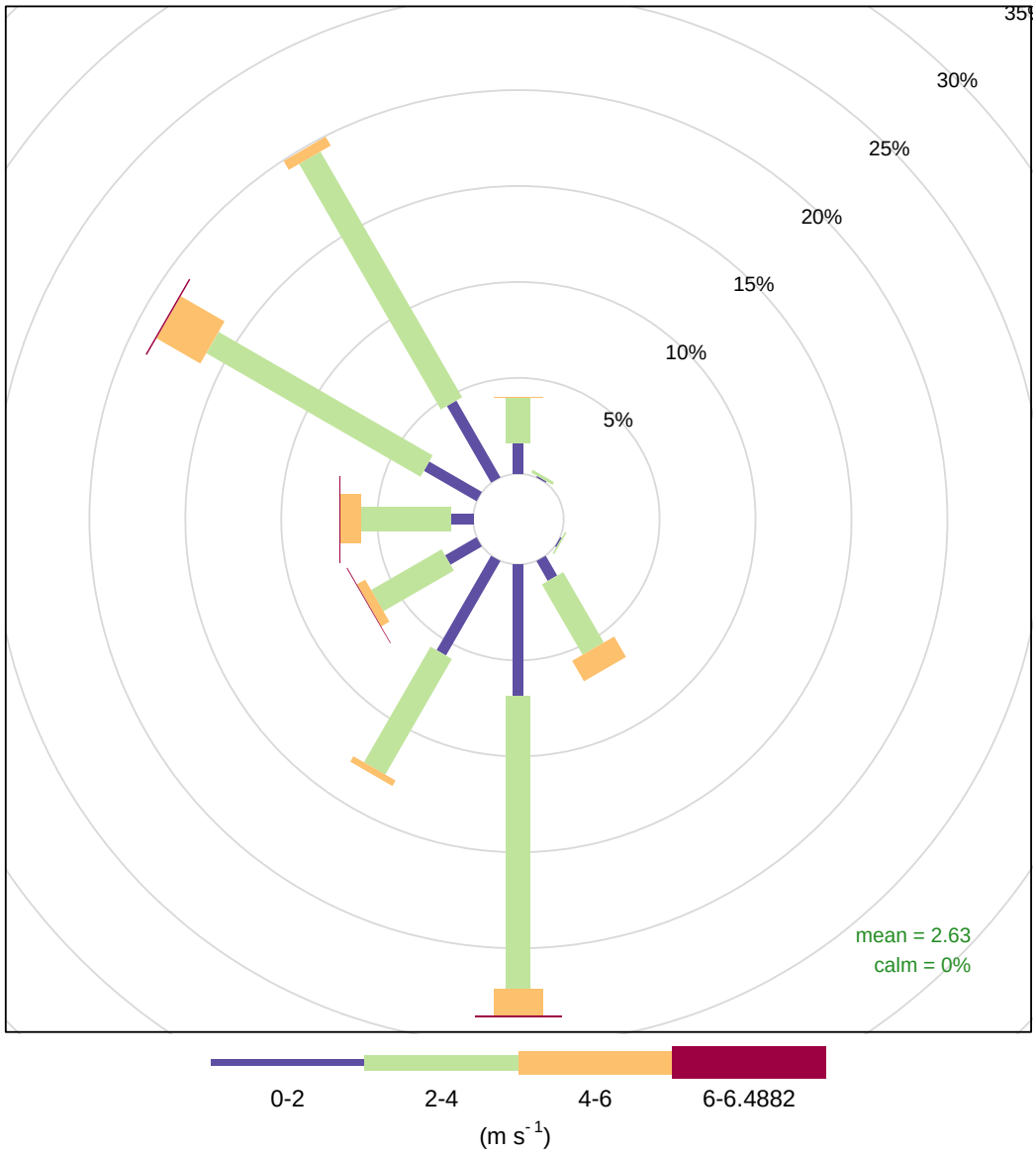

Figure S3.3: Wind rose showing trends in the wind at the research site for the final eddy covariance data used in this study.